Electronic Thesis and Dissertation Repository

7-25-2023 10:00 AM

Elucidating the Biomechanics of MERTK-Mediated Efferocytosis

Brandon Hayato Dickson, *Western University*

Supervisor: Heit, Bryan, *The University of Western Ontario*

A thesis submitted in partial fulfillment of the requirements for the Master of Science degree in Microbiology and Immunology

© Brandon Hayato Dickson 2023

Abstract

Macrophages are key mediators of efferocytosis – the phagocytic engulfment and removal of apoptotic cells. During engulfment, the coordinated activity of efferocytic receptors induces the remodeling of the actin cytoskeleton, which facilitates the envelopment of the cell by the plasma membrane. Mer receptor tyrosine kinase (MERTK) is a crucial efferocytic receptor, but its role during actin remodeling is not well understood. Previously, our lab showed that MERTK is an activator of β_2 integrins – which are comprised of receptors known to induce the actin polymerization that is required for engulfment. We hypothesized that MERTK is an indirect stimulator of actin polymerization via the stimulation of the actin-remodeling β_2 integrins. Herein, the biomechanics of efferocytosis were investigated by fluorescence imaging of the efferocytic synapse. In a frustrated efferocytosis model – where macrophages attempted to engulf a planar substrate that mimicked apoptotic cells, MERTK formed discrete clusters within the centre of the efferocytic synapse, where the periphery of the synapse was delineated by an expanding ring of actin-associated β_2 integrins. This suggests that integrins, not MERTK, are local directors of actin polymerization. Single particle tracking revealed that MERTK was less restricted in its free diffusion compared to the highly confined β_2 integrins, indicating these receptors play unique biomechanical roles during engulfment. Finally, we began the development of a traction force microscopy assay to characterize the biophysics of MERTK-dependent engulfment. Preliminary data revealed that frustrated efferocytosis on opsonized hydrogels required the simultaneous activity of MERTK and efferocytic integrin receptors. We expect that integrins transduce the forces required for engulfment via the actin cytoskeleton, whereas MERTK stimulates the initial activation of the integrins. Further elucidation of the mechanism of MERTK-mediated engulfment will be critical in our understanding of pathologies where efferocytosis is defective, such as systemic lupus erythematosus and atherosclerosis.

Keywords: MERTK, β_2 integrin, Efferocytosis, Biomechanics

Summary for Lay Audience

Macrophages are a type of immune cell that engulf and destroy dying cells, a process known as efferocytosis. This is required to prevent the accumulation of dead cells that would otherwise cause autoimmune disease or inflammation. MERTK is a receptor that is required for the recognition and engulfment of dying cells, how this works is not understood. Our laboratory previously showed that MERTK activates another group of receptors called the β_2 integrins. Integrins are known to directly manipulate the structure of the actin cytoskeleton, a network of protein fibers that are responsible for altering the shape of cells. By reshaping the cell, reorganization of actin allows a macrophage to extend its membrane around a target, thus engulfing material from their surrounding environment. We predicted that MERTK activates the β_2 integrins to induce the actin remodeling required for the engulfment of dying cells. In other words, we expect that the MERTK indirectly induces actin restructuring by working through integrins. To test this, we used fluorescence microscopy to observe the structures formed by macrophages during efferocytosis. In this project, we found that macrophages formed structured interactions with the dying cell being engulfed. β_2 integrins were located at the outer edges of the extending membrane, where extensive actin remodeling also occurred. MERTK failed to localize at these sites, and instead was found in the centre of the macrophage. Analysis of the movement of MERTK and β_2 integrins showed that the integrins were immobilized by their direct linkage with the actin cytoskeleton, while MERTK was not. Finally, we started the development of an experiment that will measure the forces induced by the actin cytoskeleton during efferocytosis. We expect that integrins are responsible for direct force production whereas MERTK plays a passive role by stimulating the initial activation of the integrins. Together, this work has revealed key insights into how MERTK and integrins coordinate the clearance of dying cells. This may represent a targetable pathway to treat conditions where MERTK's activity is defective, such as heart attack, stroke, lupus, arthritis, or other severe inflammatory disorders.

Acknowledgments

I'd like to acknowledge all who have supported me over the last two years.

To Dr. Bryan Heit: Thank you for giving me a chance by bringing me along to your lab. I started as an inexperienced, recently graduated bachelor's student from a different institution and city. My development into an emerging independent researcher would not have been possible without your guidance. I will miss our meetings where we would spend ages talking about science. No matter where I end up, I will always remember my roots as a Heit Lab alumnus.

To my committee members, Dr. Jimmy Dikeakos and Dr. Lakshman Gunaratnam: Thank you for your invaluable insight and support throughout my project. You are both amazing role models in academia and I will continue to carry on the values of what it means to be a scientist. I will strive to do my best throughout my scientific career, to be unfaltering in the jaws of failure, and to someday become a role model myself for the next generation of researchers.

I would like to extend my gratitude to everyone that I have worked with in the Heit Lab: Austin Le Lam, Kasia Wodz, Paul Mun, Catherine Jung, Peter Guo, Alex Lac, Dr. Nima Taefehshokr, Kerolos Kolta, Agata Wolochacz, Oneeb Hassan, Alice Kim, Tasnia Rahman, Maddy Dusick, Sarah Kwok, Amena Aktar, Mark Kwok, Matthew Arbolino, and Angela Vrieze. Austin and Angela, you two were especially important for teaching me a lot of the techniques that I know to this day; I appreciate that this was a luxury that not every new student gets when they join a new lab!

To mom and dad: Thank you for providing me this beautiful life. The sacrifices you made for my brothers and I are indescribable. I'm going to make you proud.

To Grammy: Thank you for the love and support you've given me. I'm going to work with many incredible people to help develop effective treatments for cancer and autoimmune disease. I promise.

It would not be an exaggeration to say that coming to Western was the best decision of my life. I would have never imagined that I would make so many friends in our department. It pains me to leave all of this behind so I can pursue my studies at Toronto. I could not have done this without you all.

Table of Contents

List of Tables

List of Figures

List of Abbreviations

AC	Apoptotic cell
ADAM17	A disintegrin and metalloprotease 17
ARP2/3	Actin-related protein 2/3 complex
APAF1	Apoptotic protease activating factor 1
APS	Ammonium persulphate
APTMS	(3-aminopropyl)-trimethoxysilane
BAI1	Brain-specific angiogenesis inhibitor 1
CAD	Caspase-activated DNase
DAG	Diacylglycerol
DAMP	Danger-associated molecular pattern
DC	Dendritic cell
DMEM	Dulbecco's Modified Eagle's Medium
DOCK180	Dedicator of cytokinesis 1
EGF	Epidermal growth factor
ERK	Extracellular signal regulated kinase
ERM	Ezrin/radixin/moesin
Fab	Fragment of antigen binding
FAK	Focal adhesion kinase
FADD	FAS associated death domain protein
FBS	Fetal bovine serum
FcγR	Fc-gamma receptor
FRET	Fluorescence resonance energy transfer
Gas6	Growth arrest-specific protein 6
Gla	Gamma carboxyglutamic acid-rich domain
GPCR	G-protein coupled receptor

Grb2	Growth factor receptor-bound protein 2
GULP	GULP PTB Domain Containing Engulfment Adaptor
HEPES	4-(2-hydroxyethyl)piperazine-1-ethanesulfonic acid
HMGB1	High mobility group box 1
ICAD	Inhibitor of caspase-activated DNase
ICAM	Intracellular adhesion molecule
IFN	Interferon
IFNAR	Interferon α/β receptor
Ig	Immunoglobulin
IL	Interleukin
ILK	Integrin-linked kinase
IP3	Inositol 1,4,5-trisphosphate
ITAM	Immunoreceptor tyrosine-based activation motif
LAT	Linker for activation of T cells
LRP1	Low density lipoprotein receptor-related protein 1
LXR	Liver X receptor
MAPK	Mitogen-activated protein kinase
MERTK	Mer receptor tyrosine kinase
MFG-E8	Milk factor globule EGF factor 8
MHC	Major histocompatibility complex
NF-κB	Nuclear factor kappa-light-chain-enhancer of activated B cells
PAA	Polyacrylamide
PAMP	Pathogen-associated molecular pattern
PBS	Phosphate-buffered saline
PI3K	Phosphoinositide 3 kinase
PI(3)P	Phosphatidylinositol-3-phosphate

PI(3,4)P₂	Phosphatidylinositol-3,4-bisphosphate
PI(4,5)P₂	Phosphatidylinositol-4,5-bisphosphate
PIP₃	Phosphatidylinositol-3,4,5-trisphosphate
PKC	Protein kinase C
PLCγ	Phospholipase C gamma
PMA	Phorbol 12-myristate 13-acetate
ProS	Protein S
PRR	Pattern recognition receptor
PtdCho	Phosphatidylcholine
PtdEth	Phosphatidylethanolamine
PtdSer	Phosphatidylserine
Rac1	Ras-related C3 botulinum toxin substrate 1
RAGE	Receptor for advanced glycation end products
Rap1	Ras-related protein Rap1
RCS	Royal College of Surgeons rat
RGD	Arg-Gly-Asp
RIAM	Rap1-GTP-interacting adaptor molecule
RPE	Retinal pigment epithelial cell
RPMI	Roswell Park Memorial Institute medium
RTK	Receptor tyrosine kinase
SCARF1	Scavenger receptor class F member 1
SFK	Src-family kinase
SH2	Src-homology 2 domain
SHBG	Sex hormone binding globulin
SHP-1/2	Src homology region 2 domain-containing phosphatase-1 and -2

SHIP1	Src homology 2 (SH2) domain containing inositol polyphosphate 5-phosphatase 1
SIGLEC10	Sialic acid-binding Ig-like lectin 10
SIRPα	Signal regulatory protein α
SLE	Systemic lupus erythematosus
sMER	Soluble MERTK
SOCS	Suppressor of cytokine signaling
SPM	Specialized pro-resolving mediator
SPT	Single particle tracking
SRRF	Super resolution radial fluctuations
STED	Stimulated emission depletion microscopy
SYK	Spleen tyrosine kinase
TAM	Tyro3/Axl/MERTK
TEMED	Tetramethylethylenediamine
TFM	Traction force microscopy
TGF-β	Transforming growth factor β
TIM	T-cell immunoglobulin and mucin domain 1
TLR	Toll-like receptor
TNF-α	Tumor necrosis factor
TRAIL	TNF-related apoptosis-inducing ligand
WASP	Wiskott–Aldrich Syndrome protein

Chapter 1 - Introduction

1.1 Phagocytosis and efferocytosis

Phagocytosis is the process by which eukaryotic cells ingest large particles ($\geq$ 0.5 µm) such as bacteria and fungi[1]. After its discovery in the mid-late 1800s, phagocytosis is now widely recognized to be essential for homeostasis in all mammalian organs[2–4]. The immune system is adept at phagocytosis, where defensive immune cells such as macrophages, dendritic cells (DCs), and neutrophils protect healthy tissues by engulfing foreign material. These are collectively referred to as professional phagocytes, owing to their robust capacity to perform phagocytosis.

Foreign pathogens are recognized by a variety of phagocytic receptors expressed by professional phagocytes. Foremost, pattern recognition receptors (PRRs) are specific for various pathogen-associated molecular patterns (PAMPs) on the surface of the pathogen. For example, Dectin-1 binds to β-glucans on the surface of fungi, whereas the scavenger receptor MARCO recognizes cell-wall constituents on bacteria[1]. Other receptors indirectly bind their targets via opsonins that are deposited on the surface of the pathogen. These include complement receptors and Fc gamma receptors (FcγRs), which bind to complement proteins or IgG immunoglobulins, respectively. Phagocytic receptors collectively bind to their prey and signal to induce the remodeling of the actin cytoskeleton (Figure 1.1). This causes the plasma membrane to enwrap the pathogen in a structure called the phagocytic cup. Actin polymerization at the advancing edges of the cup causes the membrane to progress over the surface of the target. The membrane eventually fuses at the distal ends to form the intracellular vacuole termed the phagosome[1].

Phagocytosis leads to the removal of the pathogen and is followed by an immune response. First, the phagosome fuses with endosomes and lysosomes, which forms an acidic environment filled with degradative enzymes that destroy the internalized pathogen[5]. Furthermore, professional phagocytes will initiate a pro-inflammatory response via the release of chemokines such as CXCL8, and cytokines such as interleukin
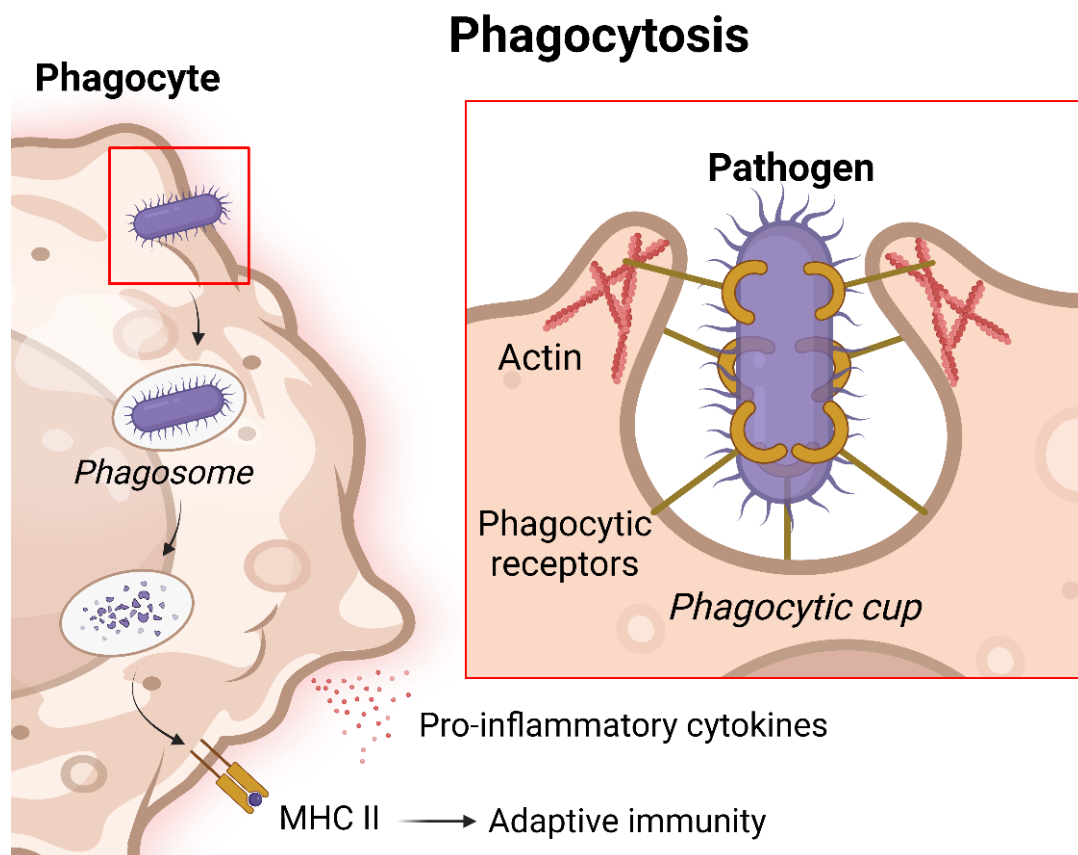
Figure 1.1: Overview of phagocytosis. Pathogens are recognized by phagocytic receptors, which induce remodeling of the actin cytoskeleton to form the phagocytic cup. The target is internalized into the phagosome, followed by its destruction by degradative enzymes. The phagocyte launches a pro-inflammatory immune response and loads pathogen-derived peptides onto MHC-II to activate the adaptive arm of the immune system. Figure produced with BioRender.

(IL)-1β, Tumor necrosis factor-alpha (TNF-α), and IL-12, which recruit and activate other immune cells to promote clearance of the infection[6,7]. Finally, DCs can load pathogen-derived peptides onto major histocompatibility complex class II (MHC-II), which activates antigen-specific CD4+ T cells[8,9]. These CD4+ T cells can differentiate into effector cells that release pro-inflammatory cytokines at the site of infection to license other immune cells to eliminate the pathogen[10]. Moreover, antigen-educated CD4+ follicular helper T cells interact with B lymphocytes in the lymph nodes, a process required for the production of pathogen-specific antibodies[11]. Finally, DCs can phagocytose and cross-present antigens onto MHC-I, which instructs CD8+ T cells to launch a precision attack against pathogen-infected cells[12]. In summary, professional phagocytes act as the first line of defense against infection and are an essential component of cellular immunity.

Efferocytosis is a subset of phagocytosis that involves the engulfment of apoptotic cells (ACs) (Figure 1.2). Apoptosis is a form of programmed cell death that occurs when host cells become old, damaged, or no longer needed. Over 100 billion cells within the human body undergo apoptosis on a daily basis and are cleared by phagocytes, herein termed as "efferocytes" in the context of efferocytosis[13]. Of the professional phagocytes, macrophages reign supreme in their ability to perform efferocytosis. Furthermore, non-professional phagocytes, which are comprised of specialized epithelial cells, can also act as efferocytes. Combined, efferocytes rapidly engulf ACs before their progression to secondary necrosis, a lytic form of cell death that leads to the uncontrolled release of danger-associated molecular patterns (DAMPs) and intracellular autoantigens[14,15]. DAMPs such as High mobility group box 1 (HMGB1), IL-1α, and heat shock proteins lead to an inflammatory response that promotes tissue injury and leukocyte infiltration[14]. Moreover, prolonged exposure of intracellular autoantigens such as DNA can lead to activation of self-reactive T- and B-lymphocytes. Therefore, ACs can be considered as "ticking time bombs" that must be rapidly cleared by efferocytosis.

In contrast to the engulfment of pathogens, efferocytosis induces an anti-inflammatory response. For instance, macrophages release cytokines such as Transforming growth factor Beta (TGF-β) and IL-10 during efferocytosis, which inhibits other immune cells
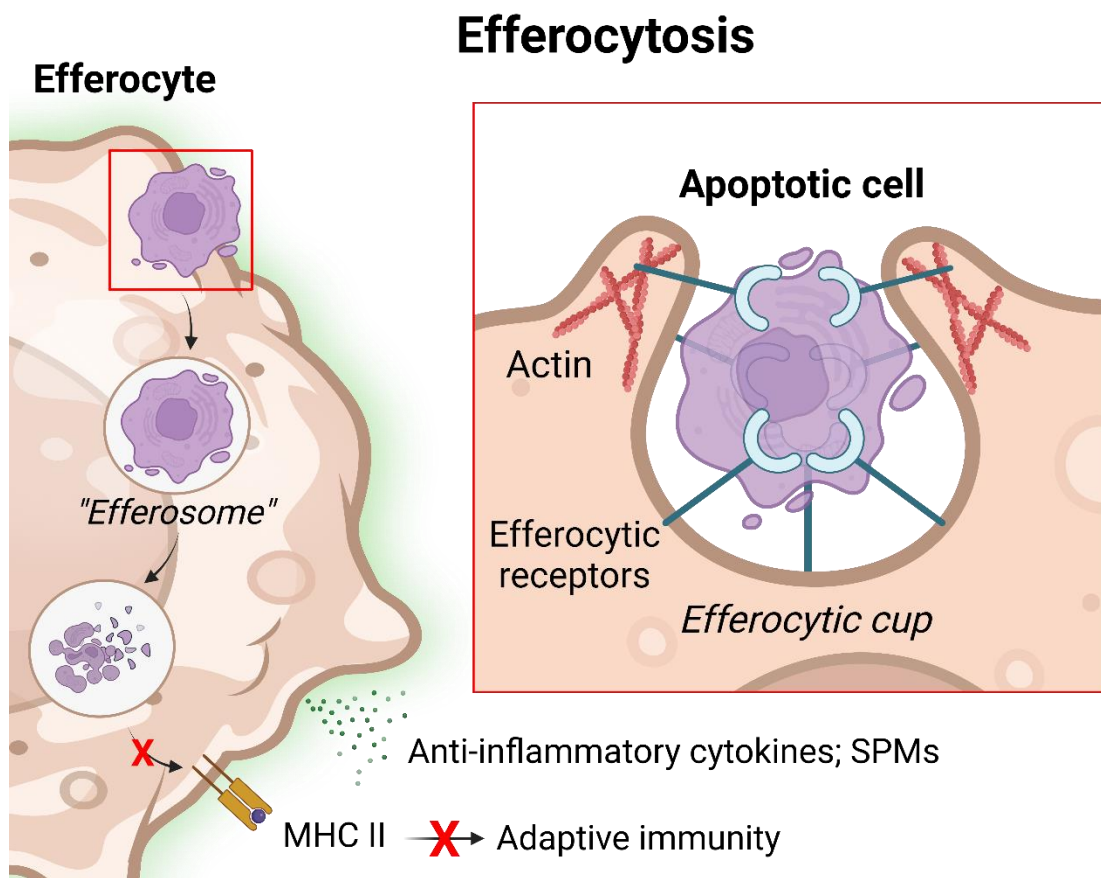
Figure 1.4: Overview of efferocytosis. Apoptotic cells are recognized by a group of phagocytic receptors collectively termed the efferocytic receptors, which induce remodeling of the actin cytoskeleton to form the efferocytic cup. The cell is internalized into the efferosome, followed by its destruction by degradative enzymes. The efferocyte responds by releasing anti-inflammatory cytokines and SPMs that promote tissue repair. Antigen loading onto MHC-II is circumvented to prevent the activation of autoreactive T cells. Figure produced with BioRender.

and promotes tissue repair[16,17]. Simultaneously, the expression of pro-inflammatory cytokines TNF-α and IL-12 are suppressed after the engulfment of ACs[18–20]. In macrophages, lipids derived from ACs promote the activity of 12/15-lipoxygenase and 5-lipoxygenase, which act to synthesize lipid molecules called specialized pro-resolving mediators (SPMs)[21,22]. SPMs such as lipoxin A4 and resolvin D1 are secreted in the local tissue, which further enhances efferocytic activity and anti-inflammatory signaling by other macrophages[23–25]. Finally, efferocytes recruit the vesicle trafficking regulator Rab17 to the apoptotic cell-containing phagosome (also called the "efferosome"), which prevents their fusion with MHC-II-containing vesicles[26]. This circumvents the loading of self-derived antigens onto MHC-II, thereby preventing the activation of autoreactive CD4$^+$ T cells[26]. The basis for the differential immune response between the phagocytosis of pathogens and the efferocytosis of ACs is not fully understood, but likely involves the combined activity of cell-surface- and phagosomal-receptors that sample the internalized cargo.

Efferocytes have the incredible responsibility of clearing hundreds of quintillions of cells over an individual's lifetime, with defects in this process leading to devastating pathological consequences. This comprises the foundation for many inflammatory- and autoimmune-mediated conditions including atherosclerosis, systemic lupus erythematosus (SLE), multiple sclerosis, and rheumatoid arthritis[15]. These diseases affect hundreds of millions of patients and pose a considerable threat to healthcare systems across the globe. Effective treatments for these pathologies are contingent on understanding the mechanism for AC-engulfment and subsequent anti-inflammatory signaling. Currently, the signaling pathways that carry out efferocytosis are not fully understood, but are being investigated for their therapeutic targetability against diseases where efferocytosis is defective.

1.1.1   Apoptotic cells signal for their clearance by efferocytosis

Apoptosis involves a series of regulated pathways to ensure the clearance of ACs by efferocytes. First, apoptosis is triggered by intrinsic stressors or by extracellular death factors. In the intrinsic pathway, signals such as DNA damage, hypoxia, or withdrawal of survival factors induces the oligomerization of pro-apoptotic proteins BAX and BAK on

the outer mitochondrial membrane[27]. BAX:BAK oligomers form pores in the mitochondria that causes the release of cytochrome C into the cytoplasm[14,27]. Cytochrome C forms a heptameric complex with Apoptotic protease activating factor 1 (APAF1), which activates caspase-9[27]. Finally, caspase-9 cleaves the executioner caspases -3 and -7 into their activated forms[28]. In the extrinsic cell death pathway, extracellular death signals such as FasL, TNF-related apoptosis-inducing ligand (TRAIL), and TNF induce their receptors to oligomerize at the plasma membrane[14]. These receptors form a complex with FAS associated death domain protein (FADD) and procaspase-8, which causes procaspase-8 to autoactivate[29]. Finally, caspase-8 can cleave and activate caspases -3 and -7, and also directly induces cytochrome C release via the cleavage of Bid, which translocates to the mitochondria to promote BAX:BAK oligomerization[30].

The executioner caspases-3 and -7 can cleave thousands of different proteins to initiate cell death. For example, the executioner caspases cleave and activate the actin-severing protein gelsolin, as well as the myosin contractility regulator Rho-associated protein kinase (ROCK)[31,32], with these effectors causing actin-disassembly and membrane blebbing. Furthermore, the Inhibitor of caspase-activated DNase (ICAD) is cleaved by caspase-3 to cause its dissociation from caspase-activated DNase (CAD), where CAD then mediates DNA fragmentation and chromatin condensation[33]. Caspase effectors further act to disassemble additional organelles such as the Golgi apparatus and endoplasmic reticulum[34,35]. The cellular debris is packaged into apoptotic blebs that are eaten directly by efferocytes, or shed into the milieu as apoptotic bodies that are engulfed individually[24]. The combined activity of caspase effectors results in a shift in cellular physiology and morphology that are characteristic of ACs, which are cleared in an immunologically silent manner. However, prolonged caspase activity results in the progressive loss of membrane integrity, eventually leading to secondary necrosis[36]. Therefore, it is imperative that ACs signal to efferocytes to mediate their own clearance from the tissue.

ACs must undergo a rapid change in molecular signature to allow efferocytes to discriminate them from healthy cells. Foremost, ACs actively generate a chemotactic gradient in a caspase-dependent manner, which promotes the recruitment of efferocytes

into regions of cell death. These so called "find-me" signals, such as lysophosphatidylcholine, sphingosine-1-phosphate, CX3CL1, adenosine triphosphate, and uridine triphosphate, act on chemotactic receptors on efferocytes to induce migration towards dying cells[37]. Recent evidence also suggests that ACs can shed apoptotic bodies that are bound by chemokines such as CCL12, CCL21, and CXCL10, which induces robust macrophage chemotaxis *in vitro*[38].

ACs express "eat-me" signals that bind to AC-recognizing phagocytic receptors, herein termed efferocytic receptors. While several "eat-me" signals have been described, phosphatidylserine (PtdSer) is the most abundant "eat-me" signal and is the most extensively characterized[39]. PtdSer is a phospholipid that is normally restricted to the inner leaflet of the plasma membrane by the flippases ATP11A and ATP11C[40,41]. These flippases are cleaved and inactivated by the executioner caspases during apoptosis[40,41]. In parallel, caspase-3 activates the scramblase XKR8, which translocates PtdSer to the outer leaflet of the plasma membrane[42]. The exposure of "eat-me" signals is concomitantly matched by a decrease in "don't eat-me" signals that are normally expressed by healthy cells to prevent their engulfment. "Don't eat-me" signals such as CD47 and CD24 are ligands for the inhibitory receptors Signal regulatory protein α (SIRPα) and Sialic acid-binding Ig-like lectin 10 (SIGLEC10) respectively, expressed by efferocytes[43–45]. Upon their activation, SIRPα and SIGLEC10 recruit phosphatases such as Src homology region 2 domain-containing phosphatase-1 and -2 (SHP-1/SHP-2) and Src homology 2 domain containing inositol polyphosphate 5-phosphatase 1 (SHIP1), which induces a dephosphorylation cascade that inhibits efferocytic receptor signaling[44,45]. How cells downregulate "don't eat-me" signals upon apoptosis are not well understood. Nevertheless, the surface expression of "eat-me" and "don't eat-me" signals is intricately balanced during apoptosis to promote the clearance of the cell via efferocytosis.

Macrophages express an array of efferocytic receptors including Stabilin-2, CD300b, Scavenger receptor class F member 1 (SCARF1), T-cell immunoglobulin and mucin domain 1 (TIM)-1, TIM-4, Brain-specific angiogenesis inhibitor 1 (BAI1), Receptor for advanced glycation end products (RAGE), MERTK, $\alpha_v\beta_3$ integrin, $\alpha_v\beta_5$ integrin, and others, which all recognize PtdSer to mediate the engulfment of the dying cell[14,15]. Other

"eat-me" signals, including differentially glycosylated intracellular adhesion molecules (ICAMs)[46], calreticulin[47], and oxidized phospholipids[48], are recognized by other cognate receptors on efferocytes. For example, our lab discovered that soluble CD93 (sCD93) opsonizes ACs to promote their engulfment by $\alpha_X\beta_2$ integrins expressed by macrophages[49]. The discovery of other efferocytic receptors is still an active area of investigation in the field. Collectively, these receptors converge on a cytoskeletal remodeling pathway to form a cup-like structure that enwraps the apoptotic cell, herein termed the "efferocytic cup".

It is a mystery as to why efferocytes express so many receptors that seemingly perform the same function; with nearly half of all known efferocytic receptors recognizing PtdSer. Complicating this, the signaling pathway for each efferocytic receptor is not resolved, and the contribution of each of these receptors to engulfment is unclear. For example, some efferocytic receptors may act to merely tether ACs into place, while other receptors may play a direct role in actin polymerization to form the efferocytic cup. The development of specific therapies to treat inflammatory- and autoimmune-disease relies on our understanding of how different efferocytic receptors cooperate to engulf ACs. To identify the differential roles of these receptors, the biomechanics of engulfment must be investigated at the cellular level.

1.2 Biomechanics of phagocytosis and efferocytosis

The remodeling of the actin cytoskeleton is foundational to the biomechanics of all types of phagocytosis, including efferocytosis. At steady-state, monomeric globular actin (G-actin) is readily assembled into filamentous actin (F-actin), which are elongated microfilaments that form a cortical meshwork underlying the plasma membrane[50]. The meshwork is physically crosslinked with the membrane via the ezrin/radixin/moesin (ERM)-family proteins[51], which link F-actin to phosphatidylinositol-4,5-bisphosphate (PI(4,5)P$_2$) and with transmembrane proteins such as CD44[52,53]. F-actin is also tethered to integrins via adaptor proteins such as talin and vinculin[54]. Together, this meshwork is aptly referred to as the actin cytoskeleton, which supports the shape and integrity of the cell.

The cytoskeleton is a dynamic structure that can be rapidly remodeled to induce changes in cellular morphology. During phagocytosis, actin polymerization occurs at the leading edges of the phagocytic cup, which causes the membrane to extend over the surface of the target[55]. Polymerization is initiated by the Rho GTPases Rac1 and Cdc42, which activate nucleation promoting factors of the Wiskott–Aldrich Syndrome protein (WASP) family – WASP/N-WASP and SCAR/WAVE[56,57]. Upon their activation, these factors stimulate the Actin-related protein 2/3 (ARP2/3) complex, which nucleates new F-actin filaments in a branching pattern[58,59]. This forms an actin-enriched outer-ring that surrounds the surface of the particle, which gradually pushes the advancing edges of the phagocytic cup around the target[60]. Simultaneously, F-actin is disassembled at the base of the phagocytic cup by actin-severing proteins including cofilin and gelsolin[55]. Actin disassembly is required to remove the dense meshwork of actin that would otherwise prevent the internalization of the particle. Phagocytic cup progression is also mediated by force-transducing F-actin bundles linked by non-muscle myosin II. Myosin II acts to contract the actin ring at the leading edge of the cup via a purse-string-like mechanism[60–62]. Finally, when the phagocytic cup reaches the end of the target, these contractile forces act to close off the membrane to form the phagosome[60]. Although not explicitly demonstrated, it is assumed that efferocytosis relies on the same series of actin reorganization events to engulf ACs.

Phagocytic and efferocytic receptors bind to their target and coordinate a signaling cascade that remodels the actin cytoskeleton. Although phagocytic receptors such as $Fc\gamma R$ and $\alpha_M\beta_2$ integrin have been extensively studied, the role of efferocytic receptors during actin remodeling are less understood. We believe that some efferocytic receptors do not possess intrinsic actin polymerization capability; but mediate engulfment through indirect means – herein referred to as "stimulating receptors". In contrast, other efferocytic receptors that directly drive the polymerization of actin will be referred to as "engulfment receptors". Stimulating receptors bind to ACs, then signal to amplify the activity of the engulfment receptors. For example, TIM-4 is a stimulating receptor that can activate members of the β_1- and β_3-integrin families, with the integrins acting as engulfment receptors that direct the internalization of the apoptotic cell[63,64]. Other members, such as the essential efferocytic receptor MERTK, are yet to be fully

characterized. Thus, there is a need for further biomechanical characterization of efferocytic receptors. This can be accomplished by investigating: 1) the downstream signaling pathways of the receptor, 2) the organization of the synapse between efferocytes and ACs, 3) the kinetics of receptor diffusion during efferocytosis, and 4) the contribution of the receptor towards force transduction.

1.2.1   Cytoskeletal remodeling is induced by receptor signaling

The signaling pathways of conventional phagocytic receptors are better understood compared to efferocytic receptors. Phagocytic receptors usually activate Rho GTPases such as Rac1 and Cdc42 to drive actin polymerization. Many phagocytic receptors such as Dectin-1 and FcγRIIA/C possess a cytoplasmic immunoreceptor tyrosine-based activation motif (ITAM)[1,65,66]. Others such as Dectin-2, FcγRI, and FcγRIIIA form a complex with the ITAM-containing FcR common gamma chain[66]. ITAMs act as signaling hubs that are tyrosine-phosphorylated by Src-family kinases (SFKs) upon receptor stimulation[1]. This post-translational modification promotes the recruitment and activation of Spleen tyrosine kinase (SYK), where SYK can recruit transmembrane scaffolding proteins such as the Linker for activation of T cells (LAT)[1,67]. This forms a platform that recruits members of the Rac1-activation machinery such as CrkII, an adaptor protein for Dedicator of cytokinesis 1 (DOCK180)[1,68]. DOCK180 heterodimerizes with Engulfment and cell motility protein (ELMO), forming a complex that acts as a guanine exchange factor that activates Rac1 GTPase[69]. SYK can also activate the adaptor protein Nck to induce Cdc42-mediated actin polymerization[70].

The integrins $\alpha_M\beta_2$ and $\alpha_X\beta_2$ mediate complement-dependent phagocytosis but do not contain ITAM motifs. However, $\alpha_M\beta_2$ can associate with the ITAM-containing FcR common gamma chain to signal through SYK, which appears to represent the predominant complement-dependent phagocytosis pathway[71]. Otherwise, integrins recruit SFKs and focal adhesion kinase (FAK), where FAK recruits the p130[CAS] adaptor protein[72]. This forms a scaffold for the CrkII:DOCK180:ELMO complex, promoting local Rac1 activation and actin polymerization[73,74]. FAK and Integrin linked kinase (ILK)further act to recruit adaptor proteins such as talin and vinculin to strengthen the integrin:actin linkage.[75]Integrins can also recruit other guanine exchange factors

including Vav, an activator of the GTPase RhoA[76,77]. RhoA is thought to promote the depolymerization of actin[78], but this view is controversial. RhoA appears to be essential for integrin-mediated phagocytosis via downstream activation of ROCK and myosin II, which has been shown to promote membrane progression at the leading edge of the phagocytic cup in an ARP2/3-independent manner[79–82]. FcγRs and complement receptors are known to cooperate with each other during phagocytosis, as Fc-mediated phagocytosis is delayed upon knockdown of $\alpha_M\beta_2$ integrins, even in the absence of complement deposition[71]. Thus, several phagocytic receptors likely signal in concert to form the phagocytic cup, and their coordination improves phagocytic efficiency (Figure 1.3).

Lipid signaling within the phagocytic cup is also crucial for its progression. Many phagocytic receptors are activators of Class I Phosphoinositide 3 kinase (PI3K), which phosphorylates $PI(4,5)P_2$ to phosphatidylinositol-3,4,5-trisphosphate (PIP_3). PI3K activity is essential for the phagocytosis of large targets (>0.5 μm)[83]. PIP_3 is concentrated to the actin-depleted base of the phagocytic cup, where it can deactivate Cdc42 and activate actin-severing proteins to promote actin disassembly[84]. PIP_3 is also an activator of RhoA, which may further promote local disassembly of the cytoskeletal network[78]. In contrast, phosphatidylinositol-3,4-bisphosphate ($PI(3,4)P_2$) and $PI(4,5)P_2$ are localized at the F-actin enriched advancing edges of the phagocytic cup[85]. Although $PI(4,5)P_2$ is constitutively present on the membrane, $PI(3,4)P_2$ is generated when PIP_3 is dephosphorylated by phosphoinositide 5-phosphatases at the advancing edge of the phagocytic cup[85]. $PI(3,4)P_2$ and $PI(4,5)P_2$ recruit actin-polymerization effectors such as lamellipodin, which amplifies WASP/N-WASP and SCAR/WAVE activity[85]. Thus, PIP_3 is likely generated by a subset of receptors that are found in the actin-depleted base of the phagocytic cup. Other receptors that play a direct role in actin polymerization are likely found at the advancing edges of the cup, where $PI(4,5)P_2$ and $PI(3,4)P_2$ are enriched.

The signaling pathways of most efferocytic receptors vary significantly from each other and are poorly understood. For example, the PtdSer receptor BAI1 directly recruits the DOCK180:ELMO complex to activate Rac1[86]. CD300b binds to PtdSer, then interacts with the ITAM-containing adaptor protein DAP12, likely leading to conventional
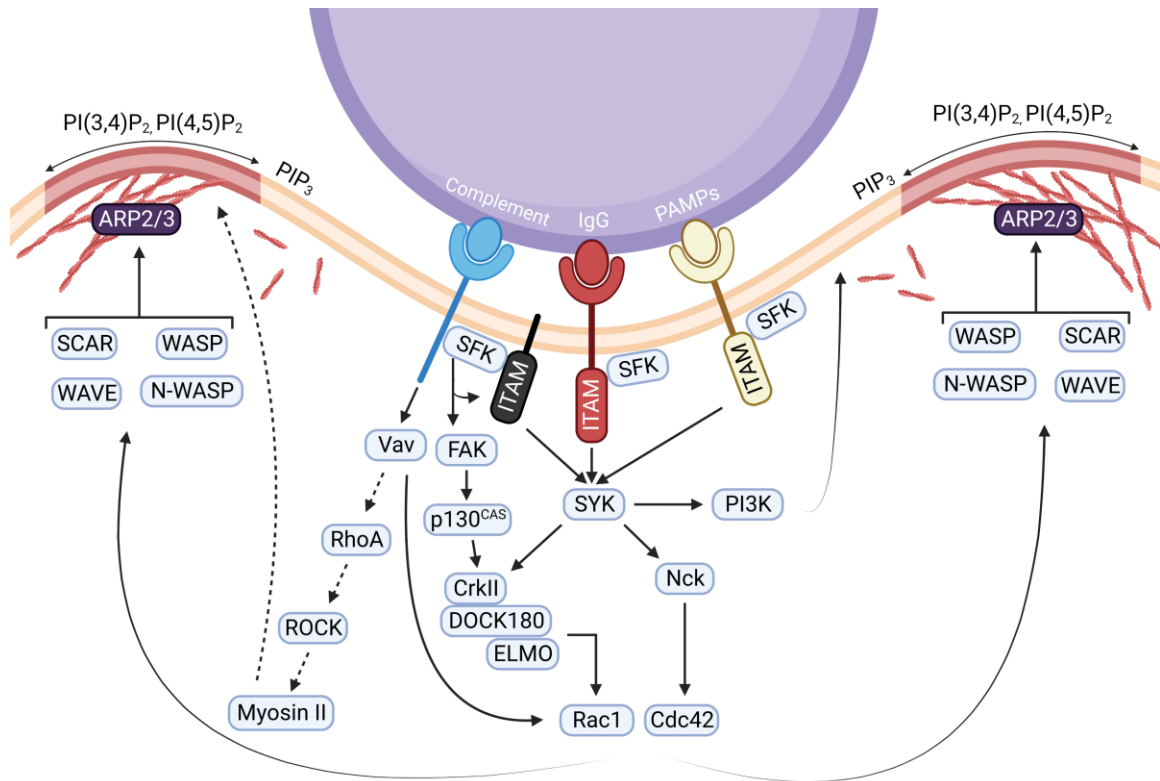
Figure 1.3: Conventional phagocytic receptor signaling. Phagocytic receptors including complement receptors, FcγRs, and PRRs either signal via intrinsic ITAM motifs or by interaction with ITAM-containing adaptor proteins. This promotes the SYK-dependent activation of Rac1 and Cdc42, which coordinates with WASP-family proteins to activate ARP2/3-mediated branched actin polymerization. Integrin complement receptors can also directly signal through Vav or FAK to also activate Rac1. Vav also activates RhoA to drive Myosin II activity. PI3K activity promotes PIP_3 generation at the base of the phagocytic cup, whereas $PI(4,5)P_2$ and $PI(3,4)P_2$ are localized at the leading edge of the phagocytic cup. Dashed arrows represent ARP2/3-independent pathways. Figure produced with BioRender.

phagocytic signaling (Figure 1.3)[87]. The calreticulin receptor Low density lipoprotein receptor-related protein 1 (LRP1), and the PtdSer receptor Stabilin-2 are both known to activate GULP PTB Domain Containing Engulfment Adaptor 1 (GULP), an activator of Rac1, but this mechanism is unresolved[88,89]. The PtdSer receptor TIM-1 contains a cytoplasmic tail with a tyrosine phosphorylation motif, but how it mediates engulfment is unexplored[90]. Its paralog, TIM-4, does not require its cytoplasmic tail to promote efferocytosis[91]. Rather, TIM-4 acts as a coreceptor for β_1 and β_3 integrins, with the latter recruiting the actin-polymerization machinery required for engulfment[63,64]. The integrins $\alpha_V\beta_3$ and $\alpha_V\beta_5$ are receptors for Milk factor globule EGF factor 8 (MFG-E8), an opsonin for PtdSer on ACs[74,92]. These integrins signal through the classical pathway involving SFKs and FAK, which recruits the CrkII:DOCK180:ELMO signaling complex to activate Rac1[73,74]. The integrin $\alpha_X\beta_2$ is a complement receptor, but we have also found that it promotes the engulfment of ACs opsonized by sCD93[49]; likely through the conventional phagocytic pathway (Figure 1.3). Finally, MERTK is an opsonic receptor for PtdSer bridged by Growth arrest-specific protein 6 (Gas6) or Protein S (ProS)[93]. MERTK possesses a tyrosine kinase domain that stimulates SFKs and PI3K[94], with some evidence suggesting this cascade can activate the $\alpha_V\beta_3$ and $\alpha_V\beta_5$ integrins[73,95]. However, whether MERTK is a stimulating receptor or engulfment receptor is unclear.

Identifying downstream signaling pathways of efferocytic receptors will provide insight into its biomechanical contribution during engulfment. Efferocytic receptors that directly recruit actin polymerization machinery are likely engulfment receptors. Stimulating receptors may mediate adhesion to the apoptotic cell and modulate the activity of engulfment receptors. Thus, stimulating receptors only induce actin polymerization by proxy. As this mechanism is unresolved, further work is required to elucidate the intermolecular crosstalk between efferocytic receptors during engulfment.

1.2.2   The structure of the phagocytic and efferocytic synapse

Phagocytes must form a structured synapse with their prey, which coordinates the signaling cascade required to form the phagocytic cup. To investigate the structure of the synapse, frustrated phagocytosis experiments are commonly employed, where fluorescently labeled macrophages are sedimented onto an opsonized glass coverslip. The

macrophages will attempt to "engulf" the planar substrate, forming a two-dimensional phagocytic synapse that is imaged by fluorescence microscopy. There are two types of frustrated phagocytosis experiments, where 1) the entire coverslip is opsonized in a monolayer of the ligand, or 2) the ligand is micropatterned onto the coverslip in discrete clusters. In the former, the entire phagocyte spreads to form the phagocytic synapse, whereas in the latter, the cell forms individual synapses localized at each cluster. Frustrated phagocytosis experiments are used to visualize receptor distribution, actin remodeling, and the overall macroscopic structure of the phagocytic synapse.

Frustrated phagocytosis occurs in two phases (Figure 1.4). In the spreading phase, branched actin polymerization occurs at the periphery to drive the radial expansion of the synapse[96]. Some phagocytic receptors such as $\alpha_M\beta_2$ colocalize with actin, suggesting they actively induce cytoskeletal remodeling to drive membrane spreading[82,97]. Then, the contraction phase begins when the synapse has spread to its maximal size, where F-actin is bundled into parallel fibers that run along the edges of the synapse[96]. This actin-enriched "outer-ring" transduces contractile forces during late-stage phagocytosis[60,96]. This ring encapsulates the actin-depleted centre of the synapse, indicative of cytoskeletal disassembly observed at the base of phagocytic cups[55,60].

Frustrated phagocytosis experiments have revealed there are intrinsic obstacles to phagocytic receptor signaling that must be overcome during synapse formation. First, a layer of glycosylated lipids and proteins called the glycocalyx surrounds the surface of all mammalian cells. The glycocalyx is a bulky coating that inhibits receptor ligation via steric hindrance and electrostatic repulsion from phagocytic targets[98,99]. Moreover, the tyrosine-phosphatases CD45 and CD148 are a major component of the glycocalyx, which act to inhibit SFK-dependent phagocytic signaling[97]. To overcome this, integrins have been shown to form a ring-like structure alongside F-actin at the periphery of FcγR-generated frustrated phagocytic synapses[97]. This produces a tight apposition that encapsulates FcγRs within the centre of the synapse, but selectively excludes bulky glycoproteins such as CD45 from entry[97]. This phenomenon has also been observed in Dectin-1-generated phagocytic cups, suggesting this is a conserved feature of phagocytosis[100]. The integrin-actin ring has also been observed in the immunological
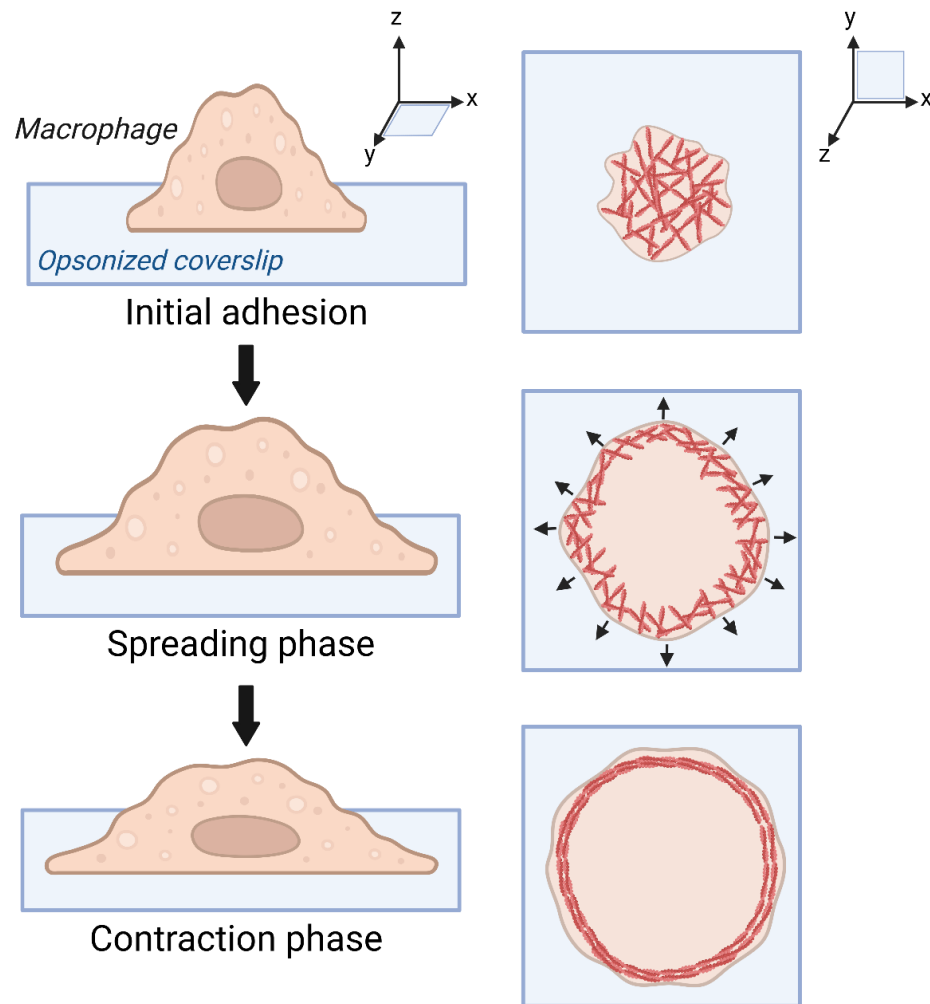
Figure 1.5: Overview of frustrated phagocytosis. Macrophages are sedimented on opsonized coverslips and the phagocytic synapse is visualized by fluorescence microscopy. The dense actin cytoskeleton during initial adhesion is rapidly restructured. In the spreading phase, branched actin polymerization occurs at the outer edges of the synapse to drive the radial expansion of the membrane. In the contraction phase, the membrane has expanded to its maximal size, and F-actin is rearranged into parallel bundles, priming the macrophage for myosin-mediated contraction. Figure produced with BioRender.

synapse between T cells and antigen presenting cells, which excludes sterically-hindering glycoproteins such as CD43[101]. CD43 and other constituents of the glycocalyx may be excluded from the phagocytic synapse in a similar manner, although this has yet to be confirmed during frustrated phagocytosis.

The synapse between a phagocyte and apoptotic cell is referred to as the efferocytic synapse. Although not fully understood, there is some speculation for the mechanisms that aid in the formation of this synapse. For example, ACs downregulate bulky glycosylated transmembrane proteins such as CD162 and CD43, which may improve access to PtdSer or other "eat-me" signals on the surface of the cell[102–104]. Furthermore, in macrophages, SIRPα is excluded from efferocytic cups surrounding PtdSer-coated silica beads, which enables enhanced integrin activation and engulfment efficiency[105]. This likely leads to the depletion of SHP-1/SHP-2 from the synapse, thereby permitting the progression of the efferocytic receptor-signaling cascade. However, whether integrins are responsible for SIRPα exclusion has not been determined. Little else is known about the structure of the efferocytic synapse and the signaling mechanisms that facilitate its generation. For example, the distribution of stimulating receptors and engulfment receptors within the synapse is yet to be explored. Thus, there is a pressing need for the development of "frustrated efferocytosis" assays, which will be crucial in determining the biomechanical role of specific receptors during the formation of the efferocytic cup.

To elucidate the structure of the efferocytic synapse, our lab[106] and others[105] have developed a frustrated efferocytosis assay in which a glass coverslip is coated with a supported lipid bilayer that mimics the surface of ACs (10-20% PtdSer). The surface can also be opsonized with serum, which contains a physiologically relevant concentration of opsonins that promote the binding of indirect PtdSer receptors such as MERTK or integrins. Our lab has observed the rapid spreading of human macrophages on AC-mimicking planar substrates, indicative of frustrated efferocytosis[106,107]. The dynamics of synapse formation, actin remodeling, and receptor localization during frustrated efferocytosis can be reliably visualized by fluorescence microscopy. These observations

will be used to make inferences on how stimulating and engulfment receptors coordinate the generation of the efferocytic cup.

1.2.3 Receptor diffusion shapes the efferocytic synapse

The standard view of the plasma membrane was established by Singer & Nicolson's fluid-mosaic model[108], which describes a semi-fluid bilayer comprised of phospholipids, sugars, cholesterol, and proteins. This provides a platform for lipids and transmembrane proteins to freely diffuse along the lateral plane of the membrane. During efferocytosis, efferocytic receptors on the surface of the efferocyte and the ligands on the surface of the apoptotic cell (e.g. PtdSer) are subject to lateral diffusion. Diffusion is known to affect receptor localization and overall synapse structure[109]. Furthermore, lateral diffusion is crucial for phenomena such as receptor oligomerization, which generates signaling platforms that enhance the recruitment of downstream effectors[109–111]. As our frustrated efferocytosis assay utilizes a supported lipid bilayer, the lateral diffusion of receptors upon their ligation to the substrate is permitted[112]. This prevents artificial receptor immobilization that would usually be observed when glass is directly opsonized, which may be more appropriate to model the phagocytosis of cell wall-expressing pathogens rather than ACs[97,109]. Thus, we expect that the structure of the efferocytic synapse and other diffusion-associated phenomena can be accurately modeled by our frustrated efferocytosis assay.

However, classical models of the plasma membrane do not account for other complexities that affect protein diffusion. Experimental observations have revealed that transmembrane protein diffusion is up to 50-fold slower than the Brownian diffusion expected in the fluid-mosaic model[113]. This was ameliorated by the now widely accepted "fences and pickets model" of the plasma membrane proposed by Akihiro Kusumi's group[114,115]. In this model, the membrane-proximal cytoskeletal meshwork act as "fences" that corral transmembrane proteins into distinct compartments within the membrane, usually less than 100 nm in diameter. This is caused by steric interactions between the cytoplasmic domain of the protein and F-actin. Compartmentalization is aided by actin-associated transmembrane proteins such as CD44, which extend through the membrane and serve as "pickets" that hinder the diffusion of other transmembrane

proteins and lipids via steric effects and hydrodynamic friction[113]. Together, these obstacles are responsible for the 50-fold diffusional slowing effect compared to predictions based on Brownian models such as the Singer-Nicolson model. The fences and pickets model also suggests that protein oligomerization causes a reduction in free diffusion due to increased steric interactions with components of the cytoskeleton[113].

The diffusive behaviour of a receptor may be reflective on its biomechanical role during engulfment. For instance, the engulfment receptors are likely highly immobilized due to their need to associate with the force-generating machinery of the actin cytoskeleton[114]. In contrast, stimulating receptors may not nucleate actin filaments directly, and thus are expected to be less constrained in their lateral diffusion[113]. Furthermore, receptors that are found within the actin-depleted centre of the efferocytic synapse are expected to become more freely diffusive as F-actin is continually disassembled as the synapse expands[116]. Oligomerization can also be inferred if a receptor becomes increasingly immobilized as the synapse matures, although this must be confirmed with other techniques such as super-resolution microscopy or step-wise photobleaching[117,118].

1.2.4   Force transduction during efferocytosis

The biomechanical role of an efferocytic receptor can be inferred by its contribution to force transduction during engulfment. Force transduction is a conserved feature across all types of phagocytosis; including FcγR-mediated phagocytosis[60,61,119], complement receptor-mediated phagocytosis[71], and efferocytosis[120]. This is driven by the interaction between myosin motor proteins and the actin cytoskeleton[62]. Myosin-family proteins play several roles during phagocytosis, with some members coordinating the structure of the phagocytic cup while others act to generate constrictive forces[60,119]. For instance, myosin 1e and myosin 1f are recruited to the leading edge of phagocytic cups to maintain receptor-actin adhesion sites by limiting uncontrolled F-actin polymerization, thereby enhancing phagocytic efficiency[61,119]. Contraction during phagocytosis is induced by a two-step mechanism. First, branched actin polymerization by ARP2/3 generates protrusive forces against the target. This forms a ring of branched F-actin that drives the leading edges of the phagocytic cup over the surface of the particle[60,96]. After most of the target has been enwrapped, myosin II arranges the ring of branched actin into parallel

fibers, forming a contractile belt[96]. Finally, myosin II enacts tension onto the belt to generate constrictive forces that are required for the final stages of cup progression and subsequent closure of the membrane[60,61,96,121].

We expect that stimulating and engulfment efferocytic receptors play differential roles in actin polymerization and thus force transduction. Stimulating receptors should not elicit the spreading of the efferocytic synapse due to their lack of intrinsic actin polymerization capability. Thus, the cytoskeletal structures required to generate contractile force should not be formed. In contrast, engulfment receptors should cause actin remodeling to transduce contractile forces onto the substrate. Furthermore, stimulating receptors may signal to amplify the activity of engulfment receptors by facilitating their activation and/or their recruitment of actin polymerization machinery[63,73], resulting in enhanced contractile force generation[82]. In summary, determining the biophysical role of stimulating and engulfment receptors can provide key insight into how they coordinate the engulfment of ACs. This will be crucial in understanding the mechanism of receptors such as MERTK, which despite their necessity for efferocytosis, remain poorly characterized during the engulfment process.

1.3   MERTK

MERTK is a member of the TYRO3/AXL/MERTK (TAM) family of receptor tyrosine kinases (RTKs)[122]. TAM receptors bind to Gas6 and/or ProS, which are soluble opsonins that bridge the receptor to PtdSer expressed by ACs[123]. Although all TAM family members bind to ACs to some capacity, MERTK is the most vital for efferocytosis. Defects in MERTK signaling or expression results in a severe drop in efferocytic efficiency, and contributes to multi-organ autoimmune and inflammatory disease[124–126]. In contrast, global deletions of TYRO3, AXL, or other PtdSer receptors causes less severe disease and are usually organ-specific[127–130]. In addition to engulfment, MERTK also induces an anti-inflammatory transcriptional program to promote tissue repair[21,131,132]. Thus, there is a substantial effort to interrogate MERTK for its therapeutic potential against diseases where efferocytosis is defective. However, the exact mechanism by which MERTK directs the engulfment of ACs is unclear.

1.3.1 MERTK structure

MERTK is a single-pass type I transmembrane protein comprised of 999 amino acids with a base molecular weight of 110 kDa[133] (Figure 1.5). The extracellular region of MERTK is heavily glycosylated for a final molecular weight of approximately 170-200 kDa[134], with N-glycosylation required for MERTK's stability[135]. Furthermore, MERTK possesses two immunoglobulin (Ig)-like repeats at its N-terminus, which is responsible for ligand binding[122,123]. This is followed by two type III fibronectin (FN3) repeats, then a membrane proximal region[122]. Proteases such as A disintegrin and metalloprotease 17 (ADAM17) can cleave MERTK at the membrane proximal region under inflammatory conditions to inhibit efferocytosis[136]. Further, MERTK possesses a helical single pass transmembrane domain[122]. The transmembrane domain facilitates self-oligomerization, causing MERTK to be expressed as distinct clusters on the membrane[137]. Our lab has shown that in human MERTK, positive selection occurred in the transmembrane domain to increase cluster size, which correlated with stronger avidity for Gas6-opsonized targets[137]. In the cytoplasmic region, MERTK consists of a tyrosine kinase domain and C-terminal tail, which are autophosphorylated at several tyrosine residues upon ligand binding[138]. This causes the recruitment of downstream signaling molecules that are required for the engulfment of ACs and subsequent anti-inflammatory signaling[21,131,139].

1.3.2 MERTK ligands

The most characterized ligands for MERTK are Gas6 and ProS. These were first discovered as serum proteins involved in the blood coagulation cascade[140], where Gas6 and ProS negatively and positively regulate coagulation, respectively[141,142]. It is now known that they also opsonize ACs to mediate their clearance from the tissue. Both of these proteins are structurally similar, and are characterized by an N-terminal gamma carboxyglutamic-acid rich (Gla) domain[143,144] (Figure 5). The Gla domain undergoes vitamin K-dependent gamma-carboxylation before its secretion by endothelial cells, osteoclasts, and hepatocytes into the blood[145–147]. This domain contains glutamic acid residues that bind to PtdSer on the surface of ACs in a Ca^{2+}-dependent manner[148]. Gas6 and ProS further contain four epidermal growth factor (EGF)-like repeats, which is required for protein stability[149,150]. Finally, the C-terminal sex hormone-binding globulin
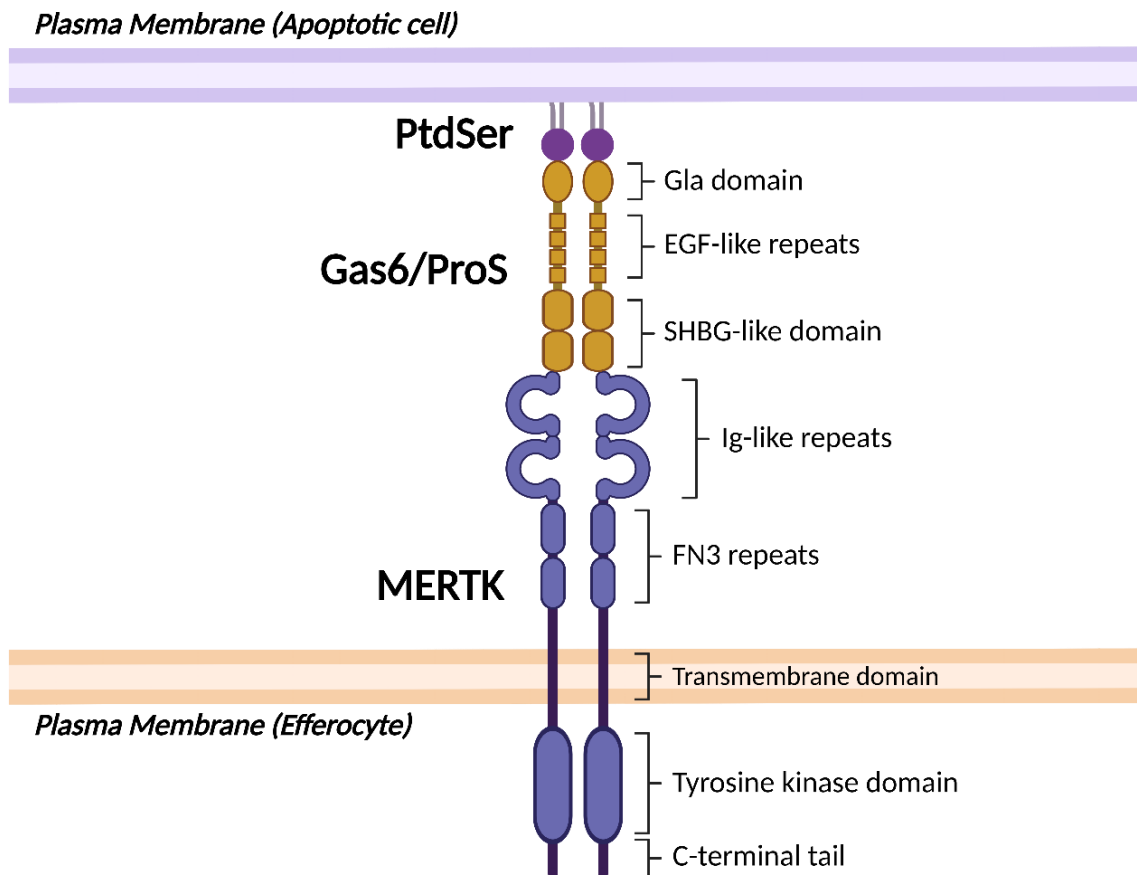
Figure 1.6: Structure of MERTK and binding to apoptotic cells opsonized by Gas6/ProS. MERTK functions as a dimer that binds to Gas6 or ProS, which opsonizes PtdSer exposed on the membrane of apoptotic cells. Gas6/ProS possess a Gla-domain that binds to PtdSer in a Ca^{2+}-dependent manner. This is followed by four EGF-like repeats and SHBG-like domain. The SHBG-like domain of Gas6/ProS binds to the N-terminal Ig-like domain of MERTK. MERTK contains two fibronectin type III repeats, and an alpha helical single pass transmembrane domain. Upon binding, the cytoplasmic tyrosine kinase domain and C-terminal tail are autophosphorylated at several tyrosine residues, leading to recruitment and activation of downstream signaling. Figure produced with BioRender.

(SHBG)-like domain binds to the Ig-like domain of MERTK[151]. Gas6 can activate MERTK in both its soluble and membrane-bound form[152]. In contrast, soluble ProS is insufficient for MERTK activation, with full activation contingent on its binding to ACs prior to ligation[152]. This may be due to its oxidation-induced oligomerization that occurs upon binding to PtdSer, which enhances ligation with MERTK[152]. Other ligands for MERTK include the proteins Tubby, Tubby-like protein 1, and Galectin-3[153,154]. These opsonins do not bind to PtdSer, but promote the efferocytosis of ACs by macrophages and MERTK-expressing epithelial cells[153,154]. The exact molecules on ACs that they bind to are not known, and their relevance to efferocytosis *in vivo* is yet to be fully explored.

1.3.3 MERTK expression

Unlike other efferocytic receptors, MERTK is expressed across a wide range of professional phagocytes. MERTK is expressed by nearly all tissue-specific macrophage subsets, including the Kupffer cells of the liver[155], cardiac macrophages[156,157], microglial cells of the nervous system[158,159], alveolar macrophages in the lungs[160], renal macrophages of the kidney[161], peritoneal macrophages[139,162], and intestinal macrophages[163]. Here, MERTK mediates the timely removal of ACs from healthy organs to prevent secondary necrosis. Furthermore, MERTK is expressed by classical DCs to promote immune tolerance against ACs, although this is an effect of MERTK's anti-inflammatory signaling cascade, rather than via direct engulfment[164]. The expression of MERTK by macrophages is dependent on the local tissue environment. Under tolerogenic conditions, endogenous TGF-β and IL-10 or exogenously administered corticosteroids can induce the polarization of macrophages into an M2c-like phenotype[165]. M2c macrophages express high levels of MERTK and are especially proficient at efferocytosis[165]. However, in inflammatory conditions, TNF-α or PAMPs such as lipopolysaccharide can polarize macrophages into an M1-like phenotype[165]. These macrophages are proficient at pathogen-targeted phagocytosis, but are characterized by lower levels of MERTK and are poor mediators of efferocytosis[165]. Furthermore, inflammation promotes the activity of ADAM17, which cleaves MERTK from the surface of macrophages to decrease efferocytosis[136,166].

The clearance of ACs from immunologically privileged sites is accomplished by non-professional phagocytes. These are specialized epithelial cells that express high levels of MERTK. In the eye, retinal pigment epithelial (RPE) cells are efferocytes that engulf dead photoreceptor outer segments to prevent their accumulation in the retina[125]. RPE cells critically rely on MERTK for efferocytosis, with defects in its expression or signaling causing congenital blindness[125,167,168]. The Sertoli cells of the testes and granulosa cells of the ovaries are specialized epithelial cells that rely on MERTK for engulfment of apoptotic germ cells[126,169,170]. MERTK-mediated efferocytosis is crucial for fertility in males whereas defects in females are associated with reduced fertility[126,170].

1.3.4   MERTK in autoimmunity and inflammatory disease

Over the last three decades, extensive research has revealed that defects in MERTK contribute to many autoimmune- and inflammatory- pathologies. In humans, certain genetic polymorphisms in *MERTK* are associated with pathologies such as atherosclerosis[171], retinitis pigmentosa[167,168], SLE[172,173], and multiple sclerosis[174]. In an effort to model these diseases, mice with global or conditional knockouts of *Mertk* are frequently used[132,175]. Furthermore, transgenic mice where MERTK's kinase activity is ablated[138,139], or mice transgenic for a cleavage-resistant form of MERTK[23,134,166] have also been employed. These studies have provided insight into diseases where efferocytosis is impaired and have demonstrated a key role of MERTK in maintaining homeostasis.

MERTK attenuates autoimmune responses by mediating the clearance of ACs before they can undergo secondary necrosis, thus preventing the release of DAMPs and intracellular autoantigens. Failure to clear ACs leads to chronic exposure to autoantigens within an inflammatory immune environment, promoting the activation of self-reactive lymphocytes. The most established link between defective efferocytosis and autoimmunity is SLE. A hallmark of SLE and other Lupus-like syndromes is the presence of anti-nuclear antibodies targeting DNA or other nuclear antigens[176]. This causes the formation of self-reactive immune complexes that promote inflammation-induced damage in the skin, joints, kidneys, and other organs[176]. A major driver of disease stems from the defective clearance of ACs. Indeed, progressive lupus-like disease is known to

develop in aged *Mertk* knockout (*Mertk*^{-/-}) mice and in mice that express a mutated form of MERTK without its kinase domain[124,177]. This is marked by elevated tissue necrosis and loss of immune tolerance, indicated by activation of self-reactive marginal zone B cells and generation of anti-DNA/anti-chromatin antibodies[124,177]. In humans, elevated levels of soluble MERTK (sMER) are correlated with more severe disease, suggesting that MERTK is cleaved under inflammatory conditions, further exacerbating the autoimmune response in SLE[172].

The link between defective efferocytosis and other autoimmune diseases are also well established, but mechanistically unresolved. For example, efferocytosis has been implicated in multiple sclerosis, an autoimmune disease characterized by progressive myelin degeneration and axonal damage in the central nervous system[159]. Microglia are the major efferocytes of the nervous system and are responsible for clearing myelin debris. In *Mertk*^{-/-} mice, myelin debris cannot be efficiently cleared, leading to Interferon (IFN)-γ-induced demyelination[178]. This corroborates with data from humans, where microglia from multiple sclerosis patients express lower levels of MERTK compared to healthy controls, and are thus impaired in their ability to clear myelin debris[179]. This likely exacerbates neuronal damage, but how this contributes to the activation of self-reactive lymphocytes is yet to be fully explored. Nevertheless, autoantibodies against intracellular self-antigens in some multiple sclerosis patients have been reported, suggesting a failure to clear dying cells to some degree[180]. In rheumatoid arthritis, an autoimmune disease that primarily affects the joints, elevated levels of cell death in the synovium and generation of self-reactive antibodies are well established phenomena[181]. Knockout of *Mertk* has been shown to increase levels of secondary necrosis in the joints of a collagen-induced mouse model of arthritis, which increased disease severity[182]. However, MERTK deletion was later reported to have no effect on autoantibody titres[183]. In humans, MERTK[+] synovial macrophages limit the immunopathology of rheumatoid arthritis, likely by enhanced efferocytosis and secretion of anti-inflammatory SPMs[184]. In summary, there is a rapidly emerging link between MERTK and autoimmune disease, but further work is required to uncover how MERTK can malfunction to promote the loss of immune tolerance.

Inflammation and cell death are critical for the progression of atherosclerosis – the buildup of fatty plaques beneath the arterial endothelium[185]. Here, intimal macrophages become overburdened by excess oxidized lipid accumulation and consequently lose their efferocytic activity[186]. These lipid-laden macrophages are commonly referred to as "foam cells" and become apoptotic[186]. As efferocytosis is compromised, a lipid-rich necrotic lesion is gradually formed, which eventually ruptures to cause cardiovascular diseases such as myocardial infarction and stroke[186]. MERTK-expressing intimal macrophages are critical in attenuating the progression of atherosclerosis. For instance, *Apoe*^{-/-} mice further expressing a kinase-dead MERTK mutant exhibit significantly elevated levels of plaque necrosis in a model of high fat diet-induced atherosclerosis[187]. Furthermore, under inflammatory conditions, MERTK is cleaved from the surface of intimal macrophages by ADAM17 to further compromise efferocytic activity[23,136,166]. Indeed, in human patients, increased sMER is correlated with increased plaque necrosis[166] and is also elevated after myocardial infarction[156]. Mice expressing a cleavage-resistant mutant of MERTK displayed increased efferocytic activity and smaller necrotic plaques in an low density lipoprotein receptor knockout model of atherosclerosis[23,166]. Cleavage resistance also played a protective role in a mouse model of myocardial ischemia reperfusion injury[156]. Thus, limiting the proteolysis of MERTK may be a promising therapeutic strategy to combat atherosclerosis.

MERTK's role during efferocytosis has been well studied in animal models of retinitis pigmentosa, a degenerative eye disease characterized by the progressive loss of photoreceptor cells[125,167]. The engulfment of photoreceptor outer segments by MERTK-expressing RPE cells is critical in preventing the accumulation of noxious debris, which contributes to cell death in the retina[125,188]. This was first discovered in The Royal College of Surgeons (RCS) rat, a model for retinitis pigmentosa that develops blindness after 60 days of age[125,188]. Genetic analysis revealed that RCS rats possess a frameshifted *Mertk* gene that terminates early during translation, thus preventing RPE-mediated efferocytosis[125]. This disease phenotype was later recapitulated in *Mertk* knockout mice[189]. Mutations in *MERTK* are known to cause retinitis pigmentosa in humans[167,168] and targeted therapies are in their early stages. For instance, a phase I clinical trial showed that eyesight could be partially restored in 3 out of 6 retinitis pigmentosa patients

with a subretinal injection of an adenoviral vector containing the *MERTK* gene[190]. These studies may establish the groundwork for personalized therapeutics against diseases where MERTK's activity is defective.

1.3.5   MERTK signaling

Although MERTK has been undeniably confirmed to be a key regulator of homeostasis *in vivo*, its signaling mechanism is considerably less understood. *In vitro* experiments have been crucial in discovering what is currently known about MERTK's signaling pathway. Like all RTKs, MERTK's kinase domain undergoes autophosphorylation upon ligand stimulation, thereby inducing its tyrosine kinase activity to modulate the activation of downstream effectors[138]. The kinase domain of MERTK was reported to interact with Src-homology 2 (SH2) domain-containing proteins including c-Src – a member of the SFK family, p85α – the regulatory subunit of Class I PI3K, Vav3 – an activator of RhoA, and Growth factor receptor-bound protein 2 (Grb2) – an initiator of the Mitogen-activated protein kinase (MAPK) pathway[94]. Although SFKs and PI3K are known to be required for phagocytosis (discussed in Chapter 1.2.1), less is known about the role of Vav3 and Grb2.

Vav3 is a guanine exchange factor that activates RhoA[191], a Rho GTPase that promotes actin disassembly[78]. Paradoxically, Vav3 also activates Rac1, the primary inducer of actin polymerization during phagocytosis[191]. Complicating this, MERTK has been shown to activate Vav1 and Vav2, which are also activators of both Rac1 and RhoA[192]. Finally, Vav proteins appear to dissociate from MERTK upon activation, suggesting their activity is not localized at the receptor itself[192]. Further work is required to determine the role of Vav1/2/3 during efferocytosis.

Grb2 is an activator of the MAPK pathway[193], which is usually associated with the induction of cellular survival, proliferation, and differentiation[194]. However, knockdown of *Grb2* was shown to decrease efferocytic efficiency in RPE cells, although the specific mechanism is yet to be discovered[94]. Grb2's role during engulfment may be indirect, as it is known to greatly increase the recruitment of Class I PI3K upon RTK stimulation[195]. In agreement with this indirect modality, inhibition of one of the final effectors of the

MAPK pathway – Extracellular signal regulated kinase (ERK) – does not affect the engulfment of apoptotic thymocytes by murine macrophages[196]. We have also observed that inhibition of p38 MAPK – another end-stage effector of the MAPK pathway – does not affect MERTK-mediated efferocytosis by human macrophages[197].

MERTK was also reported to be an activator of Phospholipase C gamma (PLCγ), an enzyme that cleaves $PI(4,5)P_2$ into diacylglycerol (DAG) and inositol 1,4,5-trisphosphate (IP_3)[198]. In macrophages, chemical inhibition of PLCγ2 prevented efferocytosis, but had no effect on tethering to ACs[198]. The role of PLCγ during efferocytosis is not fully resolved, but is believed to rely on the downstream activation of Protein kinase C (PKC). PKC is directly activated by DAG and cytosolic Ca^{2+} released from the endoplasmic reticulum by IP_3-sensitive ion channels[199]. Pan-inhibition of PKC in murine macrophages was previously reported to inhibit efferocytosis[196]. This was later discovered to be dependent on a single PKC isoform, PKCβII, which is believed to be recruited to nascent efferocytic cups in a MERTK dependent manner[200]. However, how PKC directs the structure and maturation of the efferocytic cup is not known.

The MERTK signaling pathway extends beyond just engulfment of ACs. Upon stimulation, MERTK induces a vast array of different downstream signaling processes. Firstly, MERTK induces an anti-inflammatory response that inhibits pro-inflammatory signaling cascades and promotes tissue repair. For instance, MERTK is an activator of Suppressor of cytokine signaling (SOCS)-1 and -3[131,201]. SOCS1/3 inhibits the downstream signaling pathways of toll-like receptors (TLRs) and Interferon α/β receptor (IFNAR), thus attenuating inflammation in response to PAMPs and Type I IFNs, respectively[131,202]. MERTK also upregulates the anti-inflammatory cytokines IL-10 and TGF-β through an unresolved pathway[16,17]. In addition, MERTK was reported to inhibit the activation of Nuclear factor kappa-light-chain-enhancer of activated B cells (NF-κB) – a transcription factor that induces the expression of pro-inflammatory cytokines[203]. Moreover, MERTK was shown to relieve the post-translational repression of 5-lipoxygenase via an ERK-dependent mechanism, which increases the synthesis of the anti-inflammatory SPMs – lipoxin A4 and resolvin D1[21]. Secondly, MERTK is a strong inducer of cell survival and proliferation via the PI3K/Akt/mTOR and MAPK

pathways[204]. As such, MERTK has become a major target in cancer research, as some tumors aberrantly express MERTK to promote survival and replication[204]. Finally, MERTK increases the expression of Liver X receptors (LXRs), which stimulates the transcription of the ATP-binding cassette transporter ABCA1[186,205]. This promotes the efflux of cholesterol incurred after the engulfment of ACs to limit conversion into foam cells[186,206].

In summary, MERTK activates signaling pathways required for the engulfment of ACs and for the induction of anti-inflammatory, pro-survival, and pro-proliferative transcriptional programs. Our laboratory has mostly focused on studying the engulfment pathway, although the reader should be reminded that MERTK's other functions are also highly important for homeostasis. Despite decades of progress in understanding its signaling mechanism, the role of MERTK during actin remodeling and subsequent generation of the efferocytic cup is almost completely unknown. It is also unclear whether MERTK is a stimulating receptor or an engulfment receptor. By investigating the biomechanics of MERTK-mediated efferocytosis using fluorescence microscopy (discussed in Chapter 1.2), a major gap in our understanding of efferocytosis can finally be filled. Identification of this elusive mechanism will provide insight into immunopathologies where MERTK or its downstream effectors are dysregulated.

1.4   The biomechanics of MERTK-mediated efferocytosis

It is certain that MERTK is a bonafide efferocytic receptor, given its necessity for engulfment. The conventional view held by most researchers is that MERTK directly induces Rac1-mediated actin polymerization to form the efferocytic cup, as suggested by several reviews on efferocytosis[14,15,207]. However, this does not appear to be supported by existing evidence. To our knowledge, no other RTK family members are known to coordinate the direct restructuring of actin during phagocytosis. MERTK does not contain an ITAM motif nor is it known to interact with ITAM-containing adaptor proteins like most validated phagocytic receptors[93,208]. This is required for the recruitment and activation of SYK, an important signaling molecule for both Fc- and complement-dependent phagocytosis[71,209]. Indeed, MERTK does not appear to activate SYK during efferocytosis nor by direct stimulation with Gas6[210,211]. This suggests that MERTK

should be unable to recruit the canonical Rac1-activation machinery required for actin polymerization. Therefore, biomechanical characterization of MERTK is critical to resolve this perplexing dilemma: is MERTK a stimulating receptor or an engulfment receptor?

1.4.1   The biomechanical role of MERTK during engulfment is controversial

It is possible that MERTK is a stimulating receptor that induces the engulfment of ACs through indirect mechanisms rather than by direct actin polymerization. The strongest evidence of this hypothesis was substantiated by a report in which exogenously expressed MERTK was found to activate FAK – an integrin signaling molecule – via SFK-dependent signaling in human chondrosarcoma cells[73]. FAK activation led to recruitment of p130^{CAS} to the cytoplasmic tail of β_5 integrins, forming a scaffold for the CrkII:DOCK180:ELMO complex[73]. This promoted $\alpha_V\beta_5$-mediated Rac1 activation and subsequent actin polymerization. Importantly, simultaneous expression of both MERTK and $\alpha_V\beta_5$ integrins were required for the engulfment of ACs[73]. The codependency between MERTK and $\alpha_V\beta_5$ during efferocytosis was also reported in human RPE cells[212], suggesting this mechanism is conserved. Later, MERTK was shown to activate β_3 integrins by a PI3K-dependent mechanism in platelets[213], although this axis has yet to be investigated in efferocytes. Interestingly, exogenously expressed TIM-4 was shown to tether ACs and subsequently activate $\alpha_V\beta_3$ integrins to promote efferocytosis in a murine pro B cell line, demonstrating a precedent for the crosstalk between stimulating- and engulfment-receptors[64]. These studies suggest that MERTK may be a stimulating receptor that activates integrins, with the integrins then serving as engulfment receptors that drive the actin polymerization required for engulfment.

However, the validity of the stimulating receptor hypothesis for MERTK is still questionable. Foremost, there is significant inconsistency in the choice of cells used by different laboratories. Many of the cell types that were used in the prior literature are not normally efferocytic. Thus, these experiments often involved the exogenous overexpression of MERTK and/or β_3 and β_5 integrins, which may have led to erroneous activation of signaling pathways that would not usually be induced in untransfected cells.

Although the endogenous MERTK:integrin axis was deemed essential for efferocytosis in RPE cells, there were a lack of studies investigating this pathway in professional phagocytes. Then, in a setback for the stimulating receptor hypothesis, Dransfield *et al*. reported that the blockade of endogenous $\alpha_V\beta_3$ and $\alpha_V\beta_5$ had no effect on MERTK-mediated efferocytosis[214]. Zihni *et al*. also recently reported that MERTK could directly activate Cdc42 in human macrophages[121]. It seemingly appeared as if MERTK was sufficient for cytoskeletal remodeling and engulfment of ACs[214]. Therefore, there exists a great amount of inconsistency and confusion on the biomechanical role of MERTK during engulfment, especially in macrophages. We believe this controversy is the result of a missing link in the MERTK:integrin axis that has yet to be reported – the MERTK-dependent activation of the β_2 integrin family.

1.4.2 β_2 integrins as efferocytic receptors

The β_2 integrin chain/CD18 is only expressed by leukocytes and associates with the CD11 family of integrin alpha chains: α_L/CD11a, α_M/CD11b, α_X/CD11c, or α_D/CD11d[215]. The resulting heterodimers comprise adhesion molecules involved in a variety of functions including actin-remodeling, chemotaxis/migration, differentiation, proliferation, phagocytosis, and cell-survival[215]. In particular, $\alpha_M\beta_2$ and $\alpha_X\beta_2$ can act as phagocytic receptors that coordinate the engulfment of iC3b complement-opsonized targets[216]. Although these receptors are usually studied in the context of pathogen removal, there is evidence supporting their role during efferocytosis. Foremost, apoptosis is thought to be associated with the downregulation of complement-shielding proteins CD46 and CD55[104], leading to activation of the complement pathway and iC3b deposition on the cell surface[217,218]. This results in $\alpha_M\beta_2$- and $\alpha_X\beta_2$-mediated engulfment of ACs by professional efferocytes[217,218]. Furthermore, β_2 integrins are highly promiscuous. For instance, $\alpha_M\beta_2$ is known to bind to dozens of different ligands, including the Arg-Gly-Asp (RGD) motif found in the efferocytic opsonin, MFG-E8, which is also known to mediate efferocytosis through $\alpha_V\beta_3$ and $\alpha_V\beta_5$ integrins[219]. It was also recently reported that $\alpha_M\beta_2$ drives the engulfment of non-opsonized PtdSer-coated beads[220]. Our laboratory further discovered that $\alpha_X\beta_2$ can serve as an efferocytic receptor for sCD93, which opsonizes ACs for their removal by macrophages[49]. As the integrin

α_X/CD11c is expressed by human, but not murine macrophages[221], this may explain why its role during efferocytosis had been missed by animal models. In summary, β_2 integrins can act as bonafide efferocytic receptors, but have been underappreciated because of their historical association with pathogen-removal.

1.4.3 The MERTK:β_2 integrin axis during efferocytosis

Integrins are highly regulated in their activity, especially members of the β_2 family[222,223]. Much of this regulation is driven by changes in the integrin conformation, with the conformational state of the integrin dictating whether ligation and subsequent downstream signaling can occur. Thus, integrins are only engaged under specific circumstances to limit their hyperactivity. Integrin regulation is a complex process and is the subject of several reviews[222,224,225]. Simplified, integrins assume a "bent" conformation in their inactive state, with a characteristic bend in their extracellular domain, which places the ligand-binding site near the plasma membrane where it is sterically hindered from binding ligands[222,224]. Moreover, changes to the conformation of the binding site itself greatly reduces its affinity for its cognate ligands. Intracellular signaling can induce the "extended" conformation, where the extracellular domain is straightened, increasing its binding affinity by several thousand fold[222,224]. This conformational change is induced by either intracellular signaling pathways – referred to as "inside-out" activation, or by high levels of ligand that forcibly induces activation – termed "outside-in" activation[225]. Manganese (Mn^{2+}) is also able to forcibly activate integrins by stabilizing the extended conformation[226].

Previous unpublished work from our lab had identified MERTK to be a potent inside-out activator of β_2 integrins in human macrophages[107,197]. In a microscopy-based efferocytosis assay in THP-1 macrophages, MERTK conferred tethering to Gas6-opsonized beads, but engulfment was not observed (Data not shown; schematic represented by Figure 1.6A). In contrast, $\alpha_X\beta_2$ could not mediate tethering nor engulfment of sCD93-opsonized beads (Figure 1.6B). Strikingly, engulfment was only observed when the beads were opsonized with both Gas6 and sCD93, suggesting the simultaneous activity of MERTK and $\alpha_X\beta_2$ were required for engulfment (Figure 1.6C). Addition of Mn^{2+} into solution permitted the internalization of sCD93-opsonized beads in the absence
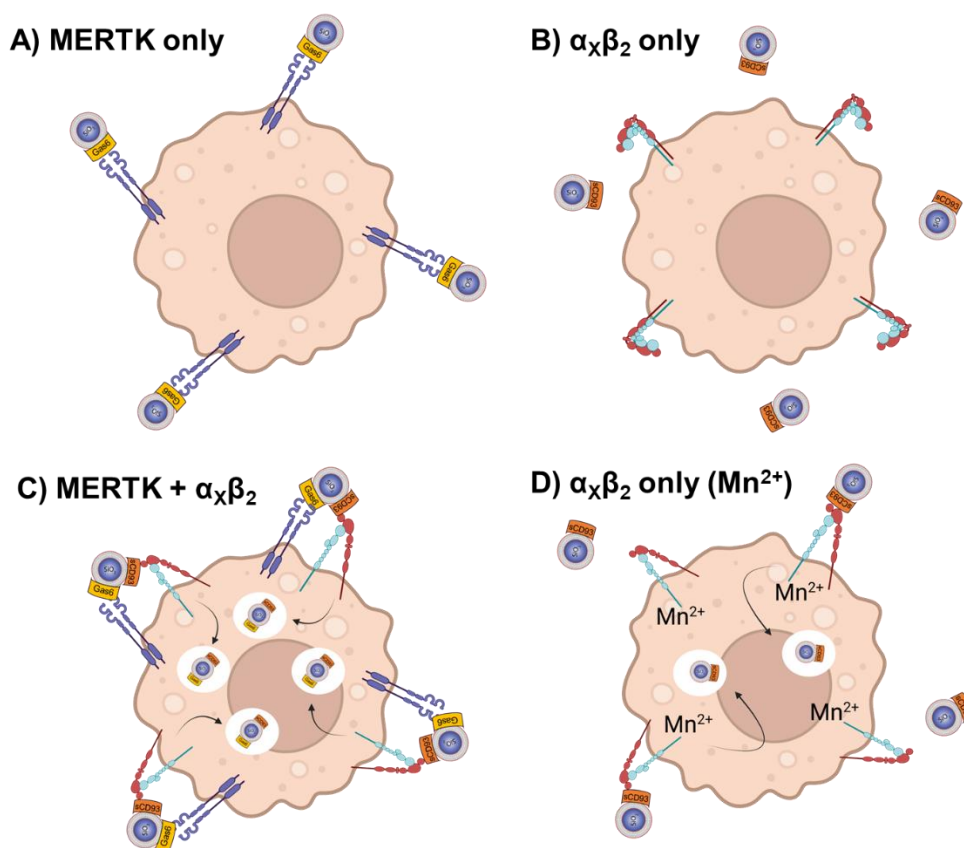
Figure 1.7: Schematic of an efferocytosis assay with Gas6- and/or sCD93-opsonized beads. Diagrams represent results from an unpublished experiment performed by Dr. Bryan Heit. THP-1 macrophages were incubated with biotinylated polystyrene beads crosslinked with Gas6 and/or sCD93 for 20 minutes. Cells were washed then fixed, and non-internalized beads were stained with fluorescent streptavidin and visualized by fluorescence microscopy. Fluorescent beads on the surface of the cell were considered to be tethered. Beads that failed to be stained by streptavidin were deemed to be fully engulfed. **A)** MERTK promoted tethering to Gas6-opsonized beads but not engulfment. **B)** $\alpha_X\beta_2$ did not induce tethering or engulfment to sCD93-opsonized beads. **C)** Simultaneous engagement of MERTK and $\alpha_X\beta_2$ were required for engulfment. **D)** $\alpha_X\beta_2$ could partially mediate engulfment of sCD93-opsonized beads upon forcible activation with Mn^{2+}. Specificity was confirmed by siRNA knockdown of *MERTK* and *CD11c* (not shown). Figure produced with BioRender.

of a MERTK ligand, implicating integrin activation as the prerequisite for internalization (Figure 1.6D). Therefore, our lab hypothesized that MERTK is an activator of the β_2 integrin family, with the latter driving the actin polymerization required for engulfment.

To visualize the inside-out activation of the β_2 integrins, previous members of our lab developed a fluorescence resonance energy transfer (FRET) assay. In these experiments, the head domain of the β_2 integrins were labeled with FITC-conjugated antibodies, while the plasma membrane was stained with octadecyl rhodamine B. In the inactive/bent conformation of the integrin, the FITC "donor" fluorophore is brought within close proximity to the membrane. When excited, this allows some of the excitation energy to be transferred from FITC to the nearby "acceptor fluorophore" – octadecyl rhodamine B, causing the latter to fluoresce at a different wavelength in a phenomenon called FRET (Figure 1.7). In the active/extended conformation, FITC is positioned further away from the membrane, effectively preventing FRET. THP-1 human macrophages were incubated with Gas6-opsonized beads, and the FRET intensity at the site of bead engagement was analyzed. Through these FRET assays, our lab revealed that MERTK was responsible for the activation of β_2 integrins through a class I PI3K-dependent mechanism[197]. The integrin signaling molecules FAK and ILK were also required for β_2 activation. FAK is known to recruit the Rac1 activation machinery and talin to the cytoplasmic tail of the β chain[73,75]. Talin is believed to promote the transition of the integrin into its extended conformation[227]. Furthermore, talin has been shown to recruit ILK, which serves as a signaling hub to strengthen the integrin-actin linkage[228]. SFKs were not required for MERTK-dependent β_2 activation, in contrast to β_5 integrins in a prior report[73]. Finally, inhibition of SYK and p38 MAPK had no effect on β_2 activation downstream of MERTK.

Our lab had confirmed that MERTK is required for the engulfment of ACs by THP-1 macrophages[197]. This was also dependent on PI3K, SFKs, SYK, FAK and ILK. Frustrated efferocytosis assays confirmed that PI3K, SFKs, FAK, and ILK were required for the spreading of the efferocytic synapse, but not SYK. Furthermore, MERTK co-immunoprecipitated with integrin components including α_X, FAK, and ILK. This was supported by ground state depletion super-resolution microscopy, which revealed the
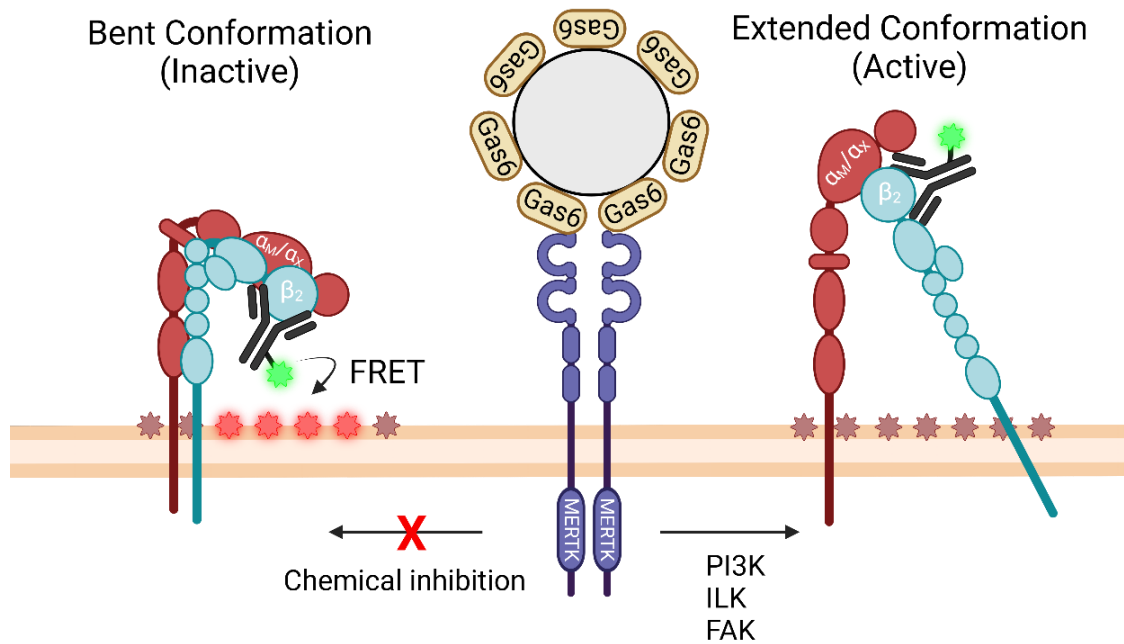
Figure 1.9: Schematic of FRET assay used to measure MERTK-dependent activation of β2 integrins. Diagram summarizes data from Tarannum Tasnim[195]. β_2 integrins were labeled with a FITC-conjugated antibody and the plasma membrane was stained with octadecyl rhodamine B. In the bent conformation, FITC excitation causes energy transfer to octadecyl rhodamine B. In the extended conformation, energy transfer does not occur. THP-1 macrophages were incubated with Gas6-opsonized beads. FRET was quantified at the membrane-bead interface, then normalized to the FRET intensity at a distal site on the membrane. Chemical inhibition of MERTK, PI3K, ILK, and FAK caused an increase in FRET. No effect was observed upon inhibition of SFK, SYK, or p38 MAPK (not shown). Figure produced with BioRender.

intimate colocalization between MERTK and β_2 integrins on the plasma membrane[229]. Thus, we have proposed that MERTK and β_2 integrins form pre-formed "signalosomes" that promote their intermolecular crosstalk during the initial stages efferocytosis. Upon MERTK-induced activation, we believe the β_2 integrins then bind to ACs to stimulate the polymerization of actin during efferocytosis.

1.5   Hypothesis and Aims

Our laboratory has identified MERTK to be a potent activator of β_2 integrins. The coordination between these receptors appears to be essential for efferocytosis. Although much of the signaling mechanism involved in the MERTK:β_2 integrin axis have been identified, we must provide biomechanical support to confirm MERTK's role during engulfment. *We hypothesize that MERTK is a stimulating receptor whereas the β_2 integrins are engulfment receptors that drive the cytoskeletal remodeling required for engulfment*. We planned on supporting this hypothesis by investigating the structure and dynamics of the efferocytic synapse using fluorescence microscopy. Three major aims were proposed to accomplish this:

Aim 1: *Determine the localization of MERTK, β_2 integrin, and F-actin within the efferocytic synapse by utilizing the frustrated efferocytosis assay*. This will determine the spatial orientation of MERTK and β_2 relative to the actin cytoskeleton. Engulfment receptors are expected to colocalize with F-actin.

Aim 2*: Characterize the diffusive behaviour of MERTK and β_2 integrins within the efferocytic synapse using single particle tracking.* Engulfment receptors are linked with F-actin and are expected to be highly immobilized, whereas stimulating receptors are likely to be more freely diffusive.

Aim 3: *Begin the development of a traction-force microscopy assay to characterize the biophysics of MERTK-mediated efferocytosis*. This assay is expected to definitively confirm the biomechanical role of MERTK during efferocytosis. Engulfment receptors play a direct role in force transduction via the actin cytoskeleton, whereas stimulating receptors do not generate force.

Chapter 2 - Methods

2.1   Materials

THP-1, HeLa, and HEK293T cells were purchased from the American Type Culture Collection (Manassas, Virginia, USA). pLVX-IRES-ZsGreen and lentiviral packaging vectors pCMV dR8.2 and pMD2.G were gifts from Dr. Jimmy Dikeakos (University of Western Ontario, London, Canada). pLVX-IRES-Puro was purchased from Takara Bio (Mountain View, California). PolyJet transfection reagent was from FroggaBio (Vaughn, Canada). rhGas6-SBP and rhMFG-E8-SBP gene fragments were ordered from Integrated DNA Technologies (Coralville, Iowa) and were cloned into pLVX-IRES-ZsGreen and pLVX-IRES-Puro. Polybrene and 100K Amicon centrifugal filters were purchased from EMD Millicore Corp (Billerica, Massachusetts). Roswell Park Memorial Institute 1640 (RPMI) medium, Dulbecco's Modified Eagle Medium (DMEM), and fetal bovine serum (FBS) were purchased from Wisent (St-Jean-Baptiste, Canada). 15 mm coverslips, 18 mm coverslips, glass bottom dishes, and 50% glutaraldehyde were ordered from Electron Microscopy Sciences (Hatfield, Pennsylvania). Rabbit polyclonal anti-human MERTK antibody was ordered from Sigma-Aldrich (Oakville, Canada), mouse monoclonal anti-human CD18 was from BioLegend (San Diego, California), mouse monoclonal anti-SBP Tag was from Santa Cruz Biotechnology (Dallas, Texas), and SiR-Actin was purchased from Spirochrome (Stein am Rhein, Switzerland). Fluorescent secondary antibodies were ordered from Cell Signalling Technology (Danvers, Massachusetts). 1-palmitoyl-2-oleoyl-sn-glycero-3-phosphocholine (PtdCho) and 1-pamitoyl-2-oleoyl-sn-glycero-3-phospho-L-serine (PtdSer) were ordered from Avanti Polar Lipids (Alabaster, Alabama), while 1,2-Dipalmitoyl-sn-glycero-3-PE-N-(cap biotin) (Biotin-PtdEth) was purchased from Cayman Chemical (Ann Arbor, Michigan). The Avanti liposome MiniExtruder kit was ordered from Avanti Polar Lipids (Alabaster, Alabama). (3-aminopropyl)-trimethoxysilane (APTMS) and Sigmacote were purchased from Sigma-Aldrich (St. Louis, Missouri). 20 000 MWCO Slide-A-Lyzer Dialysis cassettes, Pierce streptavidin agarose resin, Sulfo-SANPAH, 40 nm red carboxylate-modified FluoSpheres, Versene solution, StemPro Accutase solution, and OptiPro serum-free media were purchased from ThermoFisher (USA). 2% bis-acrylamide, 40% acrylamide, ammonium persulphate

(APS), tetramethylethylenediamine (TEMED) and 2-mercaptoethanol were from BioShop Canada Inc (Burlington, Canada). QC Colloidal Coomassie Stain was purchased from BioRad (Mississauga, Canada). rhGas6-His6 and rhMFG-E8-His6 were ordered from R&D Systems (Minneapolis, Minnesota). PRISM was licensed from GraphPad (La Jolla, California) and FIJI was downloaded from https://imagej.net/software/fiji/downloads.

2.2　　Cell culture and differentiation

THP-1 monocytes were cultured in suspension within RPMI 1640 medium supplemented with 2 mM L-glutamine, 25 mM HEPES, 1500 mg/L sodium pyruvate and 10% FBS in a cell culture incubator at 37 °C and 5% CO_2. Cells were passaged for a maximum of ten generations and cell density was kept between 5×10^5 and 1.5×10^6 cells/mL. For differentiation into THP-1 macrophages, 2×10^5 monocytes were seeded onto 18 mm coverslips in a 12-well plate and differentiated in 1 mL of culture media containing 100 ng/mL phorbol 12-myristate 13-acetate (PMA), then incubated for 72 hours.

HEK293T and HeLa cells were cultured in flasks containing DMEM supplemented with 4.5 g/L glucose, 2 mM L-glutamine, 1500 mg/L sodium pyruvate and 10% FBS at 37 °C and 5% CO_2. Cells were passaged by trypsinization for a maximum of ten generations, and confluency was kept from 10% – 95%.

2.3　　Immunostaining and F-actin labelling

To label F-actin in live THP-1 macrophages, 100 nM SiR-Actin were added to the differentiation media 12 hours before the experiment. To prevent efflux of the SiR-Actin dye, 10 μM verapamil was also added. To label MERTK and β_2 integrin, macrophages were equilibrated to 10 °C for 10 minutes. Then, cells were rinsed with 10 °C PBS to remove dead and non-differentiated cells. Macrophages were stained with a primary antibody solution containing 1 μg/mL rabbit anti-human MERTK (Sigma-Aldrich; Polyclonal; Cat# HPA075622) and 10 μg/mL mouse anti-human β_2 integrin (BioLegend; Monoclonal; Clone TS1/18; Cat# 302105) antibody in PBS for 30 minutes at 10 °C. The MERTK antibody binds to the second immunoglobulin domain of MERTK, whereas the

β_2 integrin antibody binds to the head domain of the integrin. Macrophages were rinsed with 10 °C PBS twice and a secondary antibody solution containing fluorescently labeled Fab fragments were added and incubated for 20 minutes at 10 °C, followed by two rinses with 10 °C PBS.

2.4   Frustrated efferocytosis target preparation

10 mg/mL solutions of PtdCho, PtdSer, and Biotin-PtdEth were resuspended in chloroform and stored at -20 °C. 15 μL of PtdCho, 4 μL of PtdSer, and 4 μL of Biotin-PtdEth was transferred to an amber glass vial using a gas-tight glass syringe. For negative-control experiments, liposomes were prepared with 19 μL of PtdCho and 4 μL of Biotin-PtdEth. Lipids were dried using a light stream of nitrogen gas for 5 minutes, then resuspended in 400 μL of PBS, creating a solution containing multilamellar liposomes. Unilamellar liposomes were purified from the solution using the Avanti MiniExtruder Kit fitted with a 100 nm filter, according to manufacturer's instructions. Liposomes were diluted 1:5 in PBS and stored at 4 °C for up to four days.

18 mm coverslips were acid-washed with 2 M HCl, dried with 70% ethanol, then autoclaved. Coverslips were placed in a glass vacuum chamber and the air was evacuated to < 0.1 Torr using a vacuum pump. The chamber was placed in a microwave set to max power until plasma was generated within the chamber for 10 seconds. Plasma-activated coverslips were placed in a clean 12-well plate. 200 μL of purified liposome solution was added to the centre of the coverslip in a dropwise manner, then incubated at room temperature for 25 minutes. Coverslips were rinsed three times with PBS. If biotin-PtdEth was stained, a 0.75 μg/mL solution of Streptavidin-AF647 in PBS was added for 20 minutes, followed by three rinses with PBS.

To opsonize the substrate, the coverslip was transferred to a circular live-cell microscopy chamber. 250 μL of imaging buffer (25 mM HEPES, 23.8 mM $NaHCO_3$, 150 mM NaCl, 5 mM KCl, 2 mM $CaCl_2 \cdot 2H_2O$, pH 7.4) containing 10% pooled human serum was added to the chamber, and incubated at 37 °C within a large Petri dish for 30 minutes prior to the experiment.

2.5   Microscopy

All experiments used a Leica DMI6000B inverted widefield epifluorescence microscope equipped with a Sedat Quad Filterset and 100X/1.4 NA oil immersion objective. For single particle tracking experiments, an additional 1.6x optical magnifier was used. Images were captured using a Photometrics Evolve-512 Delta EMCCD or a Hamamatsu ORCA-Flash 4.0 CMOS camera. The lens, stage, and stage lid were heated to 37 °C for at least 30 minutes prior to each experiment.

2.6   Frustrated efferocytosis assay

After immunostaining and frustrated efferocytic target preparation, cells were incubated in 1 mL of versene solution (0.48 mM EDTA in PBS) for 15 minutes at 37 °C. Then, cells were lifted by repeatedly pipetting the solution, ensuring all cells have lifted off the coverslip. The solution was transferred to a 1.5 mL microcentrifuge tube and cells were pelleted at 400×g for 5 minutes at room temperature. The versene was removed from the tube and cells were resuspended in 250 µL of pre-warmed imaging buffer containing 10% pooled human serum. Cells were added to the imaging chamber containing the opsonized coverslip within the heated microscope stage.

After 15 minutes, the position of at least 5-10 adherent macrophages were saved, and timelapse images of MERTK, β_2 integrin, and F-actin were collected as the synapse spread over time. For super-resolution radial fluctuation (SRRF) images, a 50-frame burst at 10 ms exposure was collected for each timepoint, followed by super-resolution reconstruction using the eSRRF plugin in FIJI (https://github.com/HenriquesLab/NanoJ-eSRRF)[230].

2.7   Radial distribution synapse analysis

To determine the radial distribution profile of MERTK, β_2, and F-actin within the synapse, 10-12 images of early (t = 0 min) and fully spread (t = variable) frustrated synapses were used for the radial distribution analysis. The radial profile angle plugin (http://questpharma.u-strasbg.fr/html/radial-profile-ext.html) was used to draw a circular ROI around the synapse, where the outer edge was defined by the fluorescence of the β_2

integrin signal, and the radial profile was calculated. The raw data of the radius and integrated intensities were copied into Excel. The normalized synapse position was determined by normalizing the radial positions of each cell to its respective max radius, such that the centre of the synapse = 0.0, and the outermost edge of the synapse = 1.0. The fold average intensity was calculated by normalizing the raw integrated intensities for each radial position to the average intensity within the total synapse. Finally, the fold average intensities were plotted as a function of normalized synapse position using PRISM.

2.8 Single particle tracking and diffusion analysis

Frustrated efferocytosis experiments were performed as described. For image capture, a 100×/1.4 NA oil immersion lens with the 1.6× optical magnifier was used for a total magnification of 160X. The Hamamatsu ORCA-Flash 4.0 CMOS camera was used with 4x4 binning. The synapse was imaged in 30-frame bursts spaced by 100 ms intervals, repeating every 2 minutes for a total of 20 minutes to capture the spreading of the synapse. A rectangular ROI was used to crop the synapse from the rest of the image. 30-frame intervals, representing each 2 minute timepoint, were saved as .tif files in separate folders, ranging from 0 min to 20 min.

A single particle tracking algorithm by Jaqaman *et al.*[231] adopted using an in-house MatLab GUI was used to analyze each .tif file, which generated a diffusion profile for MERTK and β_2 integrin for each timepoint. The proportion of free, confined, and linear tracks, as well as the diffusion coefficients and confinement areas were ensembled from a total of 20 cells across eight replicates in the PtdSer group and five replicates in the PtdCho negative control.

2.9 Continuous photobleaching assay

Frustrated efferocytosis experiments were performed as described, but cells were allowed to adhere to PtdSer- or PtdCho-coated substrates for 30 minutes at 37 °C/5% CO_2, ensuring the synapse was fully spread at the time of imaging. Images were captured using the Photometrics Evolve Delta-512 EMCCD with the 100×/1.4 NA oil immersion lens.

Ten cells were imaged per replicate, for a total of three experimental replicates. A 500-frame high speed (10 frames per second) burst of maximum intensity light was used to photobleach the MERTK on the basolateral surface of the macrophage. ROIs were manually drawn around each immobilized cluster of MERTK using FIJI, ignoring clusters that were clearly endocytosed. The measure stack function was used to calculate the integrated intensity for all 500 frames. All integrated intensity values were normalized to the average initial cluster intensity in the PtdSer group.

2.10   Cloning of Gas6 and MFG-E8

The cDNA sequence of recombinant human Gas6 and recombinant human MFG-E8 attached to a C-terminal linker region (GGGGSGGGGSGGGGS), followed by the streptavidin binding peptide[232,233] (SBP-Tag; MDEKTTGWRGGHVVEGLAGELE QLRARLEHHPQGQREP) was designed in SnapGene and codon-optimized for use in human cells using the IDT codon optimization tool. Sequences were purchased from IDT. rhGas6-SBP and rhMFG-E8-SBP were amplified by PCR to add 20 bp regions of homology with the MCS sequence from the pLVX-IRES-ZsGreen and pLVX-IRES-Puro backbone. pLVX-IRES-ZsGreen and pLVX-IRES-Puro vectors were linearized with XbaI, and rhGas6-SBP or rhMFG-E8-SBP were assembled into the vector by Gibson assembly. Constructs were transformed into *E. coli* DH5α and plated onto agar plates containing ampicillin and incubated overnight. Single colonies were screened by Sanger sequencing at the London Regional Genomics Centre (Robarts Research Institute, London, ON).

2.11   Lentiviral packaging and transduction

HEK293T cells were seeded to 90% confluency in DMEM + 10% FBS in T75 flasks. 4 μg pDR8.2, 10 μg pMD2.G, and 10 μg of rhGas6- or rhMFG-E8-pLVX-IRES-ZsGreen or pLVX-IRES-Puro constructs were transfected into the cells using 30 μL PolyJet according to manufacturer's instructions. Media was exchanged for fresh DMEM + 10% FBS after 12-16 hours. After 48 hours, media was collected into 50 mL tubes and topped up to a final concentration of 20% FBS. Cell debris was pelleted at 4000×g for 5 minutes

at 4 °C, and the viral supernatant was filtered through a 0.45 μm filter using a syringe. Viral supernatant was stored at -80 °C until use.

HeLa cells were grown to 80% confluency in DMEM + 10% FBS in a 6 well plate. Media was exchanged for 3 mL of viral supernatant containing 10 μg/mL polybrene. After 48 hours, cells were trypsinized and transferred to T25 flasks. For the ZsGreen cell lines, the top 3% of the brightest cells were sorted by FACS at the London Regional Flow Cytometry Facility (Robarts Research Institute, London, ON; courtesy of Dr. Kristin Chadwick). For the Puro cell lines, cells were selected using 3 μg/mL of puromycin for 2 days, followed by a 2 μg/mL maintenance dose indefinitely.

2.12   Western blot and Coomassie staining

The four HeLa cell lines expressing rhGas6 or rhMFG-E8 from the pLVX-IRES-ZsGreen or pLVX-IRES-Puro vectors were plated to 80% confluency on 6 well plates, then serum-starved with OptiPro serum-free media for 6 days. The media was transferred into 1.5 mL microcentrifuge tubes, and spun down at 21 000×g for 30 minutes at 4 °C. 1× Laemmli's buffer containing 10% 2-mercaptoethanol was added to the supernatant and boiled for 5 minutes at 99 °C. The sample was separated using a 16% SDS-PAGE gel at 100 V for 90 minutes. The gel was transferred onto a PVDF membrane using the BioRad Mini-PROTEAN Tetra Cell transfer system at 40 V for 19 hours at 4 °C. The membrane was blocked in TBS-T + 5% BSA for 2 hours on a rocker, then washed five times with TBS-T. The membrane was stained with 0.2 μg/mL mouse anti-SBP Tag antibody in 5 mL of TBS-T + 5% BSA for 16 hours at 4 °C, then washed five times with TBS-T. The membrane was incubated with 0.075 μg/mL AlexaFluor 680-conjugated anti-mouse secondary antibody in TBS-T + 5% BSA for 1 hr at room temperature. The membrane was rinsed five times with TBS-T then visualized using a LI-COR Odyssey fluorescence imaging system. Images were edited using LI-COR Image Studio.

For Coomassie staining, samples were prepared as above and separated using a 12% SDS-PAGE gel. The gel was placed in fixing solution (50% ethanol, 10% acetic acid in ddH$_2$O) for 30 minutes, followed by three rinses with distilled water. The gel was stained in 25 mL QC colloidal Coomassie solution for 20 hours at room temperature on an orbital

shaker. Three 1 hour washes with 25 mL of ddH$_2$O were used to destain the gel. The gel was imaged using a BioRad Gel Doc EZ Imager.

2.13 Protein isolation

Puro-rhGas6 and Puro-rhMFG-E8 cell lines were seeded to near-100% confluency in T175 flasks. Cells were serum starved using OptiPro serum-free media for 6 days. Media was removed and cell debris was pelleted at 4000×g for 30 minutes at 4 °C. The supernatant was concentrated using 30 kDa centrifugal filter units at 4000×g for 30 minutes at 4 °C. The concentrate was washed in the same filter unit with 15 mL of sterile PBS and spun at 4000×g for 30 minutes at 4 °C. Concentrated protein was dialyzed in a 20 000 kDa MWCO Slide-A-Lyzer Dialysis cassette in 500 mL of PBS for 2 hours at 4 °C. 500 mL of fresh PBS was added for another 2 hours, then exchanged again for 16 hours.

1 mL of streptavidin agarose resin was packed into a 10 mL chromatography tube at 4 °C for 30 minutes. The resin was equilibrated with 5 mL of streptavidin binding buffer (300 mM KCl, 40 mM Tris-base, 5 mM 2-mercaptoethanol, 2 mM EDTA, 0.1% Triton X-100, pH 7.4). The dialyzed protein sample was added to the column and collected into a tube by gravity flow, and the sample was added back to the column for a second binding step. Columns were washed with ten column volumes of streptavidin binding buffer. rhGas6 or rhMFG-E8 were eluted with elution buffer (300 mM KCl, 40 mM Tris-base, 5 mM 2-mercaptoethanol, 2 mM EDTA, 0.1% Triton X-100, 2 mM biotin, pH 7.4) in two 1 mL fractions. The sample was dialyzed again in 500 mL of PBS for 2 hours at 4 °C, followed by fresh PBS for 2 hours, and a final exchange with fresh PBS for 16 hours. Protein was quantified by Bradford assay and purity was confirmed by Coomassie staining.

2.14 Traction force microscopy

Glass bottom dishes were treated with 200 μL of 50% APTMS in ddH$_2$O for 10 minutes at room temperature. 800 μL of ddH$_2$O was added and the dish was incubated for 30 minutes on an orbital shaker. The dish was rinsed five times with ddH$_2$O. 400 μL of 0.5% glutaraldehyde was added to the dish and incubated for 30 minutes at room temperature.

Dishes were rinsed three times with ddH_2O and dried in a vacuum chamber. Simultaneously, both sides of 15 mm diameter plasma-activated coverslips were coated with 100 μL of Sigmacote for 5 minutes at room temperature, then rinsed with distilled water and dried in a vacuum chamber. 20 μL of 10X PBS, 37.5 μL of 40% acrylamide, 15 μL of 2% bisacrylamide, and 113.5 μL of ddH_2O were mixed in a 1.5 mL microcentrifuge tube and degassed in a vacuum chamber for 20 minutes. 6 μL of 40 nm red FluoSpheres (diluted 1:100 in ddH_2O), 4 μL of 3% APS, and 4 μL of 5% TEMED were added to the solution and mixed by pipetting. 8 μL of the solution was added to the centre of the glass bottom dish, and the 15 mm coverslip was added to the top of the droplet. The gel was polymerized at room temperature for 20 minutes. 2 mL of PBS was added to the glass bottom dish and the coverslip was carefully removed using forceps, revealing the gel. The gel was incubated at 4 °C for at least 12 hours prior to functionalization.

PBS was removed from the glass bottom dish and 100 μL of Sulfo-SANPAH (2 mg/mL in ice-cold ddH_2O) was added to the centre of the gel. The Sulfo-SANPAH was activated by 750 mJ/cm² of 365 nm UV light using a Stratalinker 2400. The gel was rinsed five times with PBS and the liquid was removed. 100 μL of ligand solution (15 μg/mL rhGas6, 11.25 μg/mL rhMFG-E8, 15 μg/mL rhGas6 + 11.25 μg/mL rhMFG-E8, or 1 mg/mL IgG) was added to the centre of the gel and incubated for 16 hours at 4 °C.

On the day of the experiment, the gels were washed three times with sterile PBS and incubated with live-cell imaging buffer (25 mM HEPES, 23.8 mM $NaHCO_3$, 150 mM NaCl, 5 mM KCl, 2 mM $CaCl_2 \cdot 2H_2O$, pH 7.4) for 30 minutes at 37 °C. THP-1 macrophages were lifted with versene solution and resuspended in pre-warmed live-cell imaging buffer, then added to the gel. For cells parachuted onto Gas6 + MFG-E8 dual-opsonized gels, 5 μM of the MERTK inhibitor, UNC2250[234] or DMSO vehicle control were added during resuspension. Cells were imaged 30-60 minutes post-incubation at 37 °C.

For synapse analysis, an ROI was drawn around the periphery of the cell manually using FIJI. The measure command was used to calculate synapse area, circumference, and

Feret's diameter. For force analysis, the position of 5-10 cells were saved using the acquisition software. Images of the cell were collected in DIC. A 6 μm Z-stack spaced by 0.3 μm per slice were collected for the FluoSpheres underlying each position, with these images referred to as the "strained state". Then, cells were lifted with dissociation solution (live cell imaging buffer + 5% SDS) for 15 minutes. Image acquisition was repeated for each position, with these images representing the "relaxed state".

2.15   Force-map generation

Using FIJI, a maximum intensity projection was created for the strained and relaxed state of the beads, then a two-image stack was created with the relaxed state followed by the strained state. 2D image registration using the Linear Stack Alignment with SIFT plugin was used to remove drift in the lateral axis that occurred between acquisitions. A Particle Image Velocimetry (PIV) plugin (https://sites.google.com/site/qingzongtseng/piv) was used to determine the displacement field. A Fourier-transform traction cytometry plugin was used to generate a force-magnitude and force-vector map using the displacement matrix calculated by the PIV. The value of each pixel in the force-map represents local stress in Pascal.

2.16   Statistical analysis

All statistical analyses were performed using PRISM. For the non-ensembled confined and free track proportion data, a one-way ANOVA with a Dunnett's multiple comparisons test was performed. For the ensembled data that combined all the tracks from each replicate, Fisher's exact test was used to compare the proportions of confined or free tracks over time. Welch's unequal variances t-test was used to compare the 0 vs 18 min conditions for the confinement zone and diffusion coefficient data. Student's t-test was used for the photobleaching assay.

Chapter 3 - Results

3.1 Structure of the efferocytic synapse

To investigate the structure of the efferocytic synapse, THP-1 macrophages were parachuted onto serum-opsonized PtdSer bilayer-coated coverslips, which mimics the surface of apoptotic cells. Macrophages readily spread on this planar efferocytic substrate (Figure 3.1). Super-resolution eSRRF microscopy was used to visualize the actin cytoskeleton at ~100 nm resolution; as expected, this cell spreading was accompanied by a rapid reorganization of F-actin from a dense meshwork throughout the cell into a bounding ring that localized at the edges of the synapse (Figure 3.2). This distribution has been reported as a hallmark of frustrated phagocytosis, and confirms that we have induced a similar efferocytic process[96]. In contrast, macrophages failed to spread or form an efferocytic synapse on substrates that mimic non-apoptotic cells (PtdCho-bilayer coated coverslips), where F-actin did not reorganize with the substrate (Figure 3.3). This indicates that this cell spreading and actin reorganization is due to efferocytic receptor signaling in response to PtdSer[39], and is not an adhesive response activated by contact with the surface.

We hypothesized that MERTK and β_2 integrins would be differentially localized within the efferocytic synapse, indicative of their unique biomechanical roles during engulfment. This could explain why MERTK behaved as a stimulator of integrin-dependent engulfment in our prior experiments[107,197]. To investigate this, the localization of antibody-labeled MERTK and β_2 integrin within the synapse were determined using frustrated efferocytosis experiments, where β_2 and MERTK were imaged after 30 minutes to ensure their visualization within the fully matured synapse. Strikingly, β_2 integrins localized towards the outer edge of the cell, forming an outer ring-like structure near the periphery of the synapse, but were not found within the outer edges of lamellipodia (Figure 3.4). In contrast, MERTK was distributed throughout the entirety of the synapse, including the outer lamellipodial structures (Figure 3.5). Dual-staining of MERTK and β_2 integrin further demonstrated their differential localization within the efferocytic synapse, where integrins formed a ring-structure that encapsulated the majority of MERTK, with some MERTK found in the outer lamellipodia (Figure 3.6).
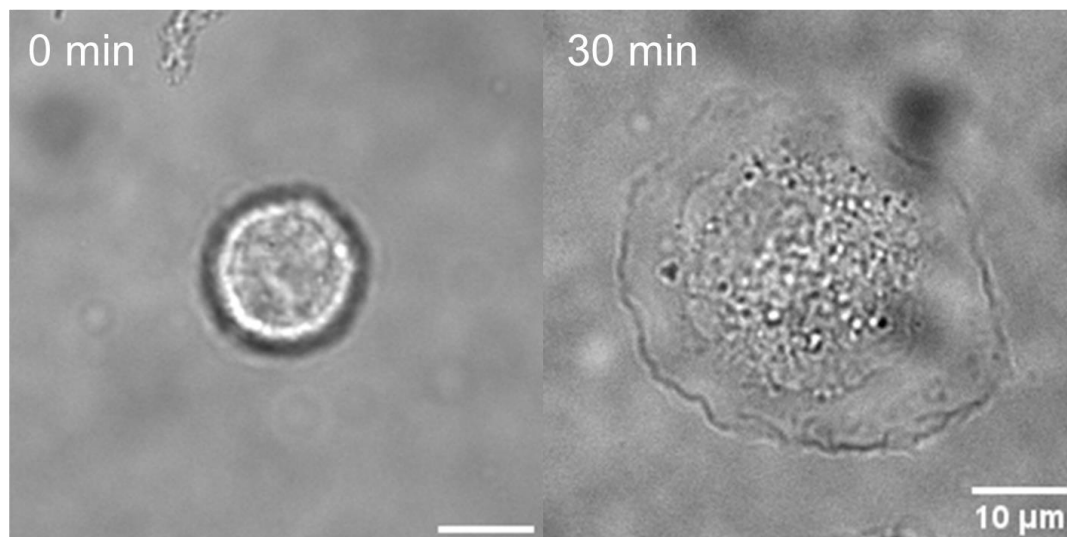
Figure 3.1: THP-1 macrophages spread on serum-opsonized PtdSer-coated coverslips. Representative DIC image of an efferocytic synapse formed by a THP-1 macrophage after 30 minutes of engagement with the planar efferocytic substrate. Images are representative of at least 10 cells imaged across three independent experiments. Scale bars are 10 μm.
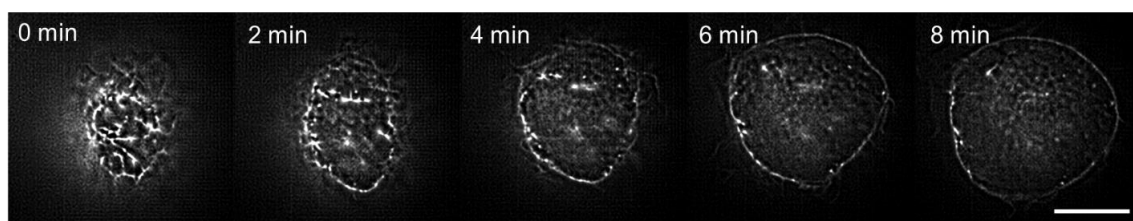
Figure 3.2: F-actin restructures into a radially expanding outer ring during frustrated efferocytosis. Super-resolution fluorescence imaging of F-actin within SiR-actin stained THP-1 macrophages undergoing frustrated efferocytosis. Images are representative of at least 5 cells imaged across three independent experiments. Scale bar is 10 μm.
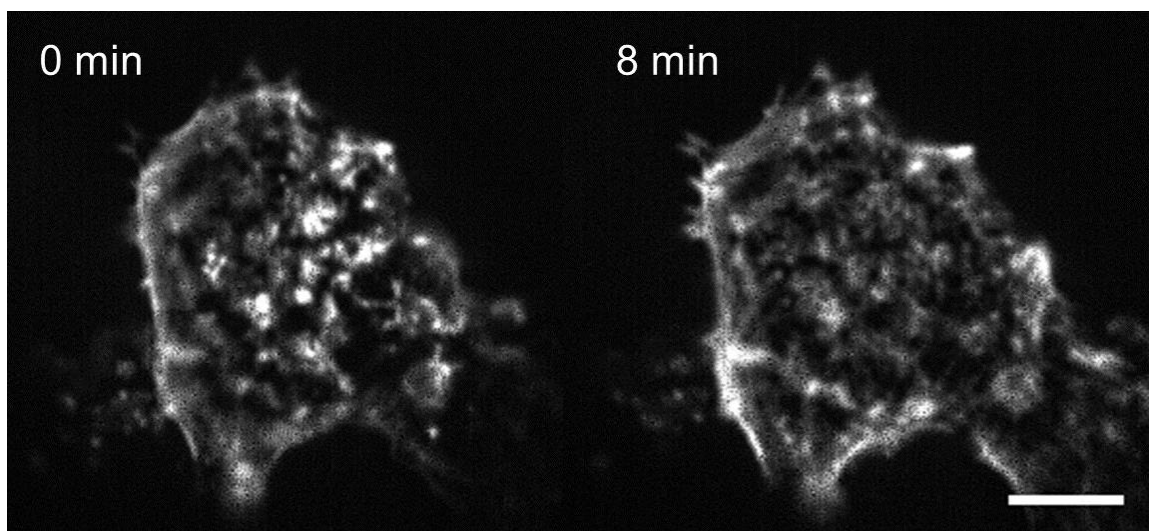
Figure 3.3: F-actin fails to reorganize upon engagement with PtdCho-bilayer coated coverslips. Fluorescence imaging of F-actin within THP-1 macrophages stained by SiR-actin. THP-1 macrophages were parachuted onto serum-opsonized PtdCho-coated coverslips and visualized using eSRRF every 2 minutes. Images are representative of at least 10 cells across three independent experiments. Scale bar is 5 μm.
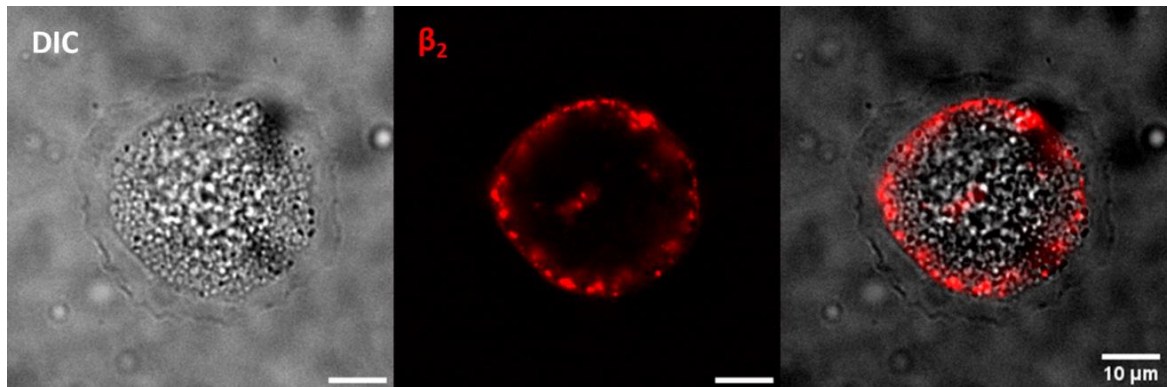
Figure 3.4: β₂ integrins form a ring-like structure in the fully matured efferocytic synapse. Fluorescence imaging of antibody-labeled β₂ integrins within the fully matured efferocytic synapse formed by THP-1 macrophages on serum-opsonized PtdSer-coated coverslips. Macrophages interacted with the substrate for 30 minutes. Images are representative of at least 10 cells imaged across three independent experiments. Scale bars are 10 μm.
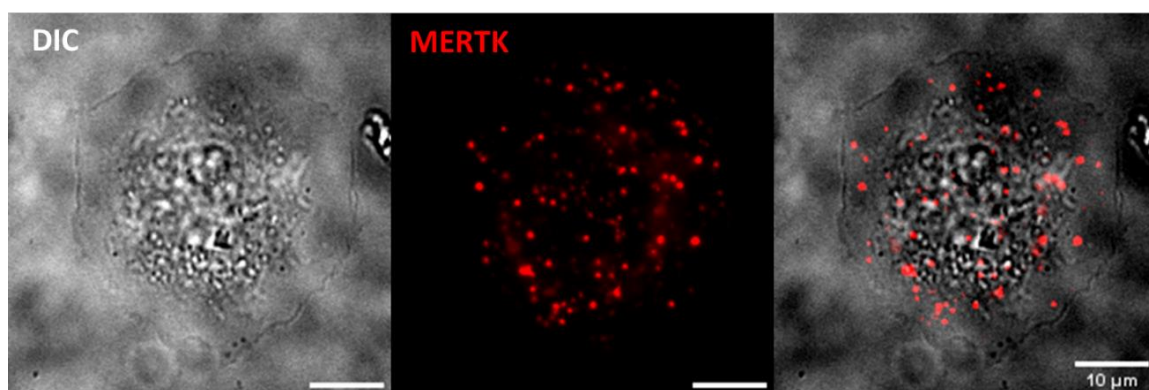
Figure 3.5: MERTK is distributed throughout the fully matured synapse.
Fluorescence imaging of antibody-labeled MERTK within the fully matured efferocytic synapse formed by THP-1 macrophages on serum-opsonized PtdSer-coated coverslips. Macrophages interacted with the substrate for 30 minutes. Images are representative of at least 10 cells imaged across three independent experiments. Scale bars are 10 μm.

**Figure 3.6: Dual-staining of MERTK and β₂ integrin shows differential localization within the efferocytic synapse**. Fluorescence imaging of antibody-labeled MERTK (red) and β₂ integrin (cyan) within the fully matured efferocytic synapse formed by THP-1 macrophages on serum-opsonized PtdSer-coated coverslips. Images are representative of at least 10 cells imaged across three independent experiments. Scale bar are 10 μm.

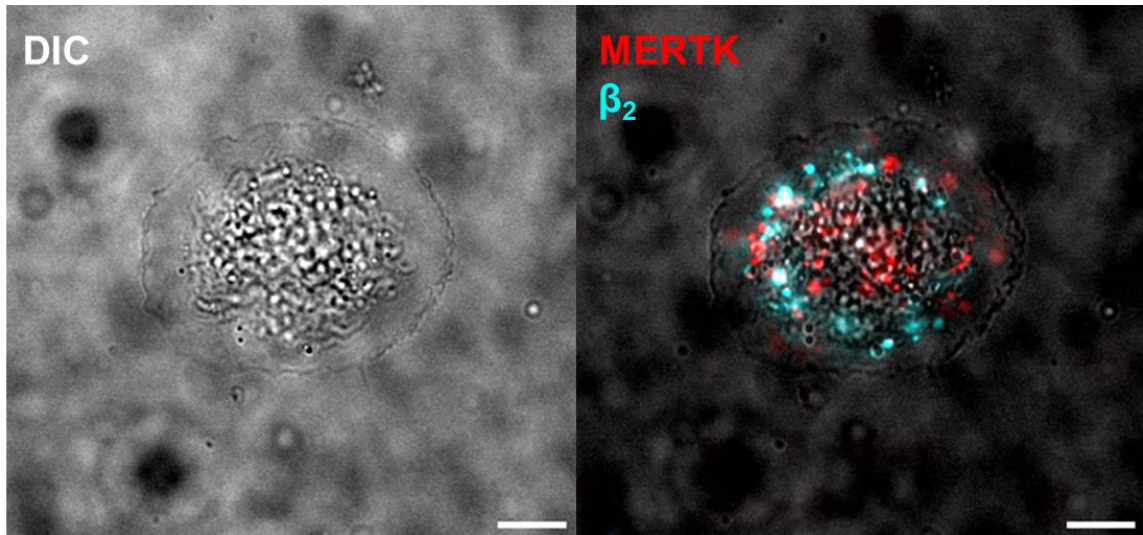To view the dynamics of synapse formation, the maturation of the synapse was visualized using timelapse microscopy. Upon first contacting the AC-mimicking substrate, both MERTK and β_2 were evenly distributed throughout the membrane (Figure 3.7; 0 min). These rapidly reorganized following contact with the substrate, with the β_2 integrins localizing to a continuous ring structure during the spreading phase (Figure 3.7; 5-10 minutes), which evolved into a discontinuous outer-ring comprised of large clusters. Interestingly, clusters of integrins appeared within the centre of the synapse during the later stages of efferocytosis (Figure 3.7; 15-25 min), although the majority of the integrins resided at the outer edge. In these experiments, these clusters appeared rapidly, rather than moving inwards from the synapse edge. Previous work in our lab demonstrated that focal exocytosis delivered integrins to the centre of the synapse, which likely explains how β_2 appears in the synapse[107]. Unlike β_2 integrin, MERTK was distributed throughout the entirety of the synapse at all timepoints. During the spreading phase, the continuous β_2 integrin ring was highly colocalized with the forming ring of F-actin at the synapse edge (Figure 3.8), suggesting that the integrins may be responsible for driving actin reorganization and the expansion of the synapse during efferocytosis. Unfortunately, SiR-actin was highly sensitive to photobleaching and prolonged imaging of the colocalization between β_2 integrins and F-actin could not be accomplished. This was especially prominent after F-actin had been cleared near the centre of the synapse after the first two minutes of spreading.

To quantitively represent the localization of MERTK, β_2 integrin, and F-actin within the maturing efferocytic synapse, a radial profile intensity analysis was performed, in which the intensity of the fluorescence signal was plotted as a function of distance from the barycentre of the synapse (Figure 3.9A). MERTK, β_2 integrin, and F-actin were evenly distributed throughout the synapse at the beginning of frustrated efferocytosis (Figure 3.9B). In the fully matured synapse, MERTK continued to be evenly distributed, whereas most of the β_2 integrin and F-actin signal was localized towards the outer edge of the synapse (Figure 3.9C). The localization pattern of β_2 and F-actin were nearly identical in the matured synapse. In summary, these data indicate that β_2 integrins likely drive the peripheral expansion of the efferocytic synapse through actin polymerization, whereas MERTK does not.
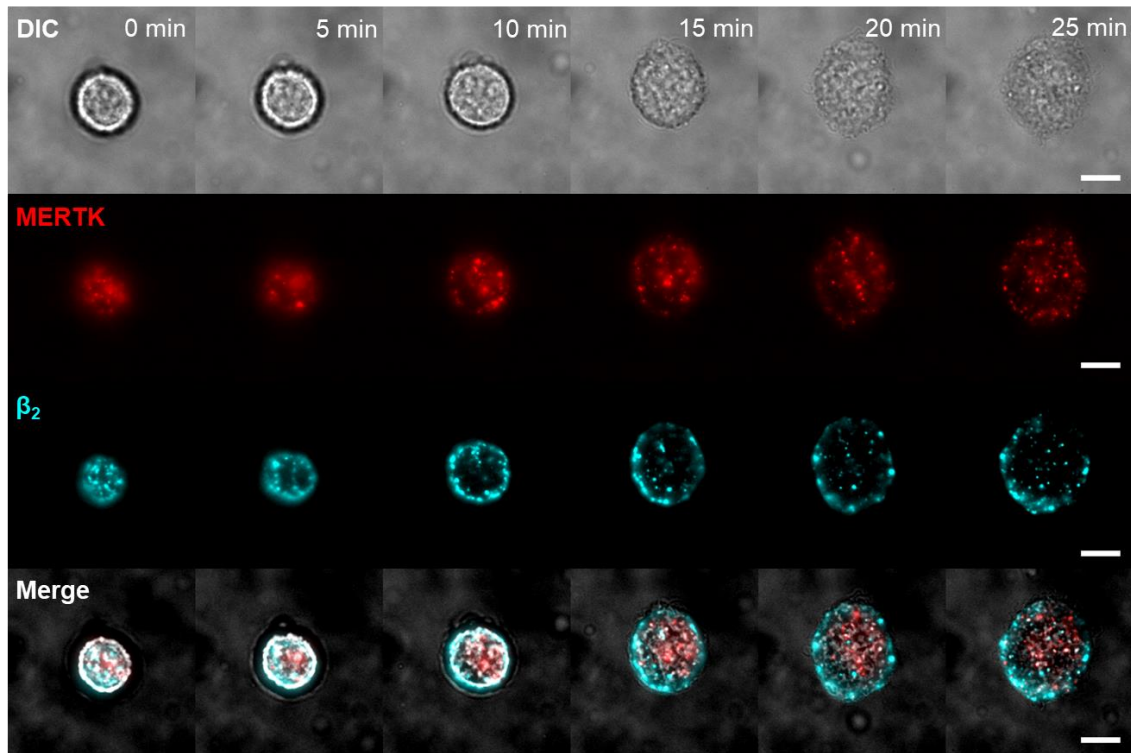
Figure 3.7: MERTK and β₂ integrin localization changes as the efferocytic synapse matures. Timelapse fluorescence imaging of antibody-labeled MERTK (red) and β₂ integrin (cyan) in THP-1 macrophages spreading on serum-opsonized PtdSer-coated coverslips. Images of the efferocytic synapse were captured every 5 minutes upon engagement with the planar efferocytic substrate. Images are representative of at least 10 cells imaged across three independent experiments. Scale bars are 10 μm.
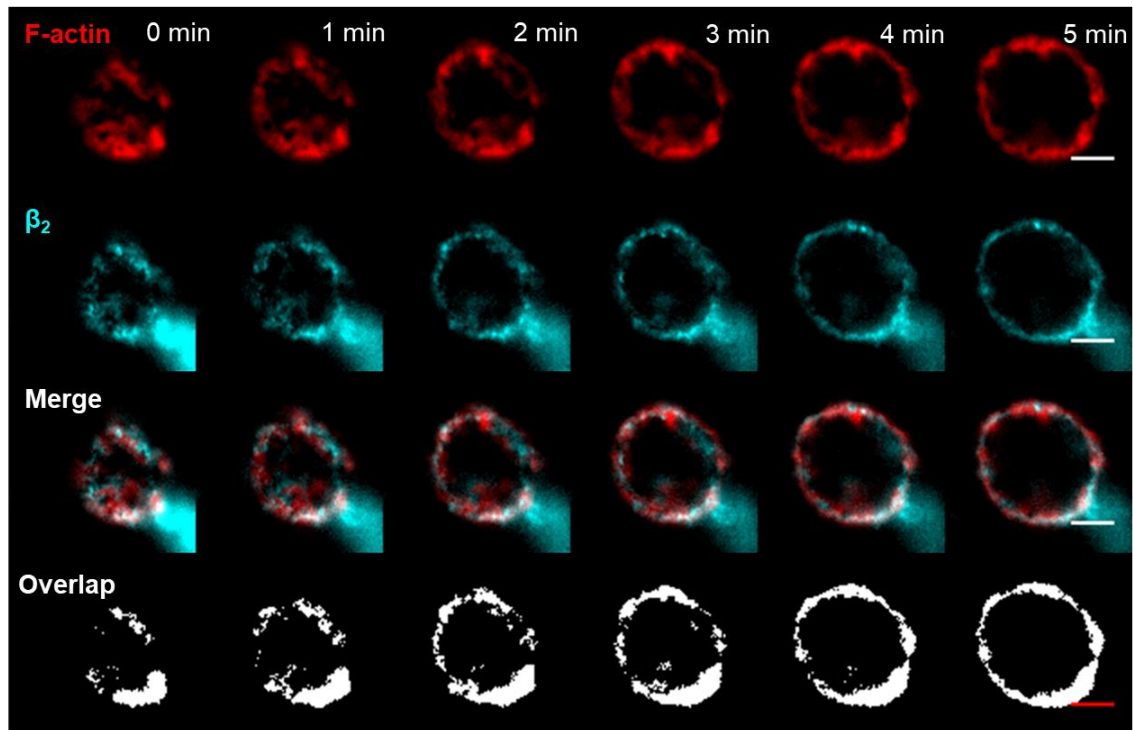
Figure 3.8: β₂ integrins colocalize with F-actin during the spreading phase of efferocytosis. Fluorescence imaging of SiR-actin labeled F-actin (red) and antibody-labeled β_2 integrin (cyan) within THP-1 macrophages spreading on serum-opsonized PtdSer-coated coverslips. Images were captured every minute. Images are representative of at least 10 cells imaged across three independent experiments. Scale bars are 10 μm.
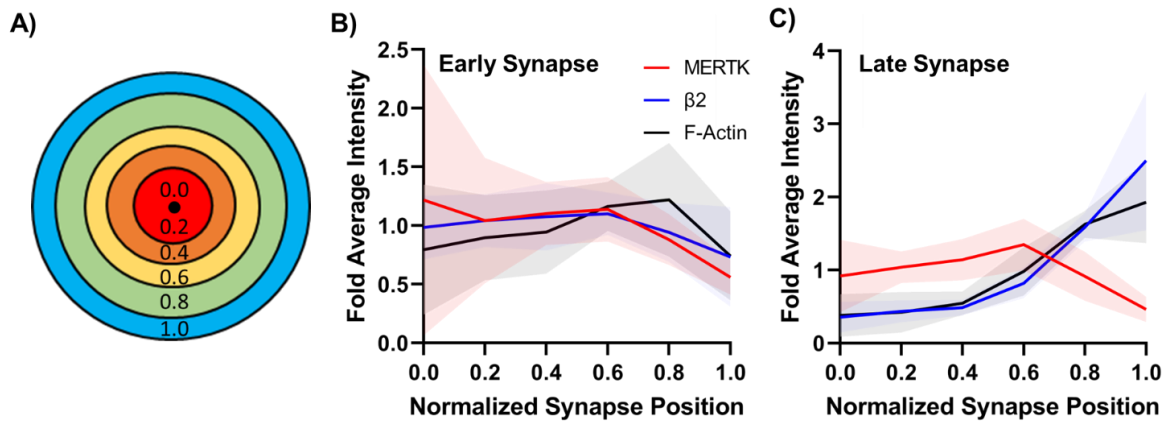
Figure 3.9: Radial profile analysis of the early and fully spread efferocytic synapse.
A) The synapse was stratified into distinct sections, where 0.0 is the centre of the synapse
and 1.0 represents the outer edge. The intensity of MERTK, β_2 integrin, and F-actin
normalized to the whole-cell average were plotted as a function of normalized synapse
position in the **B)** early synapse (t = 0 min) and **C)** fully matured synapse in THP-1
macrophages spreading on serum-opsonized PtdSer-coated coverslips. N = 10 cells for
each of the three proteins were analyzed using the Radial Profile Angle plugin on FIJI.
Shaded areas represent standard deviation for each position.

3.2 Diffusion of MERTK and β_2 during efferocytosis

Although frustrated efferocytosis assays demonstrated that the spatial organization of β_2 integrin and MERTK changed during frustrated efferocytosis, it was still unknown how these receptors separated from each other as the synapse progressed. The diffusive behaviour of phagocytic receptors is expected to change during the spreading of the synapse, and differences in the diffusion of β_2 integrin versus MERTK may account for the increasing spatial separation as synapse formation progressed. To study MERTK and β_2 integrin diffusivity, frustrated efferocytosis experiments on serum-opsonized PtdSer-coated coverslips were performed and the diffusivity of MERTK and β_2 integrin were measured using a single molecule microscopy, followed by analysis using a single particle tracking (SPT) algorithm developed by Jaqaman *et al*[231]. In this approach, MERTK and β_2 are fluorescently labeled at low density, such that individual molecules can be imaged with minimal overlap of the point-spread function of individual fluorophores. A high-speed timelapse is then acquired (~100 ms/frame), capturing 30 frames every two minutes. Each 30-frame segment is then analyzed using the SPT algorithm[231]. In brief, this algorithm identifies individual fluorophores by detecting local maxima, then determines their localization with a precision of up to 20 nm using mixed-model Gaussian fitting. Particle positions are then linked into diffusion tracks, and the diffusive behaviour of each imaged molecule is measured by a moment spectrum scaling analysis. This algorithm thus quantifies the diffusion rate of each molecule in the image, and classifies the diffusion pattern as free (unrestricted Brownian diffusion), confined (diffusion is Brownian, but is limited to a sub-region of the membrane), or linear. For confined molecules, the algorithm also calculates the size of the confinement zone.

3.2.1 SPT of MERTK and β_2 integrins within the frustrated efferocytic synapse

We hypothesized that the structure of the mature synapse was produced by the release of MERTK from pre-formed signalosome clusters, causing them to diffuse in a Brownian fashion and thus remain relatively close to the location in which it escaped the initial cluster. In contrast, we expected the β_2 integrins would demonstrate confined diffusion due to their association with actin, enabling their localization towards the actin-enriched

periphery of the synapse. In this model, MERTK would be expected to undergo an increase in its diffusion rate and an increase in the proportion of MERTK undergoing free diffusion during synapse maturation. Indeed, MERTK was found evenly distributed throughout the actin-depleted centre of the mature efferocytic synapse (Figure 3.5, 3.9), where there should be less constraint on protein diffusion. Unexpectedly, the confinement of MERTK underwent a significant increase (63.6% to 81.5%) as the synapse formed (Figure 3.10). This was accompanied by a proportional drop in the portion of MERTK undergoing free diffusion (Figure 3.11). As expected, nearly 90% of β_2 integrins were confined throughout the entire duration of synapse expansion, with no significant difference between 0 and 18 minutes of spreading (Figure 3.12). Accordingly, no change in the portion of β_2 undergoing free diffusion was observed (Figure 3.13). The confinement of β_2 integrins is consistent with their close association with the actin cytoskeleton (Figure 3.8). In sum, these data suggest that MERTK and β_2 integrins are restricted to distinct diffusional compartments in the plasma membrane, which likely accounts for their spatial dissociation during the formation of the efferocytic synapse.

MERTK's increased confinement within the actin-depleted region of the synapse was unexpected. Actin represents the primary mechanism by which protein diffusion is restricted[113,114]. Thus, the actin-depletion we observed in the centre of the synapse was expected to relieve steric constraint on MERTK, thereby increasing the portion of MERTK undergoing free diffusion. To better understand MERTK's diffusion within the synapse, we performed a more detailed analysis of the confinement zone size and of the diffusion coefficient of MERTK within these confinement zones. The confinement zone size refers to the maximum distance between any two points along the boundaries within which the receptor is observed to undergo confined diffusion (in nm), whereas the diffusion coefficient refers to how fast a receptor diffuses over a specific area within a given time (measured as mean-squared displacement, $\mu m^2/s$). Both confinement zone size and diffusion coefficient are expected to increase within actin-depleted regions of the membrane[235]. As expected, the confinement zone size of MERTK significantly increased during synapse expansion, nearly increasing by 50% from its starting value of

Figure 3.10: Proportion of MERTK undergoing confined diffusion during frustrated efferocytosis. THP-1 macrophages were immunolabelled for MERTK, and frustrated efferocytosis experiments were performed on serum-opsonized PtdSer-coated coverslips or PtdCho-coated control. The synapse was imaged at high-speed, 30 frame intervals every 2 minutes, and analyzed using an SPT algorithm. **A)** Proportion of total MERTK that demonstrates confined diffusion behaviour. **B)** Proportion of total MERTK undergoing confined diffusion as a function of time, with tracks ensembled from all experimental replicates. For **A)**, a one-way ANOVA followed by a Dunnett's multiple comparisons test was used, with data comprised of N = 8 and N = 5 experimental replicates for PtdSer and PtdCho, respectively. Error bars represent ± SEM. **B)**, Fisher's exact test was used to compare 0 vs 18 min for the 468 and 363 ensembled tracks from PtdSer and PtdCho, respectively. *** $p < 0.0002$; **** $p < 0.0001$.

Figure 3.11: Proportion of MERTK undergoing free diffusion during frustrated efferocytosis. THP-1 macrophages were immunolabelled for MERTK, and frustrated efferocytosis experiments were performed on serum-opsonized PtdSer-coated coverslips or PtdCho-coated control. The synapse was imaged at high-speed, 30 frame intervals every 2 minutes, and analyzed using an SPT algorithm. A) Proportion of total MERTK that demonstrates free diffusion behaviour. B) Proportion of total MERTK undergoing free diffusion as a function of time, with tracks ensembled from all experimental replicates. For A), a one-way ANOVA followed by a Dunnett's multiple comparisons test was used, with data comprised of $N = 8$ and $N = 5$ experimental replicates for PtdSer and PtdCho, respectively. Error bars represent $\pm$ SEM. For B) Fisher's exact test was used to compare 0 vs 18 min for the 468 and 363 ensembled tracks from PtdSer and PtdCho, respectively. *** $p < 0.0002$; **** $p < 0.0001$.
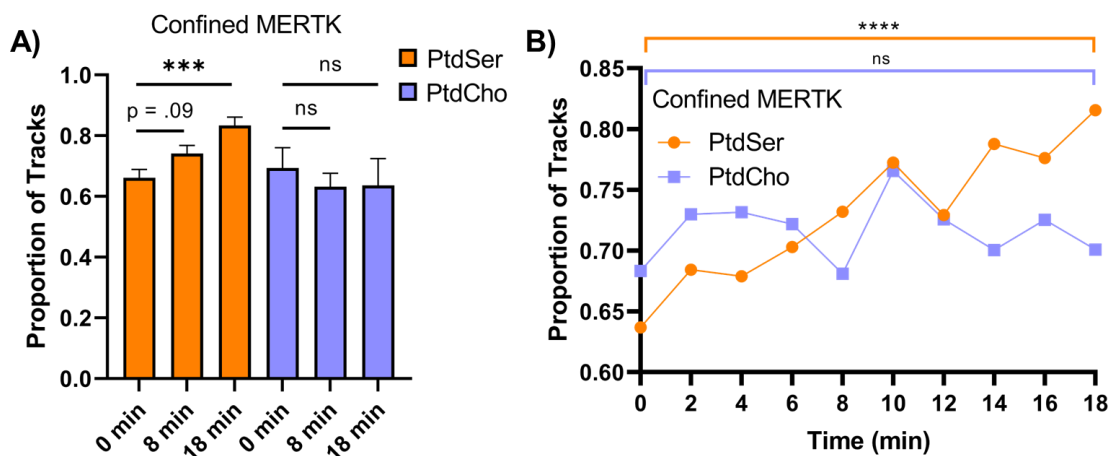
Figure 3.12: Proportion of β_2 integrin undergoing confined diffusion during frustrated efferocytosis. THP-1 macrophages were immunolabelled for β_2 integrin, and frustrated efferocytosis experiments were performed on serum-opsonized PtdSer-coated coverslips or PtdCho-coated control. The synapse was imaged at high-speed, 30 frame intervals every 2 minutes, and analyzed using an SPT algorithm. A) Proportion of total β_2 integrin that demonstrates confined diffusion behaviour. B) Proportion of total β_2 integrin undergoing confined diffusion as a function of time, with tracks ensembled from all experimental replicates. For A), a one-way ANOVA followed by a Dunnett's multiple comparisons test was used, with data comprised of N = 8 and N = 5 experimental replicates for PtdSer and PtdCho, respectively. Error bars represent $\pm$ SEM. For B) Fisher's exact test was used to compare 0 vs 18 min for the 169 and 59 ensembled tracks from PtdSer and PtdCho, respectively.
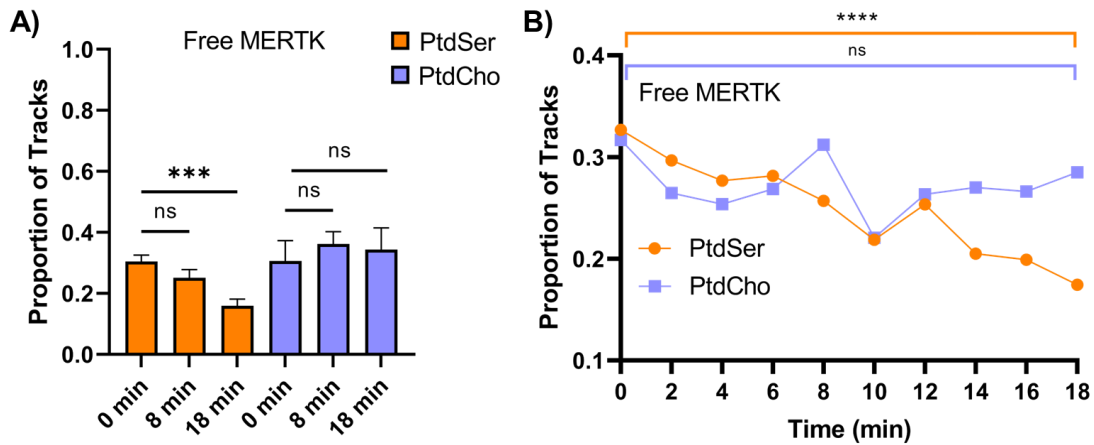
Figure 3.13: Proportion of β_2 integrin undergoing free diffusion during frustrated efferocytosis. THP-1 macrophages were immunolabelled for β_2 integrin, and frustrated efferocytosis experiments were performed on serum-opsonized PtdSer-coated coverslips or PtdCho-coated control. The synapse was imaged at high-speed, 30 frame intervals every 2 minutes, and analyzed using an SPT algorithm A) Proportion of total β_2 integrin that demonstrates free diffusion behaviour. B) Proportion of total β_2 integrin undergoing free diffusion as a function of time, with tracks ensembled from all experimental replicates. For A), a one-way ANOVA followed by a Dunnett's multiple comparisons test was used, with data comprised of N = 8 and N = 5 experimental replicates for PtdSer and PtdCho, respectively. Error bars represent ± SEM. For B) Fisher's exact test was used to compare 0 vs 18 min for the 169 and 59 ensembled tracks from PtdSer and PtdCho, respectively.
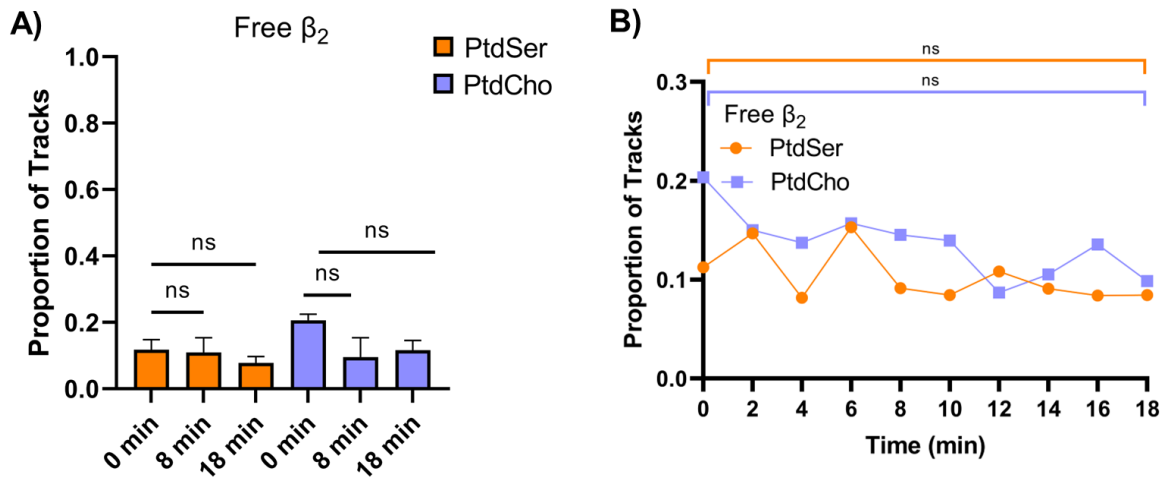
79.6 nm (Figure 3.14). No difference in confinement zone size was observed in the PtdCho control. Furthermore, MERTK exhibiting confined diffusion showed a significant increase in diffusion coefficient, roughly 50% higher than its starting value; whereas no change was observed in the PtdCho control (Figure 3.15A). Contrary to MERTK, there was no change in confinement zone or confined diffusion coefficient in the β_2 integrins within the efferocytic synapse (Figure 3.16, 3.17). Interestingly, this indicates that the β_2 integrins remain in the same (or similar) diffusive environment throughout synapse formation, whereas the diffusive environment of MERTK evolves significantly during synapse formation.

3.2.2   Assessing the oligomerization of MERTK within the efferocytic synapse

The increase in MERTK's confinement zone size and diffusion coefficient during synapse expansion is consistent with its localization in regions of the membrane undergoing progressive actin depletion. Yet, the paradoxical increase in the proportion of MERTK exhibiting confined diffusion was puzzling. A possible mechanism for this behaviour is oligomerization-induced immobilization, a process by which receptors oligomerize upon ligand binding. The steric bulk of these oligomeric complexes, in some cases augmented by immobilization of their ligands, causes them to become "trapped" on the membrane, causing their diffusion to become confined[113]. Conventional fluorescence microscopy cannot be used to directly measure cluster size, as receptor clusters are often smaller in diameter than the resolution limit of optical microscopes (>250 nm). Although we have access to super-resolution techniques that can image individual clusters with sub-20 nm precision (ground state depletion microscopy), this form of microscopy is not compatible with live cell assays. Moreover, I was unable to establish a fixation protocol that maintained adhesion of the macrophages with the planar efferocytic substrates (data not shown), precluding fixed cell imaging on this microscope. We attempted to use SRRF, but the reconstruction process requires high-speed timelapses that are sensitive to the diffusional movement of MERTK, with attempts at SRRF imaging producing a substantial streaking pattern due to the diffusion of MERTK during image
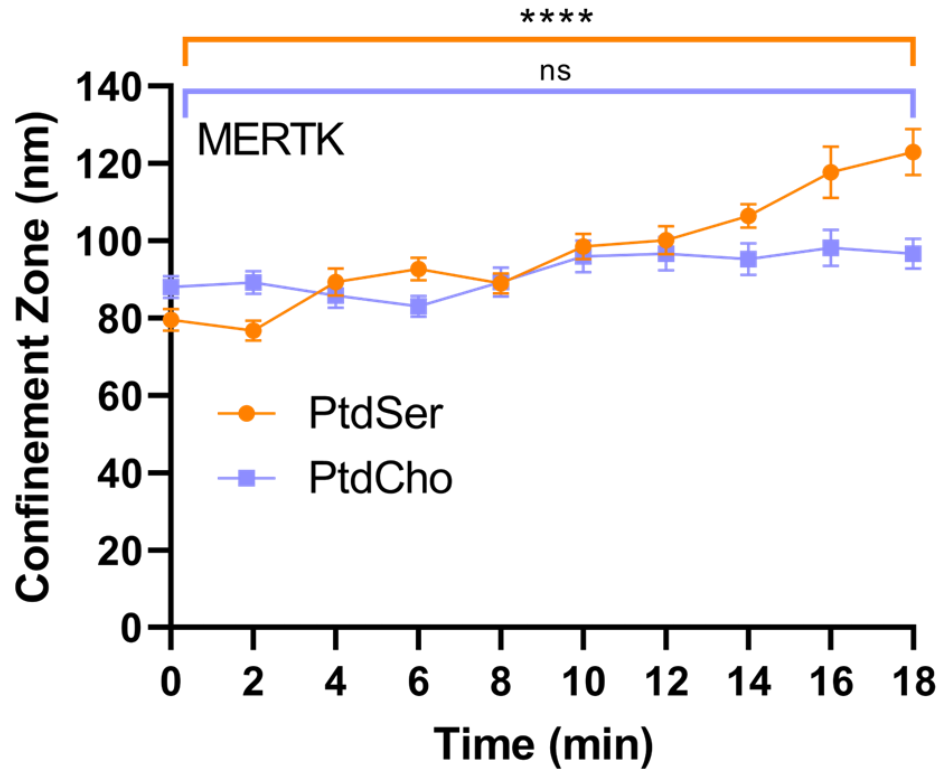
Figure 3.14: Confinement zone size (nm) of MERTK during frustrated efferocytosis. THP-1 macrophages were immunolabelled for MERTK, and frustrated efferocytosis experiments were performed on serum-opsonized PtdSer-coated coverslips or PtdCho-coated control. The synapse was imaged at high-speed, 30 frame intervals every 2 minutes, and analyzed using an SPT algorithm. Welch's unequal variances t-test was used to compare the 0 min vs 18 min confinement size, with data comprised of $N = 8$ and $N = 5$ experimental replicates for PtdSer and PtdCho, respectively. Error bars represent ± SEM. **** $p < 0.0001$.
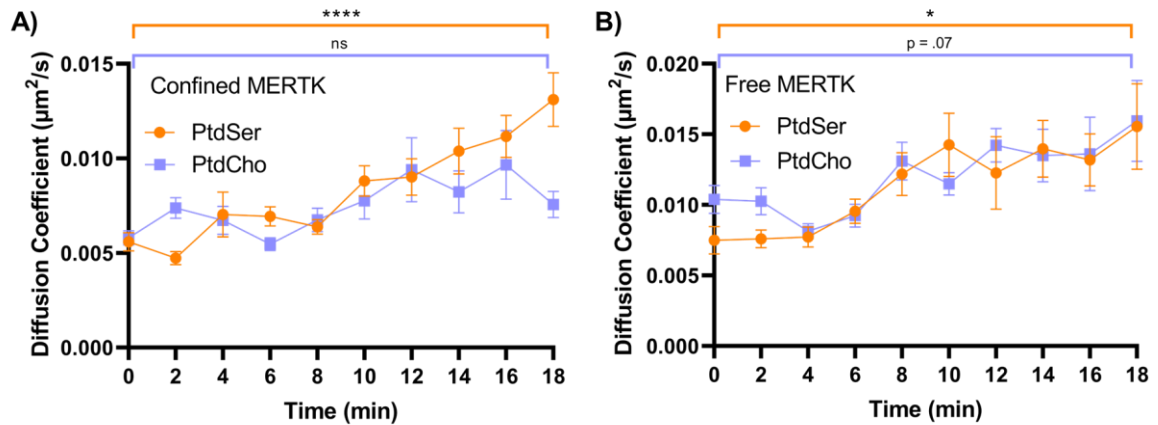
Figure 3.15: Diffusion coefficient (μm^2/s) of MERTK during frustrated efferocytosis. THP-1 macrophages were immunolabelled for MERTK, and frustrated efferocytosis experiments were performed on serum-opsonized PtdSer-coated coverslips or PtdCho-coated control. The synapse was imaged at high-speed, 30 frame intervals every 2 minutes, and analyzed using an SPT algorithm. **A)** Diffusion coefficient of MERTK receptors exhibiting confined diffusion. **B)** Diffusion coefficient of MERTK receptors exhibiting free diffusion. Welch's unequal variances t-test was used to compare the 0 min vs 18 min confinement size, with data comprised of N = 8 and N = 5 experimental replicates for PtdSer and PtdCho, respectively. Error bars represent ± SEM. * p < 0.0322; **** p < 0.0001.
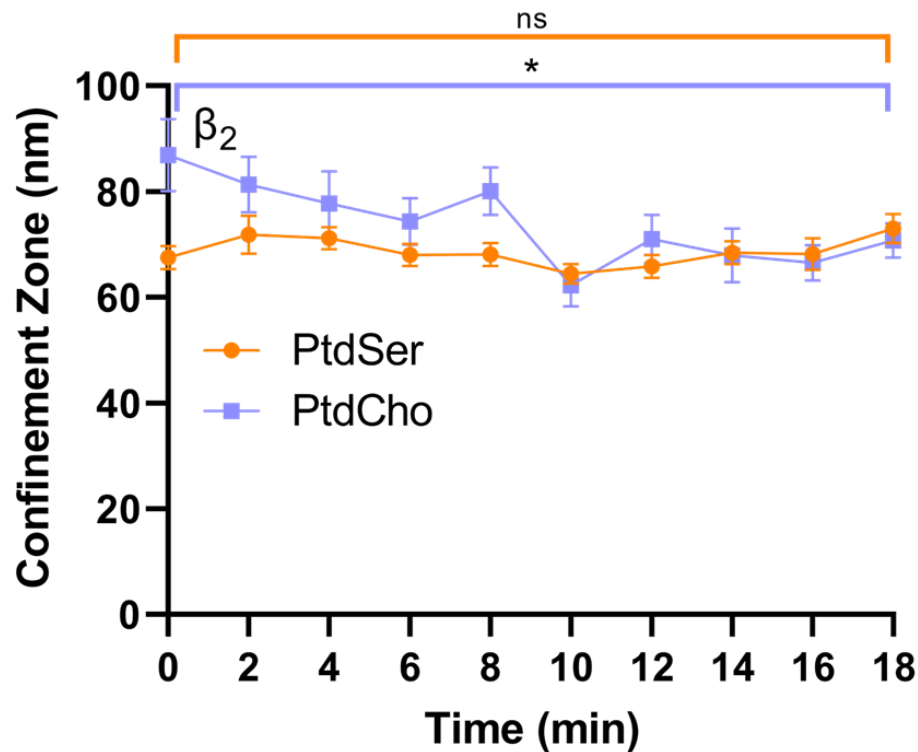
Figure 3.16: Confinement zone size (nm) of β_2 integrin during frustrated efferocytosis. THP-1 macrophages were immunolabelled for β_2 integrin, and frustrated efferocytosis experiments were performed on serum-opsonized PtdSer-coated coverslips or PtdCho-coated control. The synapse was imaged at high-speed, 30 frame intervals every 2 minutes, and analyzed using an SPT algorithm. Welch's unequal variances t-test was used to compare the 0 min vs 18 min confinement size, with data comprised of N = 8 and N = 5 experimental replicates for PtdSer and PtdCho, respectively. Error bars represent ± SEM. * p < 0.032.
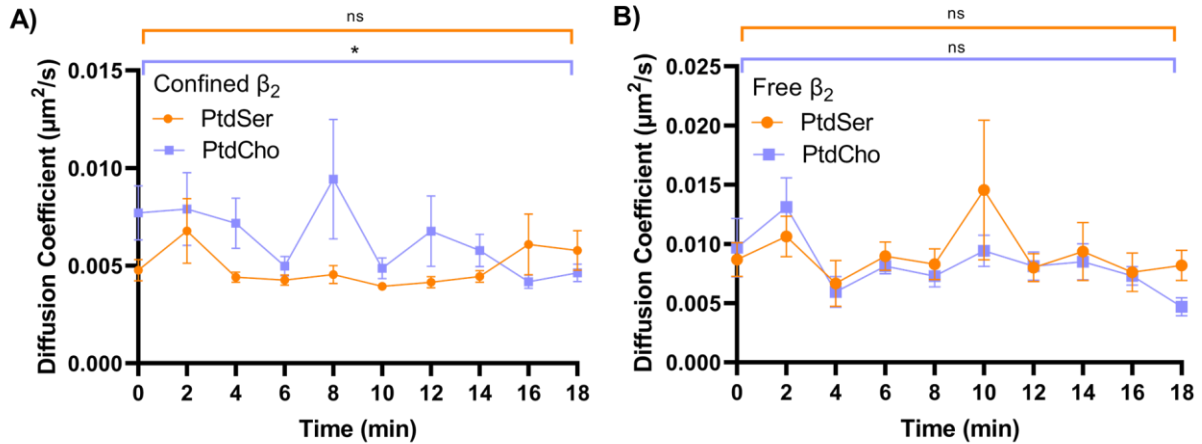
Figure 3.17: Diffusion coefficient ($\mu m^2/s$) of β_2 integrin during frustrated efferocytosis. THP-1 macrophages were immunolabelled for β_2 integrin, and frustrated efferocytosis experiments were performed on serum-opsonized PtdSer-coated coverslips or PtdCho-coated control. The synapse was imaged at high-speed, 30 frame intervals every 2 minutes, and analyzed using an SPT algorithm. **A)** Diffusion coefficient of β_2 integrins exhibiting confined diffusion. **B)** Diffusion coefficient of β_2 integrins exhibiting free diffusion. Welch's unequal variances t-test was used to compare the 0 min vs 18 min confinement size, with data comprised of N = 8 and N = 5 experimental replicates for PtdSer and PtdCho, respectively. Error bars represent ± SEM. * p < 0.0322.

acquisition (Figure 3.18). Thus, cluster sizes could not be accurately determined using this super-resolution approach.

To assess whether MERTK oligomerization was occurring, a continuous photobleaching assay was used to determine the initial cluster brightness and bleaching time of individual MERTK clusters. This assay uses prolonged, high-speed, high-intensity bursts of light to photobleach the sample. As photobleaching is a stoichiometric process[118], larger clusters will take longer to photobleach, thus allowing photobleaching time to serve as a proxy measure of oligomerization. Frustrated efferocytosis experiments were performed and MERTK-immunolabelled cells were adhered to serum-opsonized PtdSer-coated coverslips or a PtdCho control for 30 minutes. MERTK was visibly brighter on the basolateral surface of macrophages that had spread on PtdSer-coated substates compared to PtdCho control (Figure 3.19A). The average initial intensity of individual MERTK clusters were nearly 5-fold higher than MERTK in the PtdCho control (Figure 3.19B), indicative of MERTK oligomerization occurring within the synapse. Consistently, clusters within the efferocytic synapse took nearly 4 times longer to photobleach compared to control (Figure 3.19C), indicating that these clusters contain 4 times more MERTK compared to what is found on cells interacting with a non-apoptotic substrate. These data provide clear evidence that MERTK undergoes oligomerization during efferocytosis, with this oligomerization – and not trapping in actin-generated "picket fences", causing MERTK's increase in confined diffusion. However, their presence within the increasingly actin-depleted region of the synapse reduces external constraints on MERTK's diffusion, thus accounting for the increase in confinement zone size and diffusion coefficient.
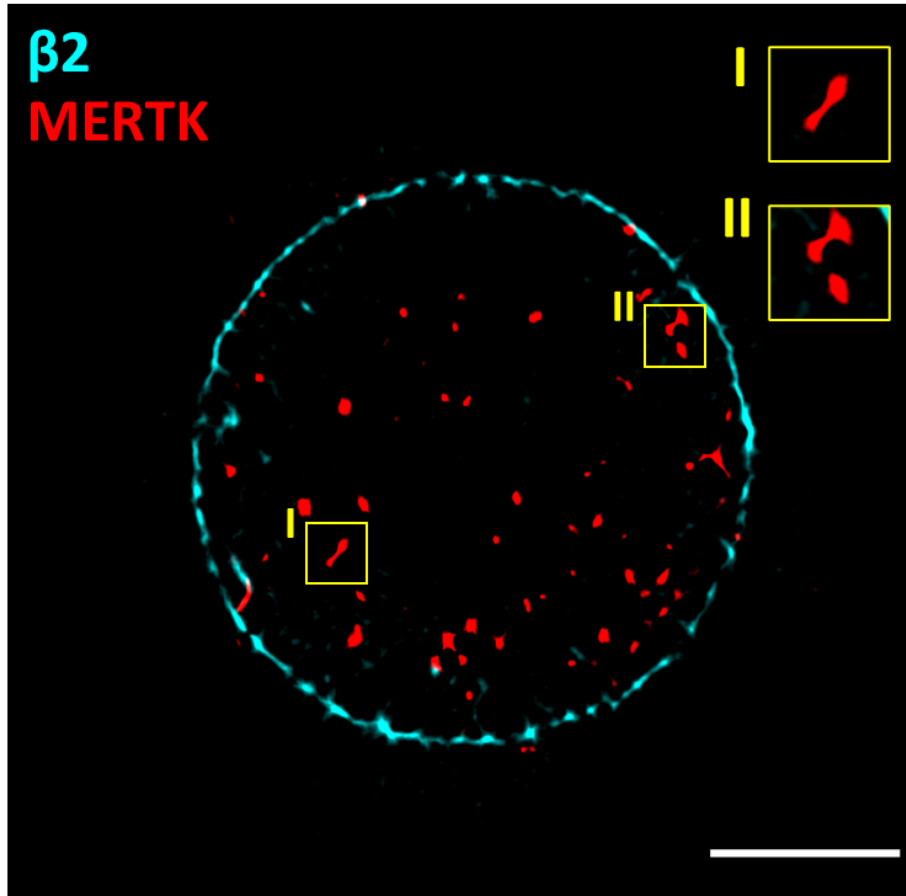
Figure 3.18: **SRRF imaging of MERTK and β2 integrin during frustrated efferocytosis.** THP-1 macrophages were immunolabelled for MERTK and β_2 integrin and parachuted onto serum-opsonized PtdSer-coated coverslips, and the image was reconstructed using a 50-frame eSRRF acquisition after the synapse had fully spread on the efferocytic substrate. Panel **I** and **II** represent areas where artifactual streaking of MERTK was observed. Scale bar is 10 μm.
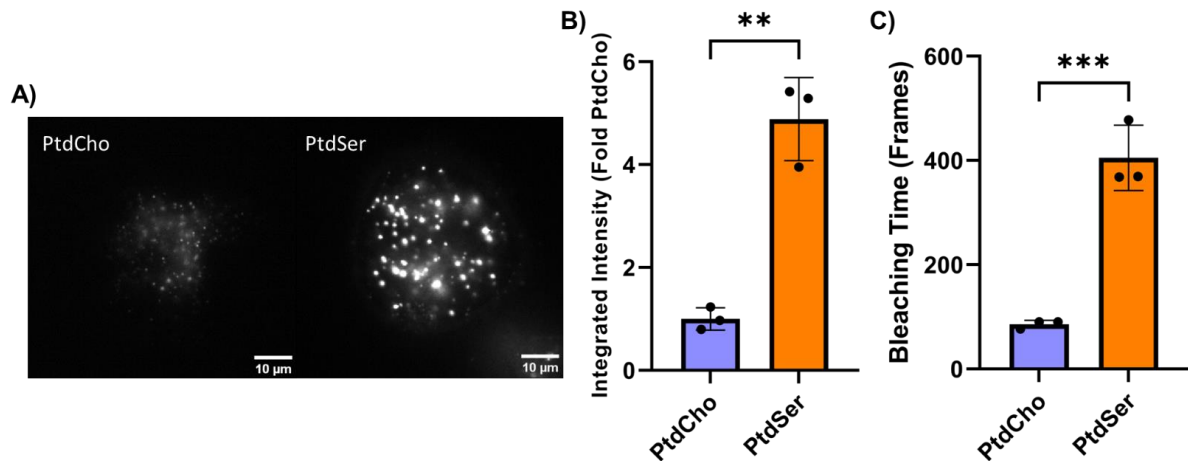
Figure 3.19: Continuous photobleaching assay to assess MERTK oligomerization during frustrated efferocytosis. THP-1 macrophages were immunolabelled for MERTK and parachuted onto serum-opsonized PtdSer-coated coverslips or PtdCho-coated control for 30 minutes to ensure maximal spreading. A 500-frame, high intensity image acquisition was used to completely the photobleach the sample. Integrated intensities at each immobilized cluster of MERTK were determined using FIJI. **A)** Representative images of MERTK clusters in macrophages interacting with PtdCho- and PtdSer-coated coverslips. **B)** Initial integrated intensity at the start of the photobleaching assay, normalized to the average intensity of MERTK in the PtdCho condition. **C)** Bleaching time expressed as the average number of frames required to reach background intensity for a cluster of MERTK. **B)** and **C)** are representative of three independent experiments comprised of 10-12 cells analyzed per replicate. Student's t-test was used to compare the PtdCho vs. PtdSer average. Error bars represent ± SD. ** $p < 0.0021$; *** $p < 0.0002$.

3.3   Development of a traction force microscopy assay

The observation that MERTK and β_2 integrin localize to different parts of the efferocytic synapse, and the preferential accumulation of actin with β_2 integrin, suggests that these receptors play different roles in efferocytosis. Combined with our signaling data obtained by prior members of our lab[107,197], I hypothesize that MERTK acts as a stimulating receptor that detects ACs, then triggers the activation of β_2 integrins to generate the forces required to engulf the cell. This is consistent with the known ability for β_2 integrins such as $\alpha_M\beta_2$ and $\alpha_X\beta_2$ to mediate phagocytosis and with the localization of β_2 integrins – but not MERTK – to the actin-dense edge of the efferocytic synapse. Indeed, actin polymerization at the leading edge of phagocytic synapses allows the membrane to wrap around a pathogen, with the observed increase in actin in the efferocytic synapse likely serving a similar role during the engulfment of ACs. This is a force-driven process, where compression from local branched-actin polymerization and contraction from myosin motor machinery help promote the internalization of the target[60,61]. Meanwhile, MERTK forms clusters that are evenly distributed throughout the synapse. MERTK could anchor the apoptotic cell into place, but are likely not involved in direct force generation like the integrins. In other words, MERTK is a coreceptor that initially activates β_2 integrins, with the latter serving as force transducers via their actin remodeling ability. To test this model, I began the development of a traction force microscopy (TFM) assay to study the forces generated by the efferocytic synapse. This experiment will provide definitive biomechanical support for MERTK's role as a stimulator for integrins during efferocytosis.

3.3.1   Overview of the 2D-TFM frustrated efferocytosis assay

Contractile forces during phagocytosis are routinely measured by two-dimensional traction force microscopy (2D-TFM) assays[82,96,236,237]. 2D-TFM involves the use of a thin polyacrylamide matrix that is polymerized on top of a glass bottom dish (Figure 3.20A). The gel is embedded with fluorescent beads that lie a few microns below the surface of the gel. Finally, the surface is opsonized with a ligand of choice using a chemical crosslinker[238]. Then, frustrated phagocytosis can be elicited by seeding macrophages onto
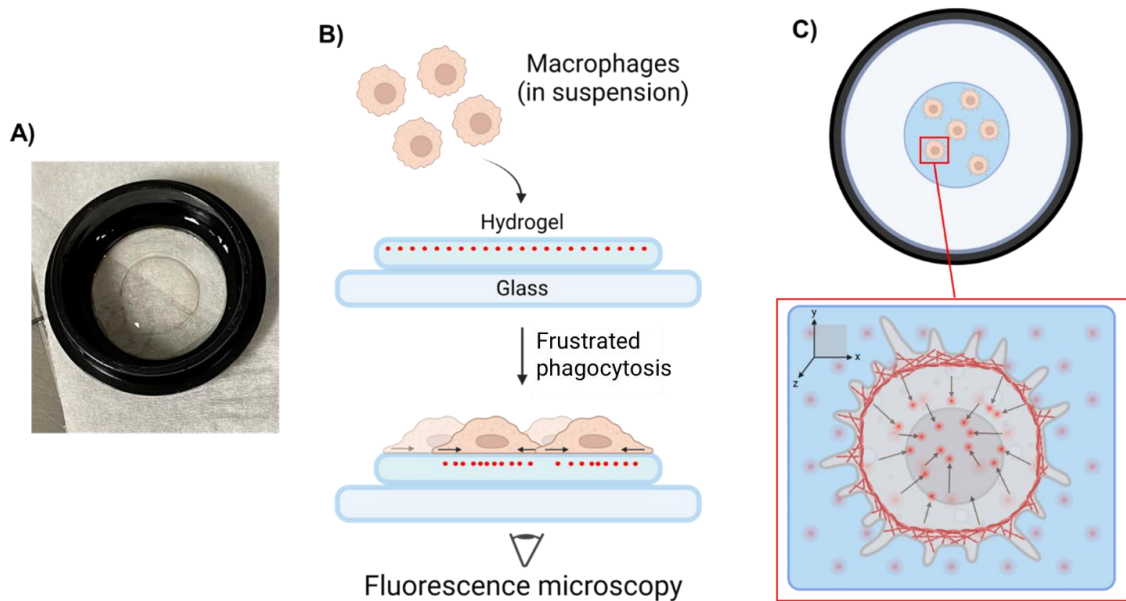
Figure 3.20: Overview of traction force microscopy. **A)** Polyacrylamide gel polymerized on top of a glass bottom dish. **B)** Macrophages are sedimented onto the opsonized gel to promote frustrated phagocytosis, which induces contractile forces that deform the underlying gel. The displacement of fluorescent beads are visualized using fluorescence microscopy. **C)** Top-down diagram of macrophages inducing contractile forces during frustrated phagocytosis. Figure produced with BioRender.

the substrate (Figure 3.20B). During frustrated phagocytosis, contractile forces mediated by the actinomyosin network induces local deformations within the gel, causing inwards displacement of the fluorescent beads (Figure 3.20C)[236,239]. A series of mathematical algorithms then generate a heat map that provides information on the magnitude and direction of the local forces[239,240].

To determine the relative roles of MERTK and integrins on force generation during efferocytosis, TFM gels will be opsonized with the MERTK ligand, Gas6, and the pan-efferocytic integrin opsonin MFG-E8. MFG-E8 is an extensively characterized opsonin that is recognized by multiple integrins known to mediate efferocytosis, including $\alpha_V\beta_3$, $\alpha_V\beta_5$, and members of the β_2 integrin family[219,241,242]. It is hypothesized that neither MERTK nor integrin activity alone are sufficient to initiate the formation of the efferocytic synapse, and thus no appreciable contractile force will be generated. When both MERTK and integrins are engaged on dual-opsonized gels, efferocytic synapse formation and force transduction is expected. This effect should be abrogated by chemical inhibition of MERTK's kinase activity, which prevents the integrin activation required for actin-remodeling. Given that integrins associate with actin in the efferocytic synapse, and that phagocytic forces are known to be produced by actinomyosin contraction, we expect all forces in the synapse to be generated by the integrins.

3.3.2   Production of Gas6 and MFG-E8

We initially planned on producing human Gas6 and MFG-E8 in-house to provide a large supply of these proteins for TFM. To accomplish this, streptavidin binding peptide(SBP)-tagged rhGas6 and rhMFG-E8 were cloned into pLVX-Puro or pLVX-ZsGreen lentiviral vectors and stably transduced into HeLa cells. HeLa cells were used as they are easy to transduce, express high levels of protein, and unlike bacterial expression systems – they contain the enzymes required for the glycosylation of both proteins[148,243] and the vitamin K-dependent carboxylation of Gas6[145], which are required for these protein's function. Moreover, the use of a mammalian cell line reduces the concern for endotoxin contamination compared to a bacterial expression system. rhGas6- and rhMFG-E8-ZsGreen cell lines were successfully generated by FACS-sorting of the top 3% brightest cells (Figure 3.21). rhGas6- and rhMFG-E8-Puro cell lines were generated by puromycin
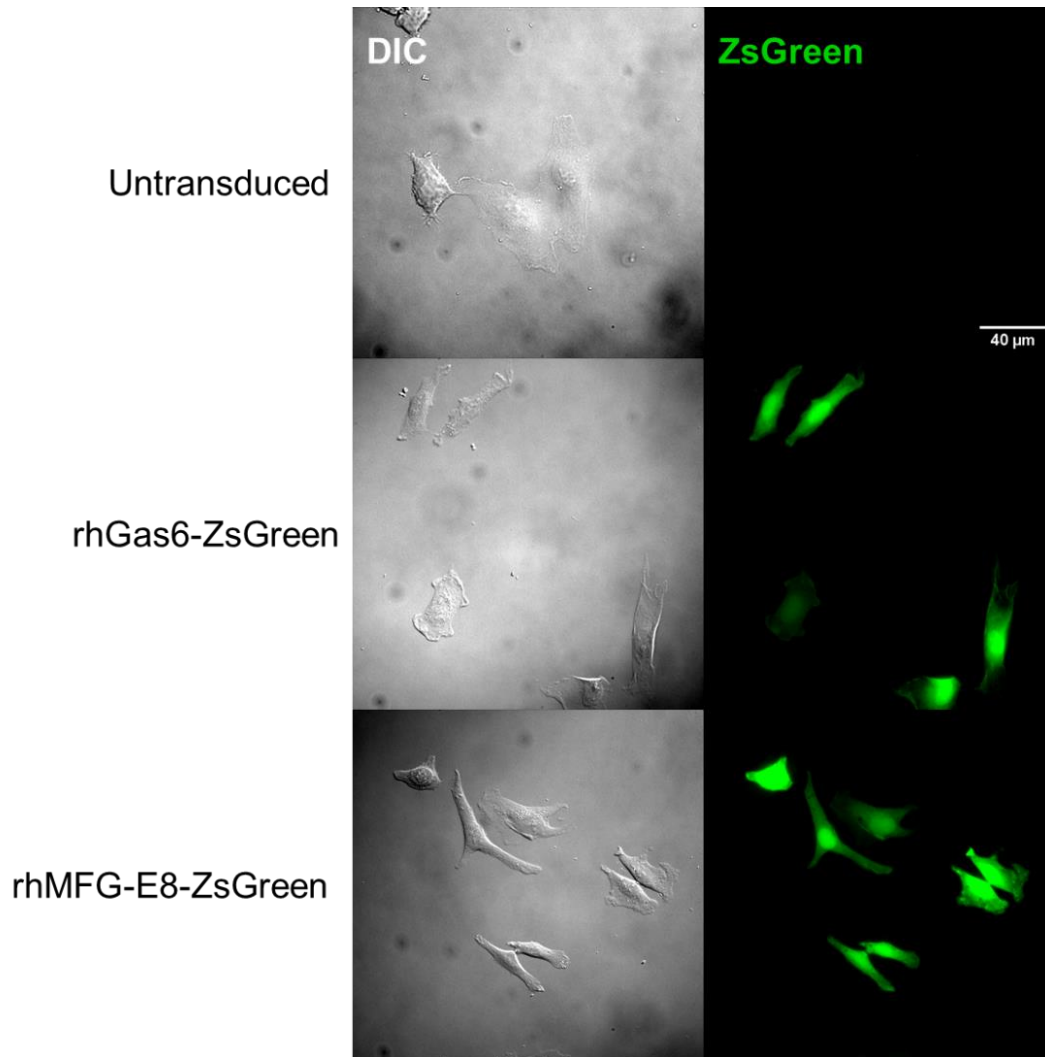
Figure 3.21: FACS-sorted rhGas6-ZsGreen and rhMFG-E8-ZsGreen HeLa cell lines visualized by fluorescence microscopy. The top 3% brightest cells were FACS-sorted at the London Regional Flow Cytometry Facility by Dr. Kristin Chadwick. Cells were visualized using fluorescence microscopy to confirm ZsGreen expression. Scale bar is 40 μm.

selection. All four cell lines secreted the expected proteins into media (Figure 3.22). The puromycin-selected cell lines showed higher Gas6 and MFG-E8 secretion than the ZsGreen-sorted cell lines, and thus were used for subsequent protein isolation. rhGas6 and rhMFG-E8 were collected from supernatants and purified by column chromatography with a streptavidin-agarose resin. Coomassie staining showed successful purification of Gas6 (Figure 3.23A), which was further supported by western blot (Figure 3.23B). However, purification of MFG-E8 was unsuccessful. A Bradford assay determined the Gas6 concentration to be 15 μg/mL. MFG-E8 could not be successfully purified in-house, and the concentration of purified rhGas6 after column chromatography was too low to be used for future experiments. Thus, rhGas6 and rhMFG-E8 were purchased from R&D Systems and reconstituted at 75 μg/mL in PBS.

3.3.3   Production of polyacrylamide substrates for TFM

Circular polyacrylamide gels with a shear modulus (stiffness) of 4.069 kPa were produced on glass bottom dishes (Table 1). This particular stiffness has been used in previous TFM studies of integrin-mediated phagocytosis[82]. Fluorescence microscopy was used to visualize the fluorescent beads embedded within the gel, revealing adequate bead density with no aggregates (Figure 3.24). Chemical crosslinking of Gas6 and MFG-E8 to the surface of the gel was confirmed by immunofluorescence staining (Figure 3.25).

THP-1 macrophages were parachuted onto Gas6- or MFG-E8 opsonized gels and incubated for 1 hr, and the resulting synapse was visualized. Importantly, cells failed to adhere to gels that were not opsonized (data not shown). Macrophages readily adhered with gels opsonized with Gas6 or MFG-E8, indicating that opsonization was successful. Gas6-opsonized gels failed to elicit synapse expansion (Figure 3.26A), whereas MFG-E8-opsonized gels caused a small cellular response characterized by a modest increase in cell diameter, but unlike synapse formation, this increase in cell diameter reduced the circularity of the cell (Figure 3.26B). This drop in circularity was due to the formation of filopodia (Figure 3.26A). We reasoned that the concentration of MFG-E8 was high enough to induce "outside-in" activation of the integrins without the need for "inside-out" signaling by other stimulating receptors such as MERTK, thus forming filopodia due to forced activation of the integrins, which are known to localize to filopodial tips to drive
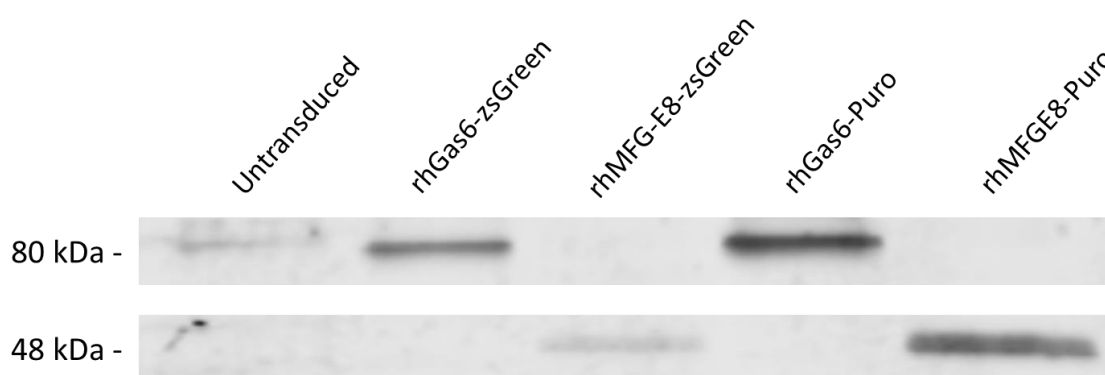
Figure 3.22: Western blot of rhGas6-SBP and rhMFG-E8-SBP secreted into media. Untransduced, rhGas6, and rhMFG-E8 HeLa cell lines were seeded onto 6 well plates and serum-starved to induce protein secretion. 10 μg of protein from the supernatant was separated on a 16% SDS-PAGE gel and transferred onto a nitrocellulose membrane. The membrane was blotted with anti-SBP-tag antibody and fluorescent secondary antibody, then imaged using the LI-COR Odyssey fluorescence imaging system. Colour, contrast, and brightness were edited using Image Studio.
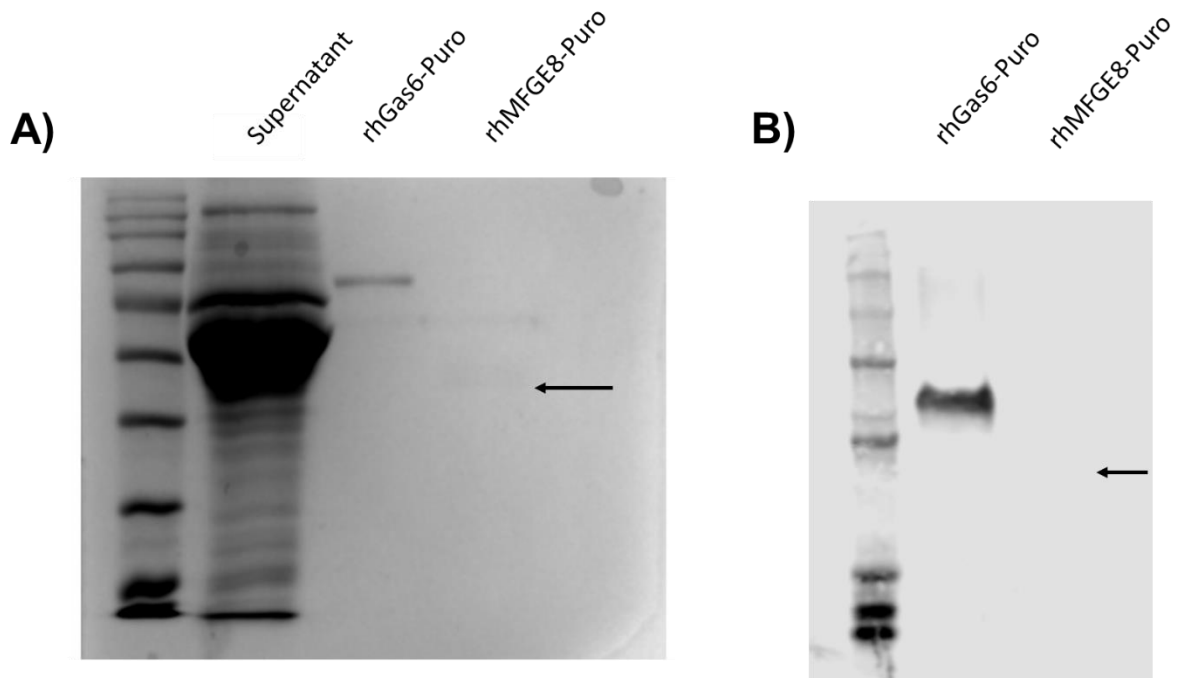
Figure 3.23: Purification of rhGas6-SBP and rhMFG-E8-SBP. Supernatant from rhGas6- and rhMFG-E8 HeLa cells were purified by column chromatography with a streptavidin agarose resin. 30 µL of concentrated samples were run on a 12% SDS-PAGE gel followed by **A)** Coomassie staining and **B)** western blot using anti-SBP antibody. The expected size of rhMFGE8 is indicated with arrows.

Table 1: Polyacrylamide mixture to produce Shear Modulus (G) = 4.069 kPa gels. PBS, acrylamide, bis-acrylamide, and ddH$_2$O are mixed and degassed for 20 minutes prior to addition of FluoSpheres, APS, and TEMED. The FluoSpheres, APS, and TEMED are diluted in ddH$_2$O. The shear modulus for this formulation has been calculated by bulk rheology from others[244,245].

10X PBS	40% acrylamide	2% bis-acrylamide	ddH$_2$O	1:100 FluoSpheres	3% APS	5% TEMED
20 μL	37.5 μL	15 μL	113.5 μL	6 μL	4 μL	4 μL
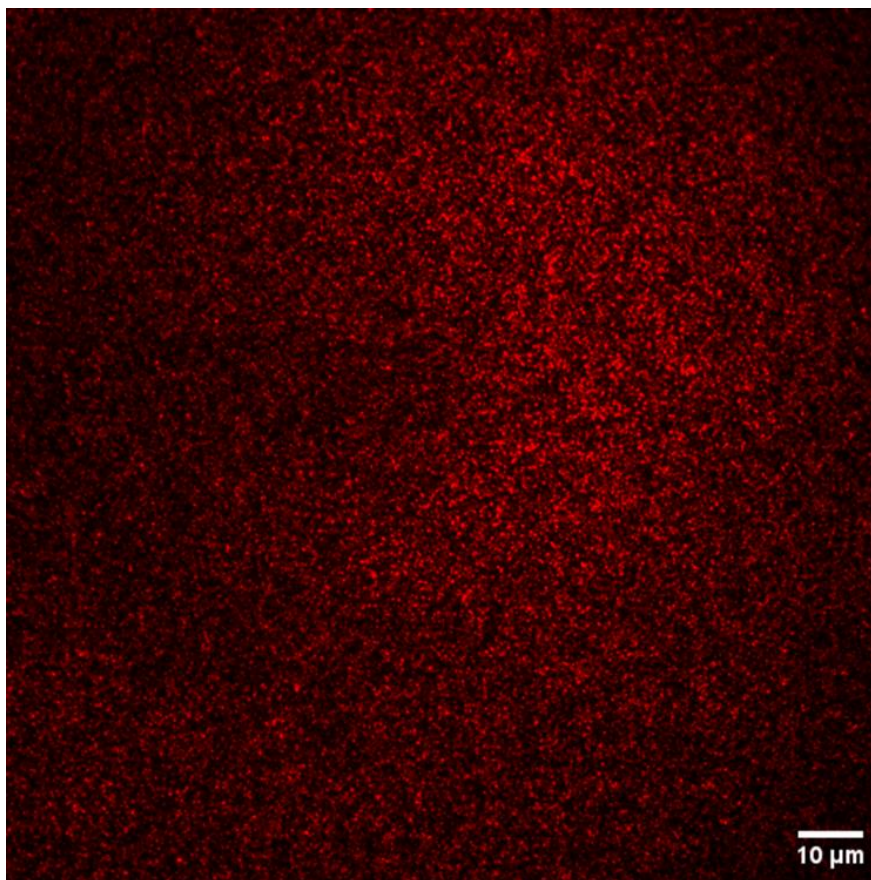
Figure 3.24: FluoSpheres embedded within polyacrylamide. Fluorescent beads were visualized with fluorescence microscopy at 100× magnification. Scale bar is 10 μm.
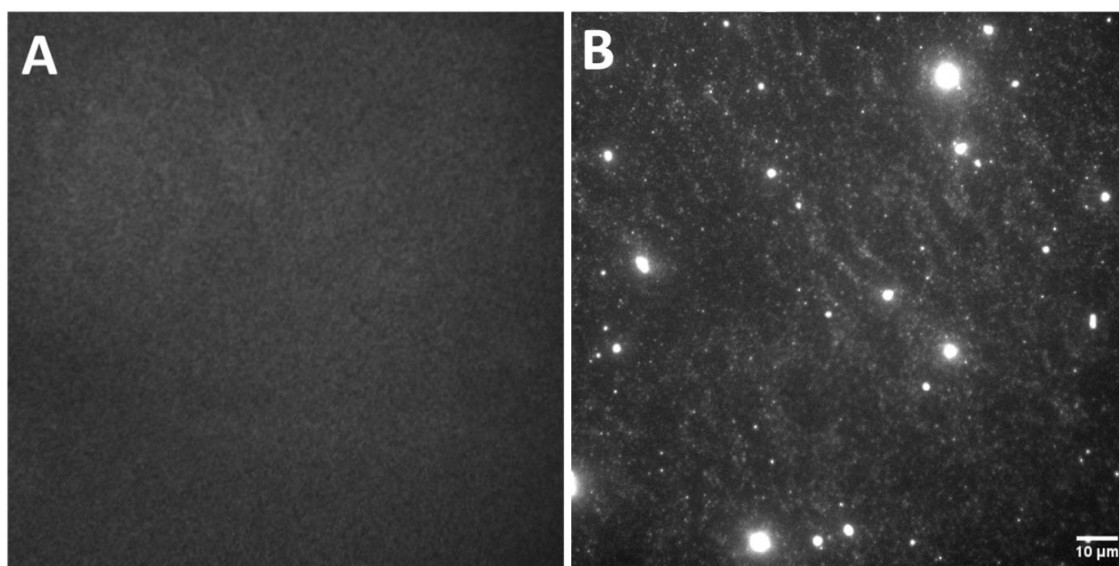
Figure 3.25: Opsonization of polyacrylamide with Gas6 and MFG-E8 visualized by fluorescence microscopy. Polyacrylamide gels were crosslinked with 15 μg/mL Gas6 and 15 μg/mL MFG-E8 using UV-activated Sulfo-SANPAH. Gels were blocked with 1 mg/mL glycine and then immunostained for the His6-tag on Gas6 and MFG-E8, and the surface of the gel was visualized by fluorescence microscopy at 100× magnification. **A)** His6 staining of a negative control (non-opsonized gel); **B)** His6 staining of a Gas6/MFG-E8 opsonized gel. To ensure equivalent staining and visualization, the gels in panels A and B were stained using the same staining buffers and imaged using the same acquisition settings. Scale bar is 10 μm.

Figure 3.26: Synapse analysis of macrophages adhered to Gas6-opsonized and MFG-E8 opsonized gels. Polyacrylamide gels with a shear modulus of 4.069 kPa were opsonized with 15 μg/mL Gas6 or 15 μg/mL MFG-E8, then THP-1 macrophages were seeded onto the gel for 1 hr. The resulting synapse was visualized by DIC microscopy. **A)** Representative images of macrophages adhered to Gas6- and MFG-E8 opsonized gels. **B)** Feret's diameter, area, perimeter, and circularity value of the synapse determined by manual ROIs drawn around the synapse using FIJI. Data are representative of 10 cells per condition from one experimental replicate. Scale bars are 10 μm.

their extension[246]. For future experiments, the MFG-E8 concentration was reduced to a level at which filopodia formation was no longer detectable. Nonetheless, the efferocytic synapse was not observed on either of the mono-opsonized gels, suggesting that neither MERTK nor integrins are sufficient for efferocytic synapse formation.

3.3.4   Frustrated efferocytosis on TFM gels and force reconstruction

Polyacrylamide gels with a stiffness of 4.069 kPa were opsonized with 15 µg/mL Gas6, 11.25 µg/mL MFG-E8, or dual-opsonized with Gas6 and MFG-E8. THP-1 macrophages adhered to Gas6- and MFG-E8-opsonized gels, but did not spread to form the efferocytic synapse (Figure 3.27, top left and top right panel). When dual-opsonized with Gas6 and MFG-E8, TFM substrates supported the formation of efferocytic synapses similar in morphology to those observed in previous experiments (Figure 3.27, bottom left panel). The spreading of the synapse was abrogated by the MERTK inhibitor UNC2250, a type II kinase inhibitor that traps the kinase domain of MERTK in an inactive conformation[234] (Figure 3.27, bottom right panel), with UNC2250-treated cells on dual-opsonized substrates showing no difference from cells adhered to Gas6- or MFG-E8 mono-opsonized gels (Figure 3.28). These data support that the activity of both MERTK and integrins are simultaneously required for the spreading of the efferocytic synapse.

To confirm that the integrins are responsible for driving force transduction during efferocytosis, we attempted to calculate the traction stresses that were induced by the synapse. It has been previously reported that contractile force is concentrated at the outer boundary of the phagocytic synapse measured by 2D-TFM[237] and at the actin-enriched forefront of phagocytic cups by 3D-TFM[60,61]. Thus, it was expected that contractile force would be highest at the periphery of the efferocytic synapse, where integrins and F-actin were localized. However, all attempts at measuring cellular traction force were unsuccessful. Despite efferocytic synapse formation, underlying bead displacement was minimal, resulting in undetectable displacement above background levels (Figure 3.29). Numerous optimizations were attempted, including changing of gel stiffness and attempts to move the beads closer to the gel surface – all without success (data not shown). Attempts to measure forces in a TFM model of classical FcγR-mediated phagocytosis
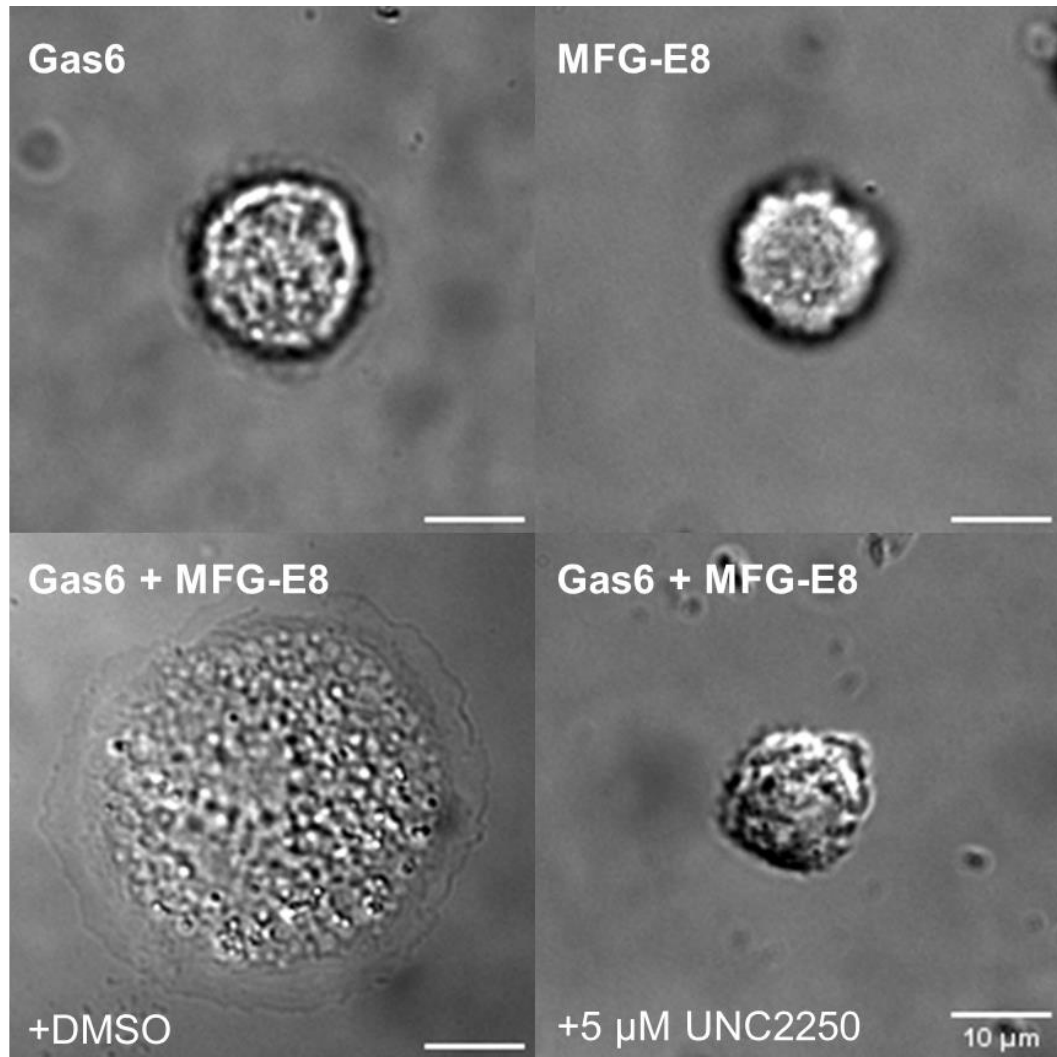
Figure 3.27: Efferocytic synapse formation on polyacrylamide requires the **simultaneous activity of MERTK and efferocytic integrins.** Polyacrylamide gels with a shear modulus of 4.069 kPa were opsonized with 15 µg/mL Gas6, 11.25 µg/mL MFG-E8, or 15 µg/mL Gas6 + 11.25 µg/mL MFG-E8. THP-1 macrophages were seeded onto the gel for 1 hr before imaging with DIC microscopy. In the Gas6 + MFG-E8 condition, cells were treated with 5 µM UNC2250 for the duration of the experiment or with DMSO control. Scale bars are 10 µm.
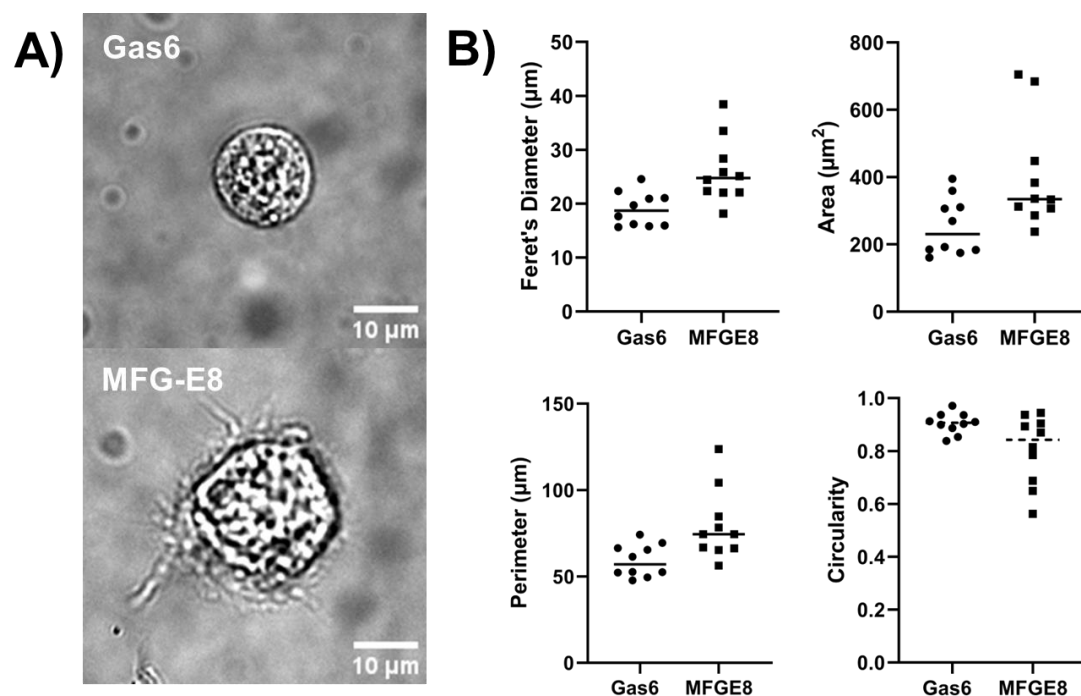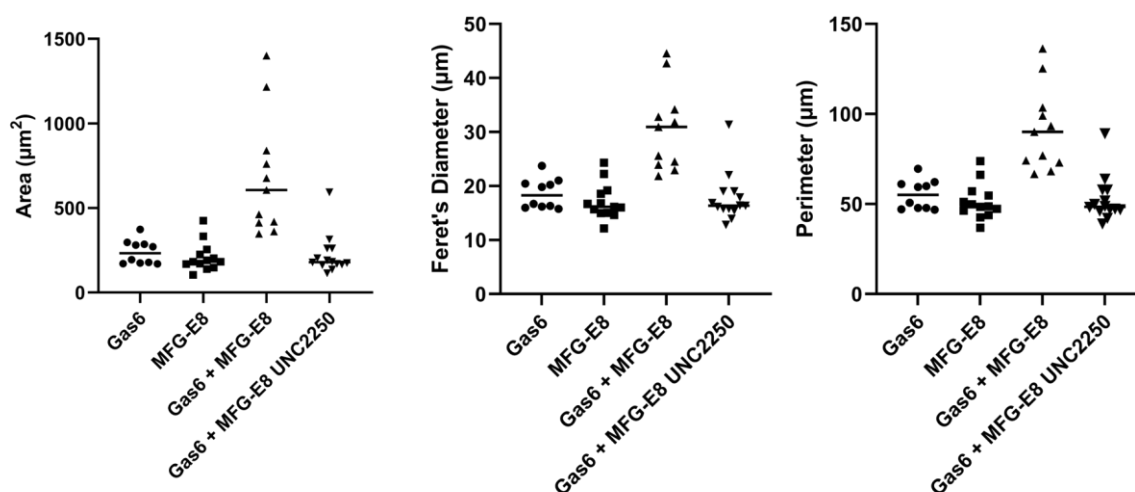
Figure 3.28: Synapse analysis of macrophages adhered to Gas6-, MFG-E8- or Gas6 + MFG-E8-opsonized gels. Polyacrylamide gels with a shear modulus of 4.069 kPa were opsonized with 15 μg/mL Gas6, 11.25 μg/mL MFG-E8, or 15 μg/mL Gas6 + 11.25 μg/mL MFG-E8. THP-1 macrophages were seeded onto the gel for 1 hr. The resulting synapse was visualized by DIC microscopy. The synapse area, diameter, and perimeter were determined by manual ROIs drawn around the synapse using FIJI. Data are representative of at least 10-14 cells per condition from one experimental replicate.
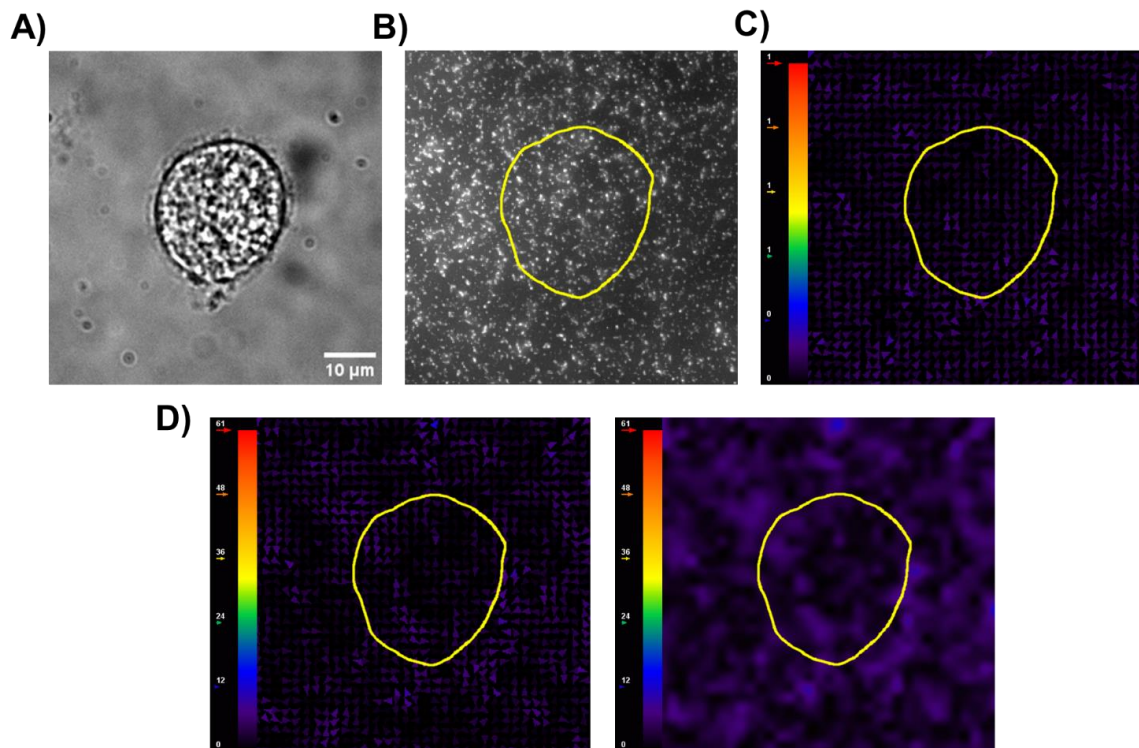
Figure 3.29: Traction forces were undetectable. THP-1 macrophages were sedimented on Gas6 + MFG-E8-dual opsonized polyacrylamide gels with a shear modulus of 4.069 kPa. A) The efferocytic synapse visualized using DIC. B) Maximum intensity projection of fluorescent beads underlying the synapse. C) Displacement vector-map calculated by the PIV algorithm. Scale represents displacement in pixels. D) Force vector map (left) and force magnitude map (right) determined by the FTTC algorithm. Scale represents local stress in Pascal. Cellular forces could not be detected above background.

using RAW264.7 macrophages, a cell line previously used by others in TFM experiments[82], also failed to produce measurable bead displacement (data not shown). This suggests that our issues were intrinsic to our gels, rather than with our cells. We are currently seeking a collaborator who has the capability of performing bulk rheology to verify gel stiffness, and we are also looking at other procedures such as direct functionalization of the gel surface with fluorescent beads. Unfortunately, these optimizations could not be completed on-time for submission of this thesis. However, the successful optimization of bead density, gel opsonization, confirmation of synapse formation, and establishment of the TFM analysis pipeline, will ensure that these experiments can be quickly completed once the gel rheology issues are addressed.

Chapter 4 - Discussion

4.1 Rationale and summary of results

MERTK is the predominant efferocytic receptor in multiple tissues including the heart and eyes. Mutations in MERTK and its opsonins predispose individuals to a range of diseases including chronic inflammatory disorders such as atherosclerosis[171], autoimmune diseases such as multiple sclerosis[174] and SLE[172,173], and to degenerative disorders including retinitis pigmentosa[167,168]. Despite its importance, the signaling mechanism used by MERTK during the engulfment of ACs is largely unknown. We had recently discovered a signaling pathway through which MERTK activates β_2 integrins, and demonstrated that this activation was required and sufficient for MERTK-dependent efferocytosis by human macrophages[107,197]. Based on these data, we hypothesized that MERTK is a stimulating receptor that does not induce actin polymerization directly, and that the β_2 integrins serve as engulfment receptors that induce the actin polymerization required for AC engulfment. To provide biomechanical support for this model, the structure and dynamics of the efferocytic synapse were investigated by fluorescence microscopy.

Using frustrated efferocytosis assays, I determined that β_2 integrins form an expanding ring-like structure near the periphery of the efferocytic synapse that colocalizes with a ring of F-actin. In contrast, MERTK formed discrete clusters that were distributed throughout the synapse. These data suggest that the β_2 integrins may be responsible for actin polymerization during efferocytosis. SPT experiments revealed that the diffusion of β_2 integrins were highly confined during frustrated efferocytosis, as expected by its interlinkage with actin. MERTK diffused more freely, consistent with its localization within the actin-depleted centre of the synapse. Paradoxically, MERTK diffusion became more confined as the synapse expanded. Photobleaching assays revealed that MERTK oligomerizes during frustrated efferocytosis, which may represent ligand-induced oligomerization, thus accounting for the increase in MERTK diffusional trapping. Finally, we began the development of a 2D-TFM assay to elucidate the relative roles of MERTK and integrins in generating engulfment forces during efferocytosis. Strikingly, neither MERTK nor the integrins were sufficient to elicit frustrated efferocytosis on

Gas6- or MFG-E8-opsonized hydrogels, respectively. The efferocytic synapse could only be formed on Gas6/MFG-E8 dual-opsonized gels, with this effect abrogated by inhibition of MERTK's kinase activity.

4.2   The structure of the efferocytic synapse

Previous studies demonstrated that several canonical phagocytic pathways were utilized by MERTK to mediate efferocytosis, including PI3K, Grb2, SFKs, and Vav3[94,138]. These results have provided only a partial view of the MERTK signaling pathway, and did not demonstrate how MERTK could interact with and regulate integrins. Our lab previously showed that the MERTK:β_2 integrin axis was necessary for efferocytosis in THP-1 macrophages[197], with immunoprecipitations and FRET assays confirming that MERTK activates β_2 integrins via a PI3K-, FAK-, and ILK-dependent mechanism[107,197]. MERTK, SFKs, PI3K, FAK, ILK, and SYK were required for efferocytosis of AC-mimicking beads. Initial frustrated efferocytosis assays showed that all of these molecules, except for SYK, were required for spreading of the synapse. These data suggested that MERTK is a stimulating receptor for the β_2 integrins – with this activation necessary for the engulfment process. Further biomechanical support was required to confirm this model. Thus, the localization of MERTK, β_2 integrins, and F-actin within the frustrated efferocytic synapse was determined by fluorescence microscopy.

4.2.1   The role of β_2 integrins at the periphery of the efferocytic synapse

On 2D surfaces, phagocytic processes typically form a ring-like synapse regardless of the ligand or phagocytic receptors involved[82,96,97,116,237]. In at least some cases, integrins form an outer edge of this structure where they provide binding, mediate actin polymerization, or act as a diffusion barrier that limits the entry of inhibitory receptors into the synapse[82,97]. Thus, our observations of an outer-ring structure of β_2 integrins that were localized at the periphery of the synapse was not unexpected. In our assays, β_2 integrins colocalized with an outer-ring of F-actin during the spreading phase of frustrated efferocytosis, which was also previously observed in models of frustrated FcγR-mediated phagocytosis[97]. This ring of integrins may play a bifunctional role during engulfment, through providing 1) the actin polymerization and mechanical force required for

membrane protrusion, and 2) exclusion of the highly glycosylated inhibitory proteins such as CD45 from the synapse.

Foremost, β_2 integrins likely induce the local polymerization of actin via their intrinsic ability to stimulate Rac1 and Cdc42 through SFK:FAK and SYK-dependent mechanisms[57,70,72,247,248]. This promotes WASP/N-WASP and SCAR/WAVE activity and subsequent ARP2/3-mediated branched actin polymerization[55], driving the radial spreading of the plasma membrane during frustrated phagocytosis[82,96]. Furthermore, during frustrated phagocytosis and during the engulfment of complement opsonized beads, $\alpha_M\beta_2$ is known to recruit formins such as mDia1 just behind the ARP2/3-enriched leading edge, which drives linear actin polymerization that enhances the coupling of the membrane to the target[82]. The intrinsic ability of integrins to stimulate branched and linear actin polymerization causes the protrusion of the plasma membrane during phagocytosis, and likely plays a similar role in efferocytosis. The β_2 integrin:F-actin ring-like structure we observed during frustrated efferocytosis is similar to what has been observed during frustrated phagocytosis on glass coverslips[97], suggesting this structure is a conserved feature of phagocytosis regardless of the ligand or whether free diffusion is permitted on the surface of the target. Finally, integrin:F-actin rings have also been observed at the advancing edges of phagocytic cups during the engulfment of three-dimensional phagocytic targets[121]. Therefore, β_2 integrins likely localize to the edge of the forming phagocytic cup to drive actin polymerization and produce the membrane protrusions required to extend the phagocytic/efferocytic cup around the target.

Secondly, the β_2 integrin:F-actin ring-like structure has been known to cause selective exclusion of the glycocalyx during phagocytosis[97]. Here, the ring forms a diffusional barrier that pushes tall, bulky glycoproteins such as CD45 and CD148 out of the expanding synapse and prevents their re-entry[97]. CD45 and CD148 possess cytoplasmic tyrosine phosphatase domains that inhibit SFKs downstream of phagocytic receptors such as FcγR and Dectin-1[97,100]. Furthermore, it is likely that the β_2-ring excludes other glycoproteins such as the mucins and CD43 from the phagocytic synapse; thereby counteracting steric occlusion and electrostatic repulsion from the glycocalyx that would otherwise inhibit phagocytic receptor ligation with the target[235]. During Fc-mediated

phagocytosis, inside-out activation of β_2 integrins by FcγRs was reported to be essential for the formation of the integrin diffusional barrier[97]. This was dependent on PLCγ activation downstream of the FcγRs, which subsequently induces DAG-mediated activation of the GTPase Rap1[82,97]. Rap1 can recruit adaptor proteins such as Rap1-GTP-interacting adaptor molecule (RIAM) to the β_2 cytoplasmic tail, promoting the extended (high affinity/active) conformation of the integrin[249]. Upon integrin activation, the extension of its extracellular domain and subsequent binding to ligands on the phagocytic target sets a size-exclusion threshold, where taller glycoproteins are pushed out from the forming phagocytic synapse whereas the shorter phagocytic receptors are retained[55,97]. It is possible that a similar mechanism takes place during efferocytosis; however, we must confirm this by performing additional frustrated efferocytosis assays where the inhibitory glycoproteins are labeled. We must also determine why MERTK – a large heavily glycosylated transmembrane protein – is not excluded from the efferocytic synapse like other large glycoproteins.

If the glycocalyx exclusion model holds true for MERTK, we would expect that the β_2 integrin ring would exclude inhibitory receptors such as SIRPα. Interestingly, Morrissey *et al*. investigated the exclusion dynamics of SIRPα during the engulfment of IgG-opsonized PtdSer-coated beads[105]. This produces a hybrid phagocytic/efferocytic cup engaged by FcγRs and PtdSer receptors, which models the engulfment of IgG-opsonized apoptotic cancer cells. They discovered that unligated SIRPα was excluded from the phagocytic cup, while CD47-ligated SIRPα remained within the cup. SIRPα within the cup inhibited the inside-out activation of $\alpha_M\beta_2$, thereby preventing actin polymerization and engulfment of the target. Forcible activation of the integrins with Mn^{2+} bypassed the inhibitory effect of CD47 to restore phagocytosis[105]. It would be interesting if we can recapitulate these findings in our frustrated efferocytosis model, where we expect to observe the exclusion of SIRPα from the efferocytic synapse. If receptor ligation is sufficient to prevent integrin-dependent exclusion, this phenomenon could also explain why MERTK is retained in the centre of the efferocytic synapse.

4.2.2   The role of MERTK within the centre of the efferocytic synapse

Preliminary work from our lab showed that MERTK and β_2 integrins are colocalized in small clusters on both the apical and basolateral surfaces of THP-1 macrophages[229]. The presence of these clusters on the apical surface implies the presence of pre-formed signalosomes, where MERTK can immediately activate the β_2 integrins upon ligation of an apoptotic cell. Remarkably, while we observed a similar colocalization early in synapse formation, we observed a clear spatial separation between MERTK and β_2 integrins as the synapse matured. MERTK's distribution throughout the actin-depleted centre of the synapse suggests it is not involved in direct actin nucleation, which although consistent with our hypothesis that MERTK acts as a stimulating receptor, leaves the role of MERTK in the mature synapse unclear and subject to speculation.

In the early synapse, we previously showed that MERTK activates the β_2 integrins through a PI3K/ILK/FAK-dependent mechanism[107,197]. Upon their activation, the integrins bind to the AC, with the resulting outside-in signaling then driving local actin polymerization to mediate the expansion of the synapse via the F-actin ring-like structure at the synapse edge. This structure may facilitate the "zippering" of MERTK onto the substrate by forming the glycocalyx exclusionary zone, likely in a similar manner to FcγRs during IgG-induced frustrated phagocytosis[97] – however, given the aforementioned conflicting data with this model, this possibility must be tested in future frustrated efferocytosis experiments.

Whether MERTK sustains the integrin activation state after their spatial separation from the β_2 integrins is not clear. It is possible that integrin activation is self- sustaining, as outside-in signaling could reinforce the integrin-mediated actin polymerization and maintain the extended conformational state[225]. Alternatively, MERTK could still play an active role in sustaining β_2 integrin activation throughout the entirety of engulfment. This would have to occur through a membrane-diffusible mediator due to MERTK's spatial separation from the integrins. This is unlikely to occur through PI3K, as PIP$_3$ is absent from the periphery of phagocytic cups[85]. However, as MERTK is an activator of PLCγ[94,198], it possible that DAG laterally diffuses to activate Rap1[97,250], thereby maintaining the integrin activation state. Indeed, $\alpha_M\beta_2$ integrin activation was reported to

be sustained well beyond the site of FcγR engagement in frustrated phagocytic cups, with DAG found to be the diffusible mediator responsible for this effect[97]. To confirm if MERTK is required to sustain β_2 integrin activation, future studies could inhibit MERTK midway through frustrated efferocytosis, followed by FRET analysis to measure the resulting conformational changes in the integrins. We must also confirm if the PLCγ/DAG/Rap1 pathway is required for MERTK-dependent integrin activation using chemical inhibitors or siRNA. We expect that the combined activity of PI3K and PLCγ are required for initial integrin activation by MERTK, while PLCγ alone sustains the integrin activation state. To test this, we can express protein-based fluorescent probes[85,251] specific for PIP_3 and DAG to visualize their localization relative to MERTK and β_2 integrins within the efferocytic cup.

The distribution of MERTK within the actin-depleted centre of the frustrated synapse can be likened to the base of the efferocytic cup in 3D space. Indeed, MERTK was also previously observed to localize at the base of efferocytic cups in RPE cells[121]. Here, actin is cleared to promote the invagination of the cup[55]. Thus, an underappreciated role of MERTK may be local actin disassembly, rather than actin polymerization as suggested by others. Lipid signaling is probably crucial for this process. Foremost, the MERTK-induced production of PIP_3 and DAG via PI3K and PLCγ respectively should locally alleviate the $PI(4,5)P_2$-mediated sequestration of actin disassembly proteins gelsolin and cofilin[55,252]. The PIP_3-enriched base of the cup should also promote the activity of RhoA, which inhibits actin polymerization by attenuating the activity of actin nucleation proteins[78]. In the future, we plan on imaging the efferocytic cup in 3D space. This could be accomplished by incubating macrophages with ACs, followed by confocal focus stacking and 3D reconstruction. We expect to observe the clustering of MERTK within the actin-depleted base, where it contributes to the formation of a PIP_3-enriched central "pit", whereas the β_2 integrins are located at the $PI(4,5)P_2$-enriched outer "rim", where local actin polymerization occurs to advance the membrane over the target (Figure 4.1).
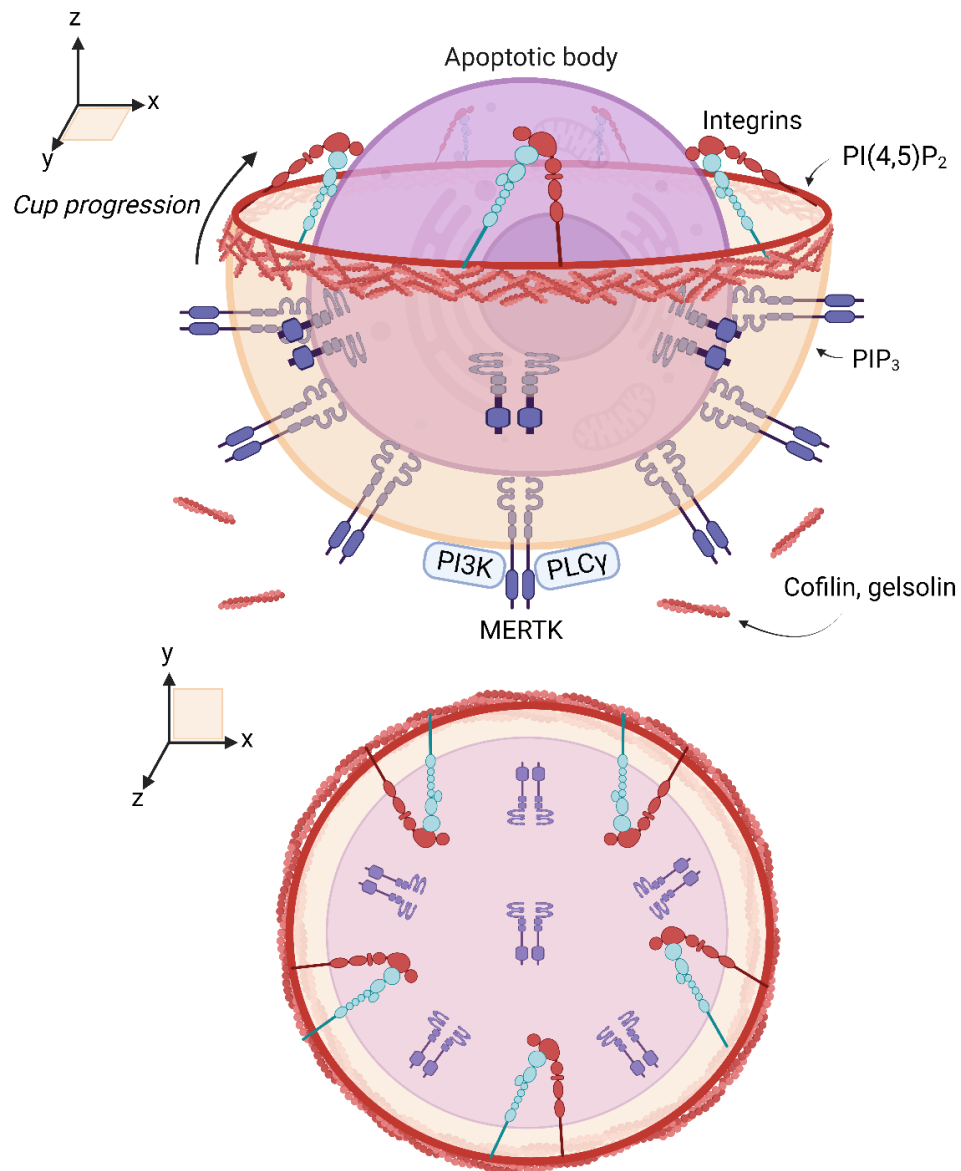
Figure 4.1: Hypothesized structure of the efferocytic cup in 3D space. MERTK is distributed throughout the base of the cup, where it activates PI3K and PLCγ to deplete PI(4,5)P$_2$. This forms a PIP$_3$-enriched pit that promotes the activity of actin-severing proteins cofilin and gelsolin. Integrins reside at PI(4,5)P$_2$-enriched rim of the efferocytic cup, where actin polymerization occurs to drive the progression of the membrane over the apoptotic body. Figure produced with BioRender.

4.3   Diffusional dynamics of MERTK and β_2 integrins

SPT provided high-resolution spatiotemporal information on the diffusional dynamics of MERTK and β_2 integrins during frustrated efferocytosis. These data demonstrated a clear dichotomy in the diffusive behaviour between these two receptors within the efferocytic synapse. Nearly 90% of β_2 integrins underwent confined diffusion throughout the entire synapse formation process. Furthermore, the slow diffusion rate and small confinement area suggested the integrins were highly restricted in their motion, which remained unchanged as the efferocytic synapse matured over time. These data are consistent with a stable mechanical linkage between the β_2 integrins and the actin cytoskeleton. This corroborates with prior literature, where just over 80% of $\alpha_M\beta_2$ was reported to be immobilized on the surface of non-activated murine macrophages[253]. Interestingly, FcγR-mediated inside-out activation was reported to transiently increase the free diffusion of $\alpha_M\beta_2$, which is believed to mobilize the integrins to promote their clustering and localization towards the phagocytic cup[253]. However, after ligation, FAK promotes the recruitment of talin and vinculin to tether the integrins to the actin cytoskeleton, effectively immobilizing it once more[54,254]. As we did not observe a transient increase in free diffusion at the beginning of frustrated efferocytosis, this suggests that the integrins have already been activated and linked with F-actin at the start of acquisition. Our diffusional analysis provides further biomechanical support for the β_2 integrins as engulfment receptors, which localize towards stable actin structures. To confirm that the immobilization effect is specific to actin, rather than other structures of the cytoskeleton, future experiments could involve the addition of latrunculin or cytochalasin, which disrupts F-actin assembly[255]. We expect that integrin immobilization should largely be abrogated upon disruption of the actin cytoskeleton[255].

In contrast, our SPT data showed that only 60% of MERTK was confined at the start of frustrated efferocytosis. We initially expected that the proportion of freely diffusive MERTK would increase due to the clearance of F-actin at the centre of the efferocytic synapse. Indeed, the significant increase in diffusion rate and in confinement size suggested that the diffusional constraint against MERTK was being alleviated as the synapse matured. Paradoxically however, the proportion of MERTK that underwent

confined diffusion significantly increased as the synapse formed, despite the clearance of actin from regions containing MERTK. We propose that oligomerization-induced trapping is responsible for this effect, supported by our continuous photobleaching experiments[113]. On a per-cluster basis, MERTK took nearly four-fold longer to photobleach within the efferocytic synapse compared to non-efferocytosing macrophages, indicative of larger cluster size. This effect was likely specific to efferocytosis rather than ligation to soluble Gas6 or ProS, as macrophages in the negative control were exposed to the same opsonin-containing media. However, discrete fusion events between individual clusters of MERTK were not observed, likely because image acquisition took place in 2 minute intervals, with each acquisition lasting only 3 seconds. Thus, oligomerization likely occurred stochastically throughout synapse formation, and most fusion events likely occurred between the time intervals.

Further work is needed to support the oligomerization-induced trapping hypothesis. Foremost, it would be interesting to perform a correlational analysis between the brightness of each fluorescent cluster with respect to its diffusive behaviour. It is expected that the brightest clusters will exhibit the greatest degree of immobilization, due to the greater steric hindrance with lipids and other proteins in the membrane, and due to increased avidity of the interaction between MERTK and its ligands on the efferocytic target. We must also measure the size of each cluster during efferocytosis to obtain visual evidence of oligomerization. As the clusters are expected to be below the resolution limit of our conventional microscope, super-resolution techniques will be required for accurate measurement of cluster size. Previously, our lab determined that human MERTK is pre-clustered in its unstimulated state, with an average cluster radius of 80-100 nm measured by ground-state depletion super-resolution microscopy[137]. However, ground-state depletion is a fixed-cell imaging technique that involves a harsh sample preparation protocol. Our initial attempts at paraformaldehyde fixation on the supported lipid bilayer were unsuccessful as the macrophages would not remain adhered to the surface (data not shown). Chemical fixation after frustrated phagocytosis on glass is commonly performed by others[96], suggesting the bilayer in our assay may have interfered with the fixation process. Although our SRRF approach has the resolution to image these clusters[230,256], the movement of the clusters during image acquisition resulted in motion artefacts that

artificially increased the apparent size of the clusters. Our recent acquisition of a stimulated emission depletion (STED) microscope, which can achieve resolutions >100 nm in live cells, may enable these experiments[257,258]. In future experiments, we can measure MERTK's cluster size from the expected 80-100 nm radius in the initial state, which may progressively increase during frustrated efferocytosis; indicating that oligomerization is truly occurring.

We speculate that the oligomerization of MERTK plays an important role during efferocytosis. Foremost, the enlargement in cluster size may enhance the avidity for ACs. We previously reported that the transmembrane domain of human MERTK underwent positive selection to increase self-cluster size, which correlated with enhanced avidity for Gas6-opsonized beads compared to MERTK from other hominids[137]. Thus, further oligomerization of the pre-existing clusters may act to strongly tether ACs into place within the efferocytic cup. Furthermore, oligomerization is believed to greatly enhance signal transduction by promoting the recruitment of downstream signaling molecules; with this effect observed in G-protein coupled receptors (GPCRs) and other RTKs[118,259]. We imagine that oligomerization could amplify the activation of MERTK effectors such as PI3K, SFKs, Grb2, Vav, PLCγ, and others, which would promote engulfment and anti-inflammatory signaling.

4.4 The biophysics of MERTK-mediated engulfment

We began the development of a 2D-TFM assay to tease apart the biophysical role of MERTK and the integrins during efferocytosis. We hypothesized that engulfment receptors, including integrins, transduce contractile forces onto the target via their intrinsic actin polymerization capability[60]. In contrast, stimulating receptors such as MERTK should not be able to transduce force, as the cytoskeletal structures required for force transduction would not be formed. Although we have yet to support this hypothesis at the biophysical level, we have produced a working model of frustrated efferocytosis on opsonized polyacrylamide gels. Our preliminary data has provided further evidence for the intermolecular crosstalk between MERTK and the integrins; such that the activity of both receptors were required for frustrated efferocytosis.

4.4.1 Predicted outcomes of the 2D-TFM frustrated efferocytosis assay

We expect that integrins will directly transduce contractile force through the actin ring-like structure. In the traction force heatmap, this would be represented by an array of inwards-facing force vectors originating from the periphery of the efferocytic synapse[96,237]. Integrins are known to mechanically couple the forces generated by actin polymerization against the surface of the particle[82]. After ligation, integrins form a "molecular clutch" that transduces centripetal traction forces onto the target, which slows the retrograde flow of F-actin during polymerization to promote the forward progression of the membrane[82,260]. Furthermore, F-actin arranges into parallel bundles after the cell has spread to its maximum size, forming a contractile belt that enacts constrictive force through the activity of myosin II[60,96]. Integrins are also crucial for this process via their activation of ROCK, which phosphorylates key regulatory proteins to stimulate myosin II activity[261].

We believe the progression of the efferocytic cup is contingent on integrin activation and ligation, as non-engaged integrins can not form the force-transducing molecular clutch required to drive membrane progression[260]. According to our preliminary observations, we predict that MERTK's stimulation of integrin activity on Gas6-opsonized gels is rendered nil because the opsonins required for integrin ligation are absent. On MFG-E8-opsonized gels, the integrins lack the activation signals required for ligation. In both cases, the force-transducing molecular clutch is not engaged and frustrated efferocytosis can not progress beyond simple adhesion. In our model, frustrated efferocytosis required the simultaneous engagement of MERTK and the efferocytic integrin receptors. We believe that MERTK activates the integrins, with the latter then inducing the actin polymerization and associated traction forces to promote membrane progression. 2D-TFM should confirm that these forces originate from integrin-dependent structures rather than at the level of MERTK; thereby providing definitive biomechanical evidence of MERTK's role as a stimulating receptor during efferocytosis. Further optimization of our 2D-TFM protocol is required to reliably measure these contractile forces.

4.4.2   Insights into the optimization of 2D-TFM

There are several possible reasons as to why our initial attempts at force measurement in our 2D-TFM experiments have been unsuccessful. We first questioned if THP-1 macrophages were inherently poor force transducers. As a positive control, we used RAW 264.7 murine macrophages on IgG-opsonized gels, which have been used by others to measure contractile forces during frustrated phagocytosis[82]. However, we failed to detect traction forces despite adhesion of RAW264.7 cells to the substrate (data not shown). Thus, we believe our technical issues likely reside in our gel preparation protocol, rather than an intrinsic issue with our cells. One possibility is that the fluorescent beads may have been embedded too far below the surface of the gel, such that local stresses at the surface were not propagated to that depth in the gel, rendering the bead displacements undetectable. Others have reported that inverting the gel during the polymerization step alleviates this[238], but this did not resolve our issues (data not shown). Alternatively, others have shown that centrifugation of the gel causes the beads to lift up to the surface[262]. Some labs are known to directly functionalize the beads to the surface of the gel prior to opsonization, thereby negating the chance for local stresses to be missed[263]. We plan on adopting these protocols for future experiments.

Another potential issue is that the stiffness of the gel may need to be optimized to elicit maximal contractile force. During FcγR-mediated frustrated phagocytosis, increasing the stiffness of the gel was reported to greatly enhance the contractile force transduced by primary murine macrophages[237], whereas gels of too low of a stiffness can prevent force generation due to absence of mechanotransduction through the integrins (Private communication, Fui Boon Kai, University of Calgary). We plan on increasing gel stiffness in future experiments to elicit stronger force transduction, although the physiological relevance could be questionable as ACs would be considerably less stiff than our existing gels[264]. There appears to be significant heterogeneity in the methods used by different laboratories, further complicating this issue. Our preliminary findings show clear evidence of the intermolecular crosstalk between MERTK and integrins during frustrated efferocytosis on polyacrylamide. However, we must design a working

2D-TFM assay before we can definitively confirm the biophysical role of MERTK and the integrins during efferocytosis.

4.5 Conclusion and implications of research

The identification of the MERTK:β_2 integrin axis may provide a resolution to the debate regarding the mechanism of MERTK-mediated efferocytosis. Previously, we had uncovered much of the signaling pathway responsible for the inside-out activation of β_2 integrins by MERTK. Herein, we investigated the structure and diffusional dynamics of the efferocytic synapse, providing biomechanical support suggesting that MERTK is not a local mediator of actin polymerization. We also showed that the cooperative activity of MERTK and the efferocytic integrins are essential for frustrated efferocytosis on a functionalized hydrogel surface. We will continue the development of a 2D-TFM assay to definitively confirm that MERTK alone is unable to form the contractile structures required for efferocytosis. We propose that MERTK is a stimulating receptor that induces actin polymerization by proxy via its activation of the β_2 integrins. This clashes with the traditional view that MERTK is a direct mediator of actin polymerization; a model that does not appear to be well supported by available evidence.

The intermolecular crosstalk between stimulating receptors and engulfment receptors may be a common theme during efferocytosis. We imagine that stimulating receptors confer specificity to ACs, which subsequently activate the engulfment receptors to induce their actin remodeling activity. Thus, autoimmune or inflammatory pathologies where MERTK's activity is defective may be secondarily characterized by a lack of integrin activity during efferocytosis. It is tempting to believe that these diseases may be alleviated by restoring the activation state of the efferocytic integrin receptors. Systemic small-molecule activators of $\alpha_M\beta_2$ and $\alpha_L\beta_2$ have been used in animal models[265,266]. However, specific targeting of tissue-resident macrophages will be necessary to avoid the dysregulation of other integrin-specific functions, as well as to prevent off-target effects on other leukocytes. Biomechanical characterization of other known efferocytic receptors will establish a clear dichotomy between stimulating- and engulfment-receptors. This will aid future therapeutic strategies to combat diseases where efferocytosis is defective.

References

1. Flannagan, R. S., Jaumouillé, V. & Grinstein, S. The Cell Biology of Phagocytosis. *Annu. Rev. Pathol. Mech. Dis.* **7**, 61–98 (2012).

2. Metschnikoff, E. Ueber die Beziehung der Phagocyten zu Milzbrandbacillen. *Archiv f. pathol. Anat.* **97**, 502–526 (1884).

3. Heifets, L. Centennial of Metchnikoff's discovery. *J Reticuloendothel Soc* **31**, 381–391 (1982).

4. Merien, F. A Journey with Elie Metchnikoff: From Innate Cell Mechanisms in Infectious Diseases to Quantum Biology. *Frontiers in Public Health* **4**, (2016).

5. Kinchen, J. M. & Ravichandran, K. S. Phagosome maturation: going through the acid test. *Nat Rev Mol Cell Biol* **9**, 781–795 (2008).

6. Acharya, D., Li, X. R. (Lisa), Heineman, R. E.-S. & Harrison, R. E. Complement Receptor-Mediated Phagocytosis Induces Proinflammatory Cytokine Production in Murine Macrophages. *Frontiers in Immunology* **10**, (2020).

7. Aderem, A. Phagocytosis and the Inflammatory Response. *The Journal of Infectious Diseases* **187**, S340-5 (2003).

8. Ramachandra, L., Simmons, D. & Harding, C. V. MHC Molecules and Microbial Antigen Processing in Phagosomes. *Curr Opin Immunol* **21**, 98–104 (2009).

9. Blander, J. M. & Medzhitov, R. On regulation of phagosome maturation and antigen presentation. *Nat Immunol* **7**, 1029–1035 (2006).

10. Abi Abdallah, D. S., Egan, C. E., Butcher, B. A. & Denkers, E. Y. Mouse neutrophils are professional antigen-presenting cells programmed to instruct Th1 and Th17 T-cell differentiation. *Int Immunol* **23**, 317–326 (2011).

11. Zou, X., Sun, G., Huo, F., Chang, L. & Yang, W. The Role of Dendritic Cells in the Differentiation of T Follicular Helper Cells. *J Immunol Res* **2018**, 7281453 (2018).

12. Joffre, O. P., Segura, E., Savina, A. & Amigorena, S. Cross-presentation by dendritic cells. *Nat Rev Immunol* **12**, 557–569 (2012).

13. Arandjelovic, S. & Ravichandran, K. S. Phagocytosis of apoptotic cells in homeostasis. *Nat Immunol* **16**, 907–917 (2015).

14. Boada-Romero, E., Martinez, J., Heckmann, B. L. & Green, D. R. The clearance of dead cells by efferocytosis. *Nat Rev Mol Cell Biol* **21**, 398–414 (2020).

15. Doran, A. C., Yurdagul, A. & Tabas, I. Efferocytosis in health and disease. *Nature Reviews Immunology* **20**, 254–267 (2020).

16. Giroud, P. *et al.* Expression of TAM-R in Human Immune Cells and Unique Regulatory Function of MerTK in IL-10 Production by Tolerogenic DC. *Front Immunol* **11**, 564133 (2020).

17. Adomati, T. *et al.* Dead Cells Induce Innate Anergy via Mertk after Acute Viral Infection. *Cell Reports* **30**, 3671-3681.e5 (2020).

18. Fadok, V. A. *et al.* Macrophages that have ingested apoptotic cells in vitro inhibit proinflammatory cytokine production through autocrine/paracrine mechanisms involving TGF-beta, PGE2, and PAF. *J Clin Invest* **101**, 890–898 (1998).

19. Huynh, M.-L. N., Fadok, V. A. & Henson, P. M. Phosphatidylserine-dependent ingestion of apoptotic cells promotes TGF-β1 secretion and the resolution of inflammation. *J Clin Invest* **109**, 41–50 (2002).

20. Kim, S., Elkon, K. B. & Ma, X. Transcriptional suppression of interleukin-12 gene expression following phagocytosis of apoptotic cells. *Immunity* **21**, 643–653 (2004).

21. Cai, B. *et al.* MerTK signaling in macrophages promotes the synthesis of inflammation resolution mediators by suppressing CaMKII activity. *Sci Signal* **11**, eaar3721 (2018).

22. Snodgrass, R. G. *et al.* Efferocytosis potentiates the expression of arachidonate 15-lipoxygenase (ALOX15) in alternatively activated human macrophages through LXR activation. *Cell Death Differ* **28**, 1301–1316 (2021).

23. Cai, B. *et al.* MerTK cleavage limits proresolving mediator biosynthesis and exacerbates tissue inflammation. *Proc Natl Acad Sci U S A* **113**, 6526–6531 (2016).

24. Gerlach, B. D. *et al.* Resolvin D1 promotes the targeting and clearance of necroptotic cells. *Cell Death Differ* **27**, 525–539 (2020).

25. Meriwether, D. *et al.* Macrophage COX2 Mediates Efferocytosis, Resolution Reprogramming, and Intestinal Epithelial Repair. *Cellular and Molecular Gastroenterology and Hepatology* **13**, 1095–1120 (2022).

26. Yin, C., Kim, Y., Argintaru, D. & Heit, B. Rab17 mediates differential antigen sorting following efferocytosis and phagocytosis. *Cell Death & Disease* **7**, e2529–e2529 (2016).

27. Garrido, C. *et al.* Mechanisms of cytochrome c release from mitochondria. *Cell Death Differ* **13**, 1423–1433 (2006).

28. Brentnall, M., Rodriguez-Menocal, L., De Guevara, R. L., Cepero, E. & Boise, L. H. Caspase-9, caspase-3 and caspase-7 have distinct roles during intrinsic apoptosis. *BMC Cell Biology* **14**, 32 (2013).

29. Lee, E.-W., Seo, J., Jeong, M., Lee, S. & Song, J. The roles of FADD in extrinsic apoptosis and necroptosis. *BMB Rep* **45**, 496–508 (2012).

30. Tummers, B. & Green, D. R. Caspase-8; regulating life and death. *Immunol Rev* **277**, 76–89 (2017).

31. Kothakota, S. *et al.* Caspase-3-generated fragment of gelsolin: effector of morphological change in apoptosis. *Science* **278**, 294–298 (1997).

32. Sebbagh, M. *et al.* Caspase-3-mediated cleavage of ROCK I induces MLC phosphorylation and apoptotic membrane blebbing. *Nat Cell Biol* **3**, 346–352 (2001).

33. Sakahira, H., Enari, M. & Nagata, S. Cleavage of CAD inhibitor in CAD activation and DNA degradation during apoptosis. *Nature* **391**, 96–99 (1998).

34. Mukherjee, S., Chiu, R., Leung, S.-M. & Shields, D. Fragmentation of the Golgi Apparatus: An Early Apoptotic Event Independent of the Cytoskeleton. *Traffic* **8**, 369–378 (2007).

35. Lane, J. D., Allan, V. J. & Woodman, P. G. Active relocation of chromatin and endoplasmic reticulum into blebs in late apoptotic cells. *Journal of Cell Science* **118**, 4059–4071 (2005).

36. Silva, M. T. Secondary necrosis: the natural outcome of the complete apoptotic program. *FEBS Lett* **584**, 4491–4499 (2010).

37. Ravichandran, K. S. Find-me and eat-me signals in apoptotic cell clearance: progress and conundrums. *J Exp Med* **207**, 1807–1817 (2010).

38. Pontejo, S. M. & Murphy, P. M. Chemokines act as phosphatidylserine-bound "find-me" signals in apoptotic cell clearance. *PLoS Biol* **19**, e3001259 (2021).

39. Fadok, V. A., Voelker, D. R., Campbell, P. A., Cohen, J. J. & Henson, P. M. Exposure of phosphatidylserine on the surface of apoptotic lymphocytes triggers specific recognition and removal by macrophages. *J Immunol* **148**, 2207–2216 (1992).

40. Segawa, K. *et al.* Caspase-mediated cleavage of phospholipid flippase for apoptotic phosphatidylserine exposure. *Science* **344**, 1164–1168 (2014).

41. Segawa, K., Kurata, S. & Nagata, S. Human Type IV P-type ATPases That Work as Plasma Membrane Phospholipid Flippases and Their Regulation by Caspase and Calcium. *J Biol Chem* **291**, 762–772 (2016).

42. Suzuki, J., Denning, D. P., Imanishi, E., Horvitz, H. R. & Nagata, S. Xk-related protein 8 and CED-8 promote phosphatidylserine exposure in apoptotic cells. *Science* **341**, 403–406 (2013).

43. Seiffert, M. *et al.* Human signal-regulatory protein is expressed on normal, but not on subsets of leukemic myeloid cells and mediates cellular adhesion involving its counterreceptor CD47. *Blood* **94**, 3633–3643 (1999).

44. Willingham, S. B. *et al.* The CD47-signal regulatory protein alpha (SIRPa) interaction is a therapeutic target for human solid tumors. *Proc Natl Acad Sci U S A* **109**, 6662–6667 (2012).

45. Barkal, A. A. *et al.* CD24 signalling through macrophage Siglec-10 is a new target for cancer immunotherapy. *Nature* **572**, 392–396 (2019).

46. Moffatt, O. D., Devitt, A., Bell, E. D., Simmons, D. L. & Gregory, C. D. Macrophage recognition of ICAM-3 on apoptotic leukocytes. *J Immunol* **162**, 6800–6810 (1999).

47. Osman, R., Tacnet-Delorme, P., Kleman, J.-P., Millet, A. & Frachet, P. Calreticulin Release at an Early Stage of Death Modulates the Clearance by Macrophages of Apoptotic Cells. *Front Immunol* **8**, (2017).

48. Fadok, V. A., Warner, M. L., Bratton, D. L. & Henson, P. M. CD36 Is Required for Phagocytosis of Apoptotic Cells by Human Macrophages That Use Either a Phosphatidylserine Receptor or the Vitronectin Receptor (αvβ3). *The Journal of Immunology* **161**, 6250–6257 (1998).

49. Blackburn, J. W. D. *et al.* Soluble CD93 is an apoptotic cell opsonin recognized by αxβ2. *European Journal of Immunology* **49**, 600–610 (2019).

50. Dominguez, R. & Holmes, K. C. Actin Structure and Function. *Annual Review of Biophysics* **40**, 169–186 (2011).

51. Arpin, M., Chirivino, D., Naba, A. & Zwaenepoel, I. Emerging role for ERM proteins in cell adhesion and migration. *Cell Adh Migr* **5**, 199–206 (2011).

52. Fievet, B. T. *et al.* Phosphoinositide binding and phosphorylation act sequentially in the activation mechanism of ezrin. *Journal of Cell Biology* **164**, 653–659 (2004).

53. Orian-Rousseau, V. *et al.* Hepatocyte Growth Factor-induced Ras Activation Requires ERM Proteins Linked to Both CD44v6 and F-Actin. *Mol Biol Cell* **18**, 76–83 (2007).

54. Boujemaa-Paterski, R. *et al.* Talin-activated vinculin interacts with branched actin networks to initiate bundles. *eLife* **9**, e53990 (2020).

55. Jaumouillé, V. & Waterman, C. M. Physical Constraints and Forces Involved in Phagocytosis. *Frontiers in Immunology* **11**, (2020).

56. Cox, D. *et al.* Requirements for Both Rac1 and Cdc42 in Membrane Ruffling and Phagocytosis in Leukocytes. *Journal of Experimental Medicine* **186**, 1487–1494 (1997).

57. Bonfim-Melo, A., Ferreira, É. R. & Mortara, R. A. Rac1/WAVE2 and Cdc42/N-WASP Participation in Actin-Dependent Host Cell Invasion by Extracellular Amastigotes of Trypanosoma cruzi. *Front Microbiol* **9**, 360 (2018).

58. Rohatgi, R. *et al.* The Interaction between N-WASP and the Arp2/3 Complex Links Cdc42-Dependent Signals to Actin Assembly. *Cell* **97**, 221–231 (1999).

59. Chen, B. *et al.* Rac1 GTPase activates the WAVE regulatory complex through two distinct binding sites. *eLife* **6**, e29795 (2017).

60. Vorselen, D. *et al.* Phagocytic 'teeth' and myosin-II 'jaw' power target constriction during phagocytosis. *eLife* **10**, e68627 (2021).

61. Barger, S. R., Vorselen, D., Gauthier, N. C., Theriot, J. A. & Krendel, M. F-actin organization and target constriction during primary macrophage phagocytosis is balanced by competing activity of myosin-I and myosin-II. *MBoC* **33**, br24 (2022).

62. Barger, S. R., Gauthier, N. C. & Krendel, M. Squeezing in a meal: myosin functions in phagocytosis. *Trends Cell Biol* **30**, 157–167 (2020).

63. Flannagan, R. S., Canton, J., Furuya, W., Glogauer, M. & Grinstein, S. The phosphatidylserine receptor TIM4 utilizes integrins as coreceptors to effect phagocytosis. *Mol Biol Cell* **25**, 1511–1522 (2014).

64. Toda, S., Hanayama, R. & Nagata, S. Two-step engulfment of apoptotic cells. *Mol Cell Biol* **32**, 118–125 (2012).

65. Schorey, J. S. & Lawrence, C. The Pattern Recognition Receptor Dectin-1: From Fungi to Mycobacteria. *Curr Drug Targets* **9**, 123–129 (2008).

66. Getahun, A. & Cambier, J. C. Of ITIMs, ITAMs, and ITAMis: revisiting immunoglobulin Fc receptor signaling. *Immunol Rev* **268**, 66–73 (2015).

67. Tridandapani, S. *et al.* The Adapter Protein LAT Enhances Fcγ Receptor-mediated Signal Transduction in Myeloid Cells. *Journal of Biological Chemistry* **275**, 20480–20487 (2000).

68. Lee, W. L., Cosio, G., Ireton, K. & Grinstein, S. Role of CrkII in Fcγ Receptor-mediated Phagocytosis*. *Journal of Biological Chemistry* **282**, 11135–11143 (2007).

69. Brugnera, E. *et al.* Unconventional Rac-GEF activity is mediated through the Dock180-ELMO complex. *Nat Cell Biol* **4**, 574–582 (2002).

70. Coppolino, M. G. *et al.* Evidence for a molecular complex consisting of Fyb/SLAP, SLP-76, Nck, VASP and WASP that links the actin cytoskeleton to Fcgamma receptor signalling during phagocytosis. *J Cell Sci* **114**, 4307–4318 (2001).

71. Walbaum, S. *et al.* Complement receptor 3 mediates both sinking phagocytosis and phagocytic cup formation via distinct mechanisms. *Journal of Biological Chemistry* **296**, 100256 (2021).

72. Meenderink, L. M. *et al.* P130Cas Src-Binding and Substrate Domains Have Distinct Roles in Sustaining Focal Adhesion Disassembly and Promoting Cell Migration. *PLoS One* **5**, e13412 (2010).

73. Wu, Y., Singh, S., Georgescu, M.-M. & Birge, R. B. A role for Mer tyrosine kinase in alphavbeta5 integrin-mediated phagocytosis of apoptotic cells. *J Cell Sci* **118**, 539–553 (2005).

74. Albert, M. L., Kim, J. I. & Birge, R. B. alphavbeta5 integrin recruits the CrkII-Dock180-rac1 complex for phagocytosis of apoptotic cells. *Nat Cell Biol* **2**, 899–905 (2000).

75. Lawson, C. *et al.* FAK promotes recruitment of talin to nascent adhesions to control cell motility. *J Cell Biol* **196**, 223–232 (2012).

76. O'TOOLE, T. E., BIALKOWSKA, K., LI, X. & FOX, J. E. B. Tiam1 Is Recruited to β1-Integrin Complexes by 14-3-3ζ Where It Mediates Integrin-Induced Rac1 Activation and Motility. *J Cell Physiol* **226**, 2965–2978 (2011).

77. Gakidis, M. A. M. *et al.* Vav GEFs are required for β2 integrin-dependent functions of neutrophils. *J Cell Biol* **166**, 273–282 (2004).

78. Sullivan, R., Price, L. S. & Koffer, A. Rho Controls Cortical F-actin Disassembly in Addition to, but Independently of, Secretion in Mast Cells*. *Journal of Biological Chemistry* **274**, 38140–38146 (1999).

79. Colucci-Guyon, E. *et al.* A role for mammalian diaphanous-related formins in complement receptor (CR3)-mediated phagocytosis in macrophages. *Curr Biol* **15**, 2007–2012 (2005).

80. Olazabal, I. M. *et al.* Rho-kinase and myosin-II control phagocytic cup formation during CR, but not FcgammaR, phagocytosis. *Curr Biol* **12**, 1413–1418 (2002).

81. Jaumouillé, V. & Grinstein, S. Molecular Mechanisms of Phagosome Formation. *Microbiology Spectrum* **4**, 4.3.06 (2016).

82. Jaumouillé, V., Cartagena-Rivera, A. X. & Waterman, C. M. Coupling of β2 integrins to actin by a mechanosensitive molecular clutch drives complement receptor-mediated phagocytosis. *Nat Cell Biol* **21**, 1357–1369 (2019).

83. Leverrier, Y. *et al.* Class I Phosphoinositide 3-Kinase p110β Is Required for Apoptotic Cell and Fcγ Receptor-mediated Phagocytosis by Macrophages. *Journal of Biological Chemistry* **278**, 38437–38442 (2003).

84. Beemiller, P. *et al.* A Cdc42 Activation Cycle Coordinated by PI 3-Kinase during Fc Receptor-mediated Phagocytosis. *Mol Biol Cell* **21**, 470–480 (2010).

85. Montaño-Rendón, F. *et al.* PtdIns(3,4)P2, Lamellipodin, and VASP coordinate actin dynamics during phagocytosis in macrophages. *Journal of Cell Biology* **221**, e202207042 (2022).

86. Park, D. *et al.* BAI1 is an engulfment receptor for apoptotic cells upstream of the ELMO/Dock180/Rac module. *Nature* **450**, 430–434 (2007).

87. Murakami, Y. *et al.* CD300b regulates the phagocytosis of apoptotic cells via phosphatidylserine recognition. *Cell Death Differ* **21**, 1746–1757 (2014).

88. Ma, C.-I. J. *et al.* Engulfment protein GULP is regulator of transforming growth factor-β response in ovarian cells. *J Biol Chem* **287**, 20636–20651 (2012).

89. Park, S.-Y. *et al.* Requirement of Adaptor Protein GULP during Stabilin-2-mediated Cell Corpse Engulfment*. *Journal of Biological Chemistry* **283**, 10593–10600 (2008).

90. Zhang, Z., Humphreys, B. D. & Bonventre, J. V. Shedding of the urinary biomarker kidney injury molecule-1 (KIM-1) is regulated by MAP kinases and juxtamembrane region. *J Am Soc Nephrol* **18**, 2704–2714 (2007).

91. Park, D., Hochreiter-Hufford, A. & Ravichandran, K. S. The phosphatidylserine receptor TIM-4 does not mediate direct signaling. *Curr Biol* **19**, 346–351 (2009).

92. Gagen, D., Filla, M. S., Clark, R., Liton, P. & Peters, D. M. Activated αvβ3 Integrin Regulates αvβ5 Integrin–Mediated Phagocytosis in Trabecular Meshwork Cells. *Invest Ophthalmol Vis Sci* **54**, 5000–5011 (2013).

93. Lemke, G. Biology of the TAM Receptors. *Cold Spring Harb Perspect Biol* **5**, a009076 (2013).

94. Shelby, S. J., Colwill, K., Dhe-Paganon, S., Pawson, T. & Thompson, D. A. MERTK Interactions with SH2-Domain Proteins in the Retinal Pigment Epithelium. *PLOS ONE* **8**, e53964 (2013).

95. Branchford, B. R. *et al.* The small-molecule MERTK inhibitor UNC2025 decreases platelet activation and prevents thrombosis. *Journal of Thrombosis and Haemostasis* **16**, 352–363 (2018).

96. Kovari, D. T. *et al.* Frustrated Phagocytic Spreading of J774A-1 Macrophages Ends in Myosin II-Dependent Contraction. *Biophys J* **111**, 2698–2710 (2016).

97. Freeman, S. A. *et al.* Integrins form an expanding diffusional barrier that coordinates phagocytosis. *Cell* **164**, 128–140 (2016).

98. Imbert, P. R. C. *et al.* An Acquired and Endogenous Glycocalyx Forms a Bidirectional "Don't Eat" and "Don't Eat Me" Barrier to Phagocytosis. *Current Biology* **31**, 77-89.e5 (2021).

99. Maschalidi, S. & Ravichandran, K. S. Phagocytosis: Sweet Repulsions via the Glycocalyx. *Current Biology* **31**, R20–R22 (2021).

100. Goodridge, H. S. *et al.* Activation of the innate immune receptor Dectin-1 upon formation of a 'phagocytic synapse'. *Nature* **472**, 471–475 (2011).

101. Delon, J., Kaibuchi, K. & Germain, R. N. Exclusion of CD43 from the Immunological Synapse Is Mediated by Phosphorylation-Regulated Relocation of the Cytoskeletal Adaptor Moesin. *Immunity* **15**, 691–701 (2001).

102. Stampfuss, J.-J. *et al.* Complete Downmodulation of P-Selectin Glycoprotein Ligand in Monocytes Undergoing Apoptosis. *Arteriosclerosis, Thrombosis, and Vascular Biology* **28**, 1375–1378 (2008).

103. Hart, S. P., Ross, J. A., Ross, K., Haslett, C. & Dransfield, I. Molecular characterization of the surface of apoptotic neutrophils: Implications for functional downregulation and recognition by phagocytes. *Cell Death Differ* **7**, 493–503 (2000).

104. Barth, N. D., Marwick, J. A., Vendrell, M., Rossi, A. G. & Dransfield, I. The "Phagocytic Synapse" and Clearance of Apoptotic Cells. *Frontiers in Immunology* **8**, (2017).

105. Morrissey, M. A., Kern, N. & Vale, R. D. CD47 Ligation Repositions the Inhibitory Receptor SIRPA to Suppress Integrin Activation and Phagocytosis. *Immunity* **53**, 290-302.e6 (2020).

106. Dickson, B. & Heit, B. Analysis of Efferocytic Receptor Dynamics and Synapse Formation in a Frustrated Efferocytosis Model. *Methods in Molecular Biology - Phagocytosis and Phagosomes 2nd Edition* **In Press**, (2023).

107. Lam, A. L. Elucidating the Role of MERTK- $\alpha x\beta 2$ Integrin Crosstalk in Efferocytic Synapse Formation. Thesis. (The University of Western Ontario, 2021).

108. Singer, S. J. & Nicolson, G. L. The Fluid Mosaic Model of the Structure of Cell Membranes. *Science* **175**, 720–731 (1972).

109. Lin, J. *et al.* TIRF imaging of Fc gamma receptor microclusters dynamics and signaling on macrophages during frustrated phagocytosis. *BMC Immunology* **17**, 5 (2016).

110. Andrews, N. L. *et al.* Actin restricts FcepsilonRI diffusion and facilitates antigen-induced receptor immobilization. *Nat Cell Biol* **10**, 955–963 (2008).

111. Needham, S. R. *et al.* EGFR oligomerization organizes kinase-active dimers into competent signalling platforms. *Nat Commun* **7**, 13307 (2016).

112. Rose, M., Hirmiz, N., Moran-Mirabal, J. M. & Fradin, C. Lipid Diffusion in Supported Lipid Bilayers: A Comparison between Line-Scanning Fluorescence Correlation Spectroscopy and Single-Particle Tracking. *Membranes (Basel)* **5**, 702–721 (2015).

113. Kusumi, A. *et al.* Paradigm Shift of the Plasma Membrane Concept from the Two-Dimensional Continuum Fluid to the Partitioned Fluid: High-Speed Single-Molecule Tracking of Membrane Molecules. *Annual Review of Biophysics and Biomolecular Structure* **34**, 351–378 (2005).

114. Kusumi, A. *et al.* Dynamic organizing principles of the plasma membrane that regulate signal transduction: commemorating the fortieth anniversary of Singer and Nicolson's fluid-mosaic model. *Annu Rev Cell Dev Biol* **28**, 215–250 (2012).

115. Ritchie, K., Iino, R., Fujiwara, T., Murase, K. & Kusumi, A. The fence and picket structure of the plasma membrane of live cells as revealed by single molecule techniques (Review). *Molecular Membrane Biology* **20**, 13–18 (2003).

116. Jaumouillé, V. *et al.* Actin cytoskeleton reorganization by the tyrosine kinase Syk regulates Fcγ receptor responsiveness by increasing its lateral mobility and clustering. *Dev Cell* **29**, 534–546 (2014).

117. Işbilir, A. *et al.* Determination of G-protein–coupled receptor oligomerization by molecular brightness analyses in single cells. *Nat Protoc* **16**, 1419–1451 (2021).

118. Chung, I. Optical measurement of receptor tyrosine kinase oligomerization on live cells. *Biochimica et Biophysica Acta (BBA) - Biomembranes* **1859**, 1436–1444 (2017).

119. Barger, S. R. *et al.* Membrane-cytoskeletal crosstalk mediated by myosin-I regulates adhesion turnover during phagocytosis. *Nat Commun* **10**, 1249 (2019).

120. Hoijman, E. *et al.* Cooperative epithelial phagocytosis enables error correction in the early embryo. *Nature* **590**, 618–623 (2021).

121. Zihni, C. *et al.* Spatiotemporal control of actomyosin contractility by MRCKβ signaling drives phagocytosis. *Journal of Cell Biology* **221**, e202012042 (2022).

122. Myers, K. V., Amend, S. R. & Pienta, K. J. Targeting Tyro3, Axl and MerTK (TAM receptors): implications for macrophages in the tumor microenvironment. *Molecular Cancer* **18**, 94 (2019).

123. Stitt, T. N. *et al.* The anticoagulation factor protein S and its relative, Gas6, are ligands for the Tyro 3/Axl family of receptor tyrosine kinases. *Cell* **80**, 661–670 (1995).

124. Cohen, P. L. *et al.* Delayed apoptotic cell clearance and lupus-like autoimmunity in mice lacking the c-mer membrane tyrosine kinase. *J Exp Med* **196**, 135–140 (2002).

125. D'Cruz, P. M. *et al.* Mutation of the receptor tyrosine kinase gene Mertk in the retinal dystrophic RCS rat. *Hum Mol Genet* **9**, 645–651 (2000).

126. Chen, Y. *et al.* Functions of TAM RTKs in regulating spermatogenesis and male fertility in mice. *Reproduction* **138**, 655–666 (2009).

127. Yanagihashi, Y., Segawa, K., Maeda, R., Nabeshima, Y. & Nagata, S. Mouse macrophages show different requirements for phosphatidylserine receptor Tim4 in efferocytosis. *Proceedings of the National Academy of Sciences* **114**, 8800–8805 (2017).

128. Tian, L. *et al.* Enhanced efferocytosis by dendritic cells underlies memory T-cell expansion and susceptibility to autoimmune disease in CD300f-deficient mice. *Cell Death Differ* **23**, 1086–1096 (2016).

129. Lee, C. S. *et al.* Boosting Apoptotic Cell Clearance by Colonic Epithelial Cells Attenuates Inflammation In Vivo. *Immunity* **44**, 807–820 (2016).

130. Manta, C.-P. *et al.* Targeting of Scavenger Receptors Stabilin-1 and Stabilin-2 Ameliorates Atherosclerosis by a Plasma Proteome Switch Mediating Monocyte/Macrophage Suppression. *Circulation* **146**, 1783–1799 (2022).

131. Lee, Y.-J. *et al.* Inhibiting Mer receptor tyrosine kinase suppresses STAT1, SOCS1/3, and NF-κB activation and enhances inflammatory responses in lipopolysaccharide-induced acute lung injury. *Journal of Leukocyte Biology* **91**, 921–932 (2012).

132. Pastore, M. *et al.* Macrophage MerTK promotes profibrogenic cross-talk with hepatic stellate cells via soluble mediators. *JHEP Reports* **4**, 100444 (2022).

133. Strick, D. J. & Vollrath, D. Focus on Molecules: MERTK. *Exp Eye Res* **91**, 786–787 (2010).

134. Law, A.-L. *et al.* Cleavage of Mer Tyrosine Kinase (MerTK) from the Cell Surface Contributes to the Regulation of Retinal Phagocytosis. *J Biol Chem* **290**, 4941–4952 (2015).

135. Liu, Y. *et al.* N-glycosylation stabilizes MerTK and promotes hepatocellular carcinoma tumor growth. *Redox Biol* **54**, 102366 (2022).

136. Thorp, E. *et al.* Shedding of the Mer tyrosine kinase receptor is mediated by ADAM17 protein through a pathway involving reactive oxygen species, protein kinase Cδ, and p38 mitogen-activated protein kinase (MAPK). *J Biol Chem* **286**, 33335–33344 (2011).

137. Evans, A. L. *et al.* Antagonistic Coevolution of MER Tyrosine Kinase Expression and Function. *Mol Biol Evol* **34**, 1613–1628 (2017).

138. Tibrewal, N. *et al.* Autophosphorylation docking site Tyr-867 in Mer receptor tyrosine kinase allows for dissociation of multiple signaling pathways for phagocytosis of apoptotic cells and down-modulation of lipopolysaccharide-inducible NF-kappaB transcriptional activation. *J Biol Chem* **283**, 3618–3627 (2008).

139. Nishi, C., Yanagihashi, Y., Segawa, K. & Nagata, S. MERTK tyrosine kinase receptor together with TIM4 phosphatidylserine receptor mediates distinct signal transduction pathways for efferocytosis and cell proliferation. *J Biol Chem* **294**, 7221–7230 (2019).

140. Manfioletti, G., Brancolini, C., Avanzi, G. & Schneider, C. The protein encoded by a growth arrest-specific gene (gas6) is a new member of the vitamin K-dependent proteins related to protein S, a negative coregulator in the blood coagulation cascade. *Mol Cell Biol* **13**, 4976–4985 (1993).

141. Angelillo-Scherrer, A. *et al.* Deficiency or inhibition of Gas6 causes platelet dysfunction and protects mice against thrombosis. *Nat Med* **7**, 215–221 (2001).

142. Burstyn-Cohen, T., Heeb, M. J. & Lemke, G. Lack of Protein S in mice causes embryonic lethal coagulopathy and vascular dysgenesis. *J Clin Invest* **119**, 2942–2953 (2009).

143. Nakano, T. *et al.* Cell adhesion to phosphatidylserine mediated by a product of growth arrest-specific gene 6. *J Biol Chem* **272**, 29411–29414 (1997).

144. Anderson, H. A. *et al.* Serum-derived protein S binds to phosphatidylserine and stimulates the phagocytosis of apoptotic cells. *Nat Immunol* **4**, 87–91 (2003).

145. Geng, K. *et al.* Requirement of Gamma-Carboxyglutamic Acid Modification and Phosphatidylserine Binding for the Activation of Tyro3, Axl, and Mertk Receptors by Growth Arrest-Specific 6. *Front Immunol* **8**, 1521 (2017).

146. van der Meer, J. H. M., van der Poll, T. & van 't Veer, C. TAM receptors, Gas6, and protein S: roles in inflammation and hemostasis. *Blood* **123**, 2460–2469 (2014).

147. Llacuna, L. *et al.* Growth arrest–specific protein 6 is hepatoprotective against murine ischemia/reperfusion injury. *Hepatology* **52**, 1371–1379 (2010).

148. Huang, M. *et al.* Structural basis of membrane binding by Gla domains of vitamin K-dependent proteins. *Nat Struct Biol* **10**, 751–756 (2003).

149. Rees, D. J. *et al.* The role of beta-hydroxyaspartate and adjacent carboxylate residues in the first EGF domain of human factor IX. *The EMBO Journal* **7**, 2053–2061 (1988).

150. Wu, G. *et al.* Molecular insights of Gas6/TAM in cancer development and therapy. *Cell Death Dis* **8**, e2700–e2700 (2017).

151. Mark, M. R., Chen, J., Hammonds, R. G., Sadick, M. & Godowsk, P. J. Characterization of Gas6, a member of the superfamily of G domain-containing proteins, as a ligand for Rse and Axl. *J Biol Chem* **271**, 9785–9789 (1996).

152. Uehara, H. & Shacter, E. Auto-Oxidation and Oligomerization of Protein S on the Apoptotic Cell Surface Is Required for Mer Tyrosine Kinase-Mediated Phagocytosis of Apoptotic Cells. *The Journal of Immunology* **180**, 2522–2530 (2008).

153. Caberoy, N. B., Alvarado, G., Bigcas, J.-L. & Li, W. Galectin-3 is a new MerTK-specific eat-me signal. *J Cell Physiol* **227**, 401–407 (2012).

154. Caberoy, N. B., Zhou, Y. & Li, W. Tubby and tubby-like protein 1 are new MerTK ligands for phagocytosis. *The EMBO Journal* **29**, 3898–3910 (2010).

155. Triantafyllou, E. *et al.* MerTK expressing hepatic macrophages promote the resolution of inflammation in acute liver failure. *Gut* **67**, 333–347 (2018).

156. DeBerge, M. *et al.* MerTK Cleavage on Resident Cardiac Macrophages Compromises Repair after Myocardial Ischemia Reperfusion Injury. *Circ Res* **121**, 930–940 (2017).

157. Jia, D. *et al.* Cardiac Resident Macrophage-Derived Legumain Improves Cardiac Repair by Promoting Clearance and Degradation of Apoptotic Cardiomyocytes After Myocardial Infarction. *Circulation* **145**, 1542–1556 (2022).

158. Park, J. *et al.* Microglial MERTK eliminates phosphatidylserine-displaying inhibitory post-synapses. *The EMBO Journal* **40**, e107121 (2021).

159. Fourgeaud, L. *et al.* TAM receptors regulate multiple features of microglial physiology. *Nature* **532**, 240–244 (2016).

160. Mohning, M. P. *et al.* Phagocytosis of microparticles by alveolar macrophages during acute lung injury requires MerTK. *American Journal of Physiology-Lung Cellular and Molecular Physiology* **314**, L69–L82 (2018).

161. Puranik, A. S. *et al.* Kidney-resident macrophages promote a proangiogenic environment in the normal and chronically ischemic mouse kidney. *Sci Rep* **8**, 13948 (2018).

162. Wanke, F. *et al.* Ligand-dependent kinase activity of MERTK drives efferocytosis in human iPSC-derived macrophages. *Cell Death Dis* **12**, 538 (2021).

163. Gautier, E. L. *et al.* Gene-expression profiles and transcriptional regulatory pathways that underlie the identity and diversity of mouse tissue macrophages. *Nat Immunol* **13**, 1118–1128 (2012).

164. Wallet, M. A. *et al.* MerTK is required for apoptotic cell–induced T cell tolerance. *Journal of Experimental Medicine* **205**, 219–232 (2008).

165. Zizzo, G., Hilliard, B. A., Monestier, M. & Cohen, P. L. Efficient Clearance of Early Apoptotic Cells by Human Macrophages Requires M2c Polarization and MerTK Induction. *J.I.* **189**, 3508–3520 (2012).

166. Cai, B. *et al.* MerTK receptor cleavage promotes plaque necrosis and defective resolution in atherosclerosis. *J Clin Invest* **127**, 564–568 (2017).

167. Ksantini, M., Lafont, E., Bocquet, B., Meunier, I. & Hamel, C. P. Homozygous Mutation in MERTK Causes Severe Autosomal Recessive Retinitis Pigmentosa. *European Journal of Ophthalmology* **22**, 647–653 (2012).

168. Al-khersan, H. *et al.* A Novel MERTK Mutation Causing Retinitis Pigmentosa. *Graefes Arch Clin Exp Ophthalmol* **255**, 1613–1619 (2017).

169. Shi, J. *et al.* Absence of MerTK disrupts spermatogenesis in an age-dependent manner. *Molecular and Cellular Endocrinology* **560**, 111815 (2023).

170. Yefimova, M. G. *et al.* Granulosa cells provide elimination of apoptotic oocytes through unconventional autophagy-assisted phagocytosis. *Hum Reprod* **35**, 1346–1362 (2020).

171. Hurtado, B. *et al.* Association study between polymorphims in GAS6-TAM genes and carotid atherosclerosis. *Thromb Haemost* **104**, 592–598 (2010).

172. Zizzo, G., Guerrieri, J., Dittman, L. M., Merrill, J. T. & Cohen, P. L. Circulating levels of soluble MER in lupus reflect M2c activation of monocytes/macrophages, autoantibody specificities and disease activity. *Arthritis Res Ther* **15**, R212 (2013).

173. Recarte-Pelz, P. *et al.* Vitamin K-dependent proteins GAS6 and Protein S and TAM receptors in patients of systemic lupus erythematosus: correlation with common genetic variants and disease activity. *Arthritis Res Ther* **15**, R41 (2013).

174. Binder, M. D. *et al.* Common and Low Frequency Variants in MERTK Are Independently Associated with Multiple Sclerosis Susceptibility with Discordant Association Dependent upon HLA-DRB1*15:01 Status. *PLoS Genet* **12**, e1005853 (2016).

175. Ait-Oufella, H. *et al.* Defective mer receptor tyrosine kinase signaling in bone marrow cells promotes apoptotic cell accumulation and accelerates atherosclerosis. *Arterioscler Thromb Vasc Biol* **28**, 1429–1431 (2008).

176. Kaul, A. *et al.* Systemic lupus erythematosus. *Nat Rev Dis Primers* **2**, 1–21 (2016).

177. Shao, W.-H. *et al.* Disrupted Mer receptor tyrosine kinase expression leads to enhanced MZ B-cell responses. *Journal of Autoimmunity* **35**, 368–374 (2010).

178. Shen, K. *et al.* Multiple sclerosis risk gene Mertk is required for microglial activation and subsequent remyelination. *Cell Reports* **34**, 108835 (2021).

179. Healy, L. M. *et al.* MerTK-mediated regulation of myelin phagocytosis by macrophages generated from patients with MS. *Neurol Neuroimmunol Neuroinflamm* **4**, e402 (2017).

180. Höftberger, R., Lassmann, H., Berger, T. & Reindl, M. Pathogenic autoantibodies in multiple sclerosis — from a simple idea to a complex concept. *Nat Rev Neurol* **18**, 681–688 (2022).

181. Baier, A., Meineckel, I., Gay, S. & Pap, T. Apoptosis in rheumatoid arthritis. *Curr Opin Rheumatol* **15**, 274–279 (2003).

182. Waterborg, C. E. J. *et al.* Protective Role of the MER Tyrosine Kinase via Efferocytosis in Rheumatoid Arthritis Models. *Front Immunol* **9**, 742 (2018).

183. van den Brand, B. T. *et al.* Therapeutic Efficacy of Tyro3, Axl, and MerTK Agonists in Collagen-Induced Arthritis. *Arthritis Rheum* **65**, 671–680 (2013).

184. Alivernini, S. *et al.* Distinct synovial tissue macrophage subsets regulate inflammation and remission in rheumatoid arthritis. *Nat Med* **26**, 1295–1306 (2020).

185. Lusis, A. J. Atherosclerosis. *Nature* **407**, 233–241 (2000).

186. Kojima Yoko, Weissman Irving L., & Leeper Nicholas J. The Role of Efferocytosis in Atherosclerosis. *Circulation* **135**, 476–489 (2017).

187. Thorp, E., Cui, D., Schrijvers, D. M., Kuriakose, G. & Tabas, I. Mertk receptor mutation reduces efferocytosis efficiency and promotes apoptotic cell accumulation

and plaque necrosis in atherosclerotic lesions of apoe-/- mice. *Arterioscler Thromb Vasc Biol* **28**, 1421–1428 (2008).

188. Tso, M. O. *et al.* Apoptosis leads to photoreceptor degeneration in inherited retinal dystrophy of RCS rats. *Investigative Ophthalmology & Visual Science* **35**, 2693–2699 (1994).

189. Duncan, J. L. *et al.* An RCS-Like Retinal Dystrophy Phenotype in Mer Knockout Mice. *Investigative Ophthalmology & Visual Science* **44**, 826–838 (2003).

190. Ghazi, N. G. *et al.* Treatment of retinitis pigmentosa due to MERTK mutations by ocular subretinal injection of adeno-associated virus gene vector: results of a phase I trial. *Hum Genet* **135**, 327–343 (2016).

191. Movilla, N., Dosil, M., Zheng, Y. & Bustelo, X. R. How Vav proteins discriminate the GTPases Rac1 and RhoA from Cdc42. *Oncogene* **20**, 8057–8065 (2001).

192. Mahajan, N. P. & Earp, H. S. An SH2 Domain-dependent, Phosphotyrosine-independent Interaction between Vav1 and the Mer Receptor Tyrosine Kinase: A MECHANISM FOR LOCALIZING GUANINE NUCLEOTIDE-EXCHANGE FACTOR ACTION*. *Journal of Biological Chemistry* **278**, 42596–42603 (2003).

193. Zhang, S. *et al.* The role of the Grb2–p38 MAPK signaling pathway in cardiac hypertrophy and fibrosis. *J Clin Invest* **111**, 833–841 (2003).

194. Zhang, W. & Liu, H. T. MAPK signal pathways in the regulation of cell proliferation in mammalian cells. *Cell Res* **12**, 9–18 (2002).

195. Jackson, J. G., St. Clair, P., Sliwkowski, M. X. & Brattain, M. G. Blockade of Epidermal Growth Factor- or Heregulin-Dependent ErbB2 Activation with the Anti-ErbB2 Monoclonal Antibody 2C4 Has Divergent Downstream Signaling and Growth Effects. *Cancer Research* **64**, 2601–2609 (2004).

196. Hu, B. *et al.* RECOGNITION AND PHAGOCYTOSIS OF APOPTOTIC T CELLS BY RESIDENT MURINE TISSUE MACROPHAGES REQUIRES MULTIPLE SIGNAL TRANSDUCTION EVENTS. *J Leukoc Biol* **71**, 881–889 (2002).

197. Tasnim, T. Identification of the Signalosome and Signaling Pathway of the Efferocytic Receptor MERTK. Thesis. (The University of Western Ontario, 2020).

198. Todt, J. C., Hu, B. & Curtis, J. L. The receptor tyrosine kinase MerTK activates phospholipase C γ2 during recognition of apoptotic thymocytes by murine macrophages. *Journal of Leukocyte Biology* **75**, 705–713 (2004).

199. Newton, A. C. Protein Kinase C: Perfectly Balanced. *Crit Rev Biochem Mol Biol* **53**, 208–230 (2018).

200. Todt, J. C. *et al.* Activation of protein kinase C beta II by the stereo-specific phosphatidylserine receptor is required for phagocytosis of apoptotic thymocytes by resident murine tissue macrophages. *J Biol Chem* **277**, 35906–35914 (2002).

201. Rothlin, C. V., Ghosh, S., Zuniga, E. I., Oldstone, M. B. A. & Lemke, G. TAM Receptors Are Pleiotropic Inhibitors of the Innate Immune Response. *Cell* **131**, 1124–1136 (2007).

202. Piganis, R. A. R. *et al.* Suppressor of cytokine signaling (SOCS) 1 inhibits type I interferon (IFN) signaling via the interferon alpha receptor (IFNAR1)-associated tyrosine kinase Tyk2. *J Biol Chem* **286**, 33811–33818 (2011).

203. Sen, P. *et al.* Apoptotic cells induce Mer tyrosine kinase–dependent blockade of NF-κB activation in dendritic cells. *Blood* **109**, 653–660 (2007).

204. Cummings, C. T., DeRyckere, D., Earp, H. S. & Graham, D. K. Molecular Pathways: MERTK Signaling in Cancer. *Clin Cancer Res* **19**, 5275–5280 (2013).

205. A-Gonzalez, N. & Hidalgo, A. Nuclear Receptors and Clearance of Apoptotic Cells: Stimulating the Macrophage's Appetite. *Frontiers in Immunology* **5**, (2014).

206. Nagata, S. Apoptosis and Clearance of Apoptotic Cells. *Annu. Rev. Immunol.* **36**, 489–517 (2018).

207. Mehrotra, P. & Ravichandran, K. S. Drugging the efferocytosis process: concepts and opportunities. *Nat Rev Drug Discov* 1–20 (2022).

208. Lemke, G. & Rothlin, C. V. Immunobiology of the TAM receptors. *Nat Rev Immunol* **8**, 327–336 (2008).

209. Kiefer, F. *et al.* The Syk Protein Tyrosine Kinase Is Essential for Fcγ Receptor Signaling in Macrophages and Neutrophils. *Mol Cell Biol* **18**, 4209–4220 (1998).

210. Canetti, C., Hu, B., Curtis, J. L. & Peters-Golden, M. Syk activation is a leukotriene B4–regulated event involved in macrophage phagocytosis of IgG-coated targets but not apoptotic cells. *Blood* **102**, 1877–1883 (2003).

211. Zhou, J. *et al.* Tyro3, Axl, and Mertk receptors differentially participate in platelet activation and thrombus formation. *Cell Communication and Signaling* **16**, 98 (2018).

212. Finnemann, S. C., Bonilha, V. L., Marmorstein, A. D. & Rodriguez-Boulan, E. Phagocytosis of rod outer segments by retinal pigment epithelial cells requires alpha(v)beta5 integrin for binding but not for internalization. *Proc Natl Acad Sci U S A* **94**, 12932–12937 (1997).

213. Angelillo-Scherrer, A. *et al.* Role of Gas6 receptors in platelet signaling during thrombus stabilization and implications for antithrombotic therapy. *J Clin Invest* **115**, 237–246 (2005).

214. Dransfield, I., Zagórska, A., Lew, E. D., Michail, K. & Lemke, G. Mer receptor tyrosine kinase mediates both tethering and phagocytosis of apoptotic cells. *Cell Death Dis* **6**, e1646–e1646 (2015).

215. Fagerholm, S. C., Guenther, C., Llort Asens, M., Savinko, T. & Uotila, L. M. Beta2-Integrins and Interacting Proteins in Leukocyte Trafficking, Immune Suppression, and Immunodeficiency Disease. *Frontiers in Immunology* **10**, (2019).

216. Vorup-Jensen, T. & Jensen, R. K. Structural Immunology of Complement Receptors 3 and 4. *Front Immunol* **9**, 2716 (2018).

217. Takizawa, F., Tsuji, S. & Nagasawa, S. Enhancement of macrophage phagocytosis upon iC3b deposition on apoptotic cells. *FEBS Lett* **397**, 269–272 (1996).

218. Verbovetski, I. *et al.* Opsonization of Apoptotic Cells by Autologous iC3b Facilitates Clearance by Immature Dendritic Cells, Down-regulates DR and CD86, and Up-regulates CC Chemokine Receptor 7. *Journal of Experimental Medicine* **196**, 1553–1561 (2002).

219. Hirano, Y. *et al.* MFG-E8-derived peptide attenuates adhesion and migration of immune cells to endothelial cells. *J Leukoc Biol* **101**, 1201–1209 (2017).

220. Vorselen, D. *et al.* Cell surface receptors TREM2, CD14 and integrin αMβ2 drive sinking engulfment in phosphatidylserine-mediated phagocytosis. 2022.07.30.502145 Preprint at https://doi.org/10.1101/2022.07.30.502145 (2022).

221. Yin, C. *et al.* Efferocytic Defects in Early Atherosclerosis Are Driven by GATA2 Overexpression in Macrophages. *Front. Immunol.* **11**, (2020).

222. Takagi, J., Petre, B. M., Walz, T. & Springer, T. A. Global Conformational Rearrangements in Integrin Extracellular Domains in Outside-In and Inside-Out Signaling. *Cell* **110**, 599–611 (2002).

223. Lu, C., Ferzly, M., Takagi, J. & Springer, T. A. Epitope mapping of antibodies to the C-terminal region of the integrin beta 2 subunit reveals regions that become exposed upon receptor activation. *J Immunol* **166**, 5629–5637 (2001).

224. Askari, J. A., Buckley, P. A., Mould, A. P. & Humphries, M. J. Linking integrin conformation to function. *J Cell Sci* **122**, 165–170 (2009).

225. Margadant, C., Monsuur, H. N., Norman, J. C. & Sonnenberg, A. Mechanisms of integrin activation and trafficking. *Current Opinion in Cell Biology* **23**, 607–614 (2011).

226. Mould, A. P., Akiyama, S. K. & Humphries, M. J. Regulation of integrin alpha 5 beta 1-fibronectin interactions by divalent cations. Evidence for distinct classes of binding sites for Mn2+, Mg2+, and Ca2+. *J Biol Chem* **270**, 26270–26277 (1995).

227. Lu, F. *et al.* Mechanism of integrin activation by talin and its cooperation with kindlin. *Nat Commun* **13**, 2362 (2022).

228. Zervas, C. G. *et al.* A central multifunctional role of integrin-linked kinase at muscle attachment sites. *J Cell Sci* **124**, 1316–1327 (2011).

229. Dickson, B. H. *et al.* MERTK Coordinates Efferocytosis by Regulating Integrin Localization and Activation. 2023.07.20.549870 Preprint at https://doi.org/10.1101/2023.07.20.549870 (2023).

230. Laine, R. F. *et al.* High-fidelity 3D live-cell nanoscopy through data-driven enhanced super-resolution radial fluctuation. 2022.04.07.487490 Preprint at https://doi.org/10.1101/2022.04.07.487490 (2022).

231. Jaqaman, K. *et al.* Robust single-particle tracking in live-cell time-lapse sequences. *Nat Methods* **5**, 695–702 (2008).

232. Wu, S.-C. & Wong, S.-L. Structure-Guided Design of an Engineered Streptavidin with Reusability to Purify Streptavidin-Binding Peptide Tagged Proteins or Biotinylated Proteins. *PLOS ONE* **8**, e69530 (2013).

233. Yang, L. & Veraksa, A. Single-Step Affinity Purification of ERK Signaling Complexes Using the Streptavidin-Binding Peptide (SBP) Tag. *Methods Mol Biol* **1487**, 113–126 (2017).

234. Zhang, W. *et al.* Pseudo Cyclization through Intramolecular Hydrogen Bond Enables Discovery of Pyridine Substituted Pyrimidines as New Mer Kinase Inhibitors. *J Med Chem* **56**, 9683–9692 (2013).

235. Mylvaganam, S. M., Grinstein, S. & Freeman, S. A. Picket-fences in the plasma membrane: functions in immune cells and phagocytosis. *Semin Immunopathol* **40**, 605–615 (2018).

236. Jaumouillé, V. Measurement of Minute Cellular Forces by Traction Force Microscopy. *Methods Mol Biol* **2440**, 125–139 (2022).

237. Rougerie, P. & Cox, D. *Spatio-temporal mapping of mechanical force generated by macrophages during FcγR-dependent phagocytosis reveals adaptation to target stiffness*. http://biorxiv.org/lookup/doi/10.1101/2020.04.14.041335 (2020) doi:10.1101/2020.04.14.041335.

238. Mustapha, F., Sengupta, K. & Puech, P.-H. Protocol for measuring weak cellular traction forces using well-controlled ultra-soft polyacrylamide gels. *STAR Protocols* **3**, 101133 (2022).

239. Tseng, Q. *et al.* Spatial organization of the extracellular matrix regulates cell–cell junction positioning. *PNAS* (2012) doi:10.1073/pnas.1106377109.

240. Tseng, Q. Etude d'architecture multicellulaire avec le microenvironnement contrôlé. (Université de Grenoble, 2011).

241. Mai, J., Wang, K., Liu, C., Xiong, S. & Xie, Q. αvβ3-targeted sEVs for efficient intracellular delivery of proteins using MFG-E8. *BMC Biotechnology* **22**, 15 (2022).

242. Akakura, S. *et al.* The opsonin MFG-E8 is a ligand for the alphavbeta5 integrin and triggers DOCK180-dependent Rac1 activation for the phagocytosis of apoptotic cells. *Exp Cell Res* **292**, 403–416 (2004).

243. Oshima, K. *et al.* Lactation-dependent expression of an mRNA splice variant with an exon for a multiply O-glycosylated domain of mouse milk fat globule glycoprotein MFG-E8. *Biochem Biophys Res Commun* **254**, 522–528 (1999).

244. Yeung, T. *et al.* Effects of substrate stiffness on cell morphology, cytoskeletal structure, and adhesion. *Cell Motility* **60**, 24–34 (2005).

245. Aratyn-Schaus, Y. & Gardel, M. L. Transient Frictional Slip between Integrin and the ECM in Focal Adhesions under Myosin II Tension. *Current Biology* **20**, 1145–1153 (2010).

246. Miihkinen, M. *et al.* Myosin-X and talin modulate integrin activity at filopodia tips. *Cell Reports* **36**, (2021).

247. Price, L. S., Leng, J., Schwartz, M. A. & Bokoch, G. M. Activation of Rac and Cdc42 by Integrins Mediates Cell Spreading. *Mol Biol Cell* **9**, 1863–1871 (1998).

248. Chang, F., Lemmon, C. A., Park, D. & Romer, L. H. FAK Potentiates Rac1 Activation and Localization to Matrix Adhesion Sites: A Role for βPIX. *Mol Biol Cell* **18**, 253–264 (2007).

249. Yang, J. *et al.* Conformational activation of talin by RIAM triggers integrin-mediated cell adhesion. *Nat Commun* **5**, 5880 (2014).

250. Delcommenne, M. *et al.* Phosphoinositide-3-OH kinase-dependent regulation of glycogen synthase kinase 3 and protein kinase B/AKT by the integrin-linked kinase. *Proc Natl Acad Sci U S A* **95**, 11211–11216 (1998).

251. Tewson, P. H., Martinka, S., Shaner, N. C., Hughes, T. E. & Quinn, A. M. New DAG and cAMP Sensors Optimized for Live-Cell Assays in Automated Laboratories. *J Biomol Screen* **21**, 298–305 (2016).

252. Hilpelä, P., Vartiainen, M. K. & Lappalainen, P. Regulation of the actin cytoskeleton by PI(4,5)P2 and PI(3,4,5)P3. *Curr Top Microbiol Immunol* **282**, 117–163 (2004).

253. Jongstra-Bilen, J., Harrison, R. & Grinstein, S. Fcγ-receptors Induce Mac-1 (CD11b/CD18) Mobilization and Accumulation in the Phagocytic Cup for Optimal Phagocytosis*. *Journal of Biological Chemistry* **278**, 45720–45729 (2003).

254. Freeman, S. A. & Grinstein, S. Phagocytosis: receptors, signal integration, and the cytoskeleton. *Immunological Reviews* **262**, 193–215 (2014).

255. Fujiwara, T. K. *et al.* Confined diffusion of transmembrane proteins and lipids induced by the same actin meshwork lining the plasma membrane. *Molecular Biology of the Cell* **27**, 1101 (2016).

256. Culley, S., Tosheva, K. L., Matos Pereira, P. & Henriques, R. SRRF: Universal live-cell super-resolution microscopy. *Int J Biochem Cell Biol* **101**, 74–79 (2018).

257. Vicidomini, G., Bianchini, P. & Diaspro, A. STED super-resolved microscopy. *Nat Methods* **15**, 173–182 (2018).

258. Kilian, N. *et al.* Assessing photodamage in live-cell STED microscopy. *Nat Methods* **15**, 755–756 (2018).

259. Palczewski, K. Oligomeric forms of G protein-coupled receptors (GPCRs). *Trends in Biochemical Sciences* **35**, 595–600 (2010).

260. Case, L. B. & Waterman, C. M. Integration of actin dynamics and cell adhesion by a three-dimensional, mechanosensitive molecular clutch. *Nat Cell Biol* **17**, 955–963 (2015).

261. Vicente-Manzanares, M., Ma, X., Adelstein, R. S. & Horwitz, A. R. Non-muscle myosin II takes centre stage in cell adhesion and migration. *Nat Rev Mol Cell Biol* **10**, 778–790 (2009).

262. Przybyla, L., Lakins, J. N., Sunyer, R., Trepat, X. & Weaver, V. M. Monitoring developmental force distributions in reconstituted embryonic epithelia. *Methods* **94**, 101–113 (2016).

263. Stubb, A. *et al.* Fluctuation-Based Super-Resolution Traction Force Microscopy. *Nano Lett.* **20**, 2230–2245 (2020).

264. Kuznetsova, T. G., Starodubtseva, M. N., Yegorenkov, N. I., Chizhik, S. A. & Zhdanov, R. I. Atomic force microscopy probing of cell elasticity. *Micron* **38**, 824–833 (2007).

265. Lokugamage, N. *et al.* Use of a small molecule integrin activator as a systemically administered vaccine adjuvant in controlling Chagas disease. *npj Vaccines* **6**, 1–14 (2021).

266. Maiguel, D. *et al.* Small Molecule–Mediated Activation of the Integrin CD11b/CD18 Reduces Inflammatory Disease. *Science Signaling* **4**, ra57–ra57 (2011).

Curriculum Vitae

Name: Brandon Dickson

Post-secondary Education: Western University; London, ON, Canada
2021-2023 MSc (Microbiology & Immunology)

McMaster University; Hamilton, ON, Canada
2017-2021 BSc (Honours Biochemistry)

Honours and Awards: Robarts Research Retreat Poster Award; 2023
RHSE Fellowship, University of Toronto; 2023
CSI Student Travel Award, CHU Ste-Justine; 2023
RGE Murray Graduate Student Seminar Award; 2023
FW Luney Graduate Travel Award; 2022, 2023
CSI Poster Award; 2022
CGS-M Scholarship, CIHR; 2022
Dean's Honour List, McMaster University; 2017-2021
The Yates Scholarship, McMaster University; 2018
President's Award, McMaster University; 2017

Related Work Experience: Teaching Assistant, Western University, 2021-2023

Publications:

Dickson BH, Tasnim T, Lam AL, Vrieze A, Blythe EN, Dekaban GA, Heit B. MERTK Coordinates Efferocytosis by Regulating Integrin Localization and Activation. *Preprint*. 2023. https://doi.org/10.1101/2023.07.20.549870

Dickson BH, Heit B. Analysis of Efferocytic Receptor Dynamics and Synapse Formation in a Frustrated Efferocytosis Model. *Methods Mol. Biol.* 2023. https://doi.org/10.1007/978-1-0716-3338-0_5

Taefehshokr N, Lac A, Vrieze AM, **Dickson BH**, Guo PN, Jung C, Blythe EN, Fink C, Dekaban GA, Heit B. SARS-CoV-2 NSP5 Antagonizes the MHC II Antigen Presentation Pathway by Hijacking Histone Deacetylase 2. *Preprint*. 2023. https://doi.org/10.1101/2023.02.10.528032

Klein TA, Grebenc DW, Shah PY, McArthur OW, **Dickson BH**, Surette MG, Kim Y, Whitney JC. Dual targeting factors are required for LXG toxin export by the bacterial type VIIb secretion system. *mBio*. 2022. https://doi.org/10.1128/mbio.02137-22